

A review on quantum dot sensitized solar cells: Past, present and future towards carrier multiplication with a possibility for higher efficiency



Anurag Sahu^a, Ashish Garg^b, Ambesh Dixit^{a,*}

^a Department of Physics & Center for Solar Energy, Indian Institute of Technology Jodhpur, Jodhpur 342037, India

^b Department of Materials Science and Engineering, Indian Institute of Technology Kanpur, Kanpur 208016, India

ARTICLE INFO

Keywords:

Quantum dots
Solar cell
QDSSC, Carrier multiplication
Absorber
Bandgap
Multiexciton generation (MEG)

ABSTRACT

Quantum Dot Sensitized Solar Cells are considered as the potential third generation solar cells due to their suitable optoelectronic properties for photovoltaic response. The possibility of size and composition tunability makes quantum dots as relevant absorber materials to match the wider solar spectrum more efficiently. In conjunction, the possibility of multiple electron-hole pair generations at the cost of single photon i.e. multiple carrier generation is showing potential to overcome the theoretical single junction power conversion efficiency limitations. Quantum dot sensitized solar cells are showing power conversion efficiencies up to 12%, very close to its counterpart dye sensitized solar cells. However, QDSSCs efficiencies are still lagging behind the conventional solid state single junction solar cells. In this review, we will discuss the initial evolution of quantum dot sensitized solar cells with their microscopic working principles. The review will also address development of key building blocks and factors such as various interfaces in QDSSCs, carrier transport and recombination across different interfaces, affecting the power conversion efficiency. Further, fundamental concepts of carrier multiplication and possible theoretical models for multiple exciton generation are discussed towards their impact on the power conversion efficiencies of quantum dot sensitized solar cells.

1. Introduction

Ever growing global energy demands and waning fossil fuels coupled with global warming, causing temperature rise, are some of the future threats, demanding continuous efforts from scientists and researchers to develop efficient and cost effective renewable energy alternatives. Earth is continuously receiving 3×10^{24} J/Year energy from Sun, while 1/10,000th part of this energy, is sufficient to satisfy the global energy demand (Pandikumar and Alagarsamy, 2018; Wang et al., 2018; Ichikawa et al., 2001). Photovoltaic systems provide an alternative way for harnessing this available renewable energy by converting it directly into electrical energy. The electrical energy production is increasing worldwide using photovoltaic systems, yet still there are issues and challenges to go a long way to play the significant role, meeting the global energy demand (Pandikumar and Alagarsamy, 2018; Wang et al., 2018; Ichikawa et al., 2001).

Solar Cells evolved significantly in the last few decades and this evolution is categorized in three generations taking into account the various technologies involved and recently the concept of fourth generation is also introduced in the photovoltaic community (Pandikumar and Alagarsamy, 2018). First generation solar cells are conventional

silicon ‘Si’ wafer based photovoltaic cells like monocrystalline silicon solar cells and polycrystalline Si solar cells. Second generation solar cells are based on thin film absorbers, aiming to reduce the cost of first generation solar cells because of expensive silicon material, used as a thick absorber in fabricating solar cells and to overcome the limitations on size of solar cells due to the restricted size silicon wafers (maximum up to 6" diameter). This includes photovoltaic technologies like CdTe solar cells (Wang et al., 2018), amorphous Si based solar cells (Ichikawa et al., 2001), heterojunction with intrinsic thin layer (HIT) solar cells (Mishima et al., 2011), copper-indium-gallium-sulphur/selenium (CIGS) based solar cells (Contreras et al., 2002), GaAs solar cells (Bauhuis et al., 2009) etc. in thin film geometries. Thus, thin film based solar cells surpassed the limitations on geometrical sizes of the solar cells. Third generation solar cells targeted reducing both the cost as well as achieving higher efficiencies. Solar cells in third generation employ more advanced concepts like integration of different bandgap junctions i.e. multijunction and inter-band based solar cells (Green, n.d.). The more recent perovskite solar cells are another class of solar cells, which are gaining attention and the field is rapidly evolving and showing record efficiencies. (Zeng et al., 2017; Wang et al., 2019) In brief, some of the representative solar cells with respective schematic

* Corresponding author.

E-mail address: ambesh@iitj.ac.in (A. Dixit).

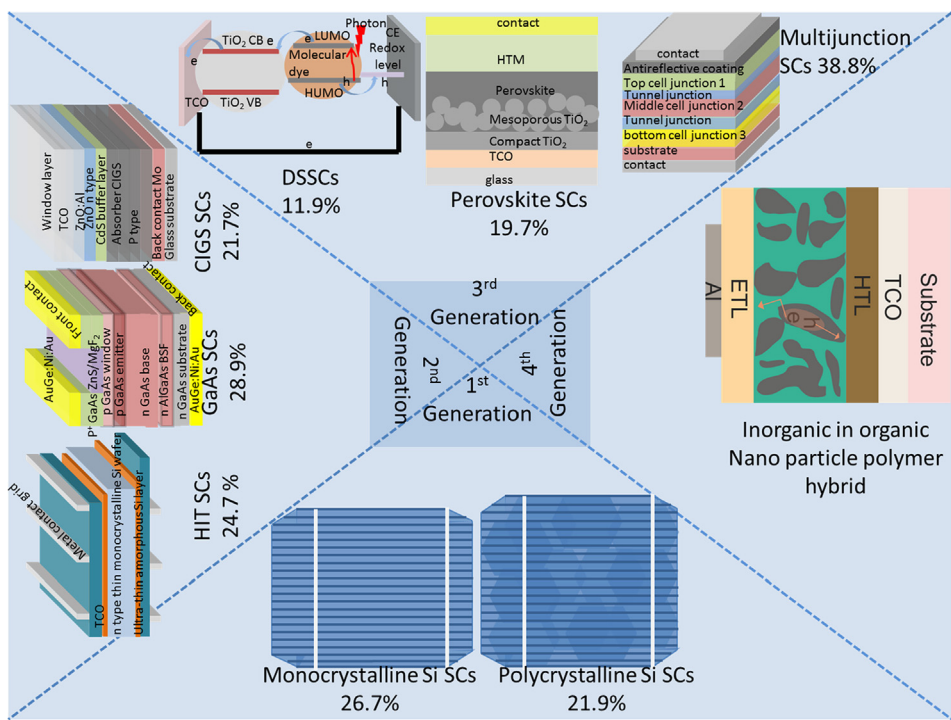


Fig. 1. Schematic diagram showing the evolution of different generations of photovoltaic solar cells with respective device structures and the current photovoltaic efficiencies.

Table 1

Summary of the best solar cells from different generations in conjunction with their respective device parameters.

Solar cell generation	Architecture of solar cell	Best reported photo-voltaic performance parameter			
		J_{SC} (mA/cm ²)	V_{OC}	FF	Efficiency (%)
1st	Monocrystalline Si Solar cell (Yoshikawa et al., 2017)	42.65	0.738	84.9	26.7 ± 0.5
2nd	Polycrystalline Si Solar cell (Benick et al., 2017)	40.76	0.6726	79.7	21.9 ± 0.4
	Amorphous Si based Solar Cell (Matsui et al., 2015)	16.36	0.896	69.8	10.2 ± 0.3
	Microcrystalline Si based Solar cell (Sai et al., 2015)	28.72	0.55	75.0	11.9 ± 0.3
	CIGS based Solar cells (Kato et al., 2017)	40.7	0.718	74.3	21.7 ± 0.5
	CdTe based solar cells (First Solar Press release 23 Feb 2016)	30.25	0.88	79.4	21.0 ± 0.4
	CZTS based solar cell (Sun et al., 2016)	21.77	0.71	65.1	10.0 ± 0.2
	GaAs based Solar cell (Kayes et al., 2011)	29.68	1.12	86.5	28.8 ± 0.9
	HIT Solar cells (Wakisaka et al., 1991; Taguchi et al., 2014)	39.5	0.75	83.2	24.7
3rd	Multi-junction based solar cell (Chiu et al., 2014)	9.56	4.77	85.2	38.8 ± 1.2
	Dye sensitized solar cell	22.47	0.74	71.2	11.9 ± 0.4
	Perovskite based solar cell (Yang et al., 2015)	24.67	1.104	72.3	19.7 ± 0.6
	Organic solar cell (Mori et al., 1737 (2015))	19.30	0.78	74.2	11.2 ± 0.3
	Quantum Dot sensitized solar cell (Du et al., 2016)	25.18	0.742	62.4	11.66 ± 0.17
4th	Nano-particle polymer hybrid solar cells	The developments are still in nascent stage and quantification may not be worthy for such initial developments.			

structures are summarized in Fig. 1, explaining the developments associated with different generations. The schematic solar cell diagrams are also explaining the respective geometrical structures with their optimal photovoltaic efficiencies. Further, Table 1 summarises various solar cells architectures for all these generations, with their optimal reported photovoltaic device parameters. This table is derived from the Solar Energy efficiency table by Green et al. (2017). The table is also listing reports with the highest efficiencies, reported so far in the literature for different generation solar cell devices.

Further, solar cells are also classified considering their working mechanism i.e. involving photoinduced carrier generation and electron-hole separation processes. The first classification is considered as a P-N

junction solar cells, which makes use of photoinduced carrier generation in bulk material, especially in the absorber layer, followed by the carrier separation with the help of a built-in junction potential (Gregg, 2003). The second classification includes excitonic solar cells, making use of excitonic absorbers. In excitonic solar cells, absorption of solar radiation results in creation of exciton (a bound electron-hole pair) rather than free electron-hole pair. These photogenerated excitons are weakly bound electron-hole pairs through Coulombic interaction, but they are also considered as the mobile excited states simultaneously (Powell and Soos, 1975; Gregg and Hanna, 2003). These excitonic solar cells make use of interfacial dissociation of exciton into free electron and hole. Excitonic solar cells include organic solar cells (Hoppe and

Sariciftci, 2004; Mori et al., 2015), dye sensitized solar cells (DSSCs) (Oregan and Gratzel, 1991; Mathew et al., 2014), and quantum dot sensitized solar cells (QDSSCs) (Ren et al., 2015) etc. The working mechanism of these excitonic solar cells is quite similar in principle. However, these differ significantly in their geometrical architectures. These solar cells make use of excitonic absorbing materials for generating excitons after absorption of incident solar radiation instead of free electron-hole pair as observed in conventional Si or other semiconductor based P-N junction cells. These photogenerated excitons are dissociated at the interface in electron and hole due to their band offsets and transported further to the selective contacts. Such selective contacts are formed by using materials, known as electron transport material (ETM) which accepts and transport electron from excitonic absorber and hole transport material (HTM) which accepts and transport holes from excitonic absorber. Apart from excitonic absorber, electron and hole transport materials are also very important components of the excitonic solar cell. The defects, interfaces, energy levels alignments and carrier lifetime in ETM and HTM can hamper device performance. Thus, a careful selection of material and their processing are very important to achieve the enhanced photovoltaic response.

DSSC excitonic solar cells became popular among other excitonic solar cells after Gratzels' (1991) work showing promise for high photovoltaic efficiency, where high surface area of porous TiO₂ electrode is used as the working electrode. The reported efficiency was the highest for an excitonic solar cell around that period (Gregg, 2003). The observed improvement in efficiency was attributed to the availability of large surface area of the electrode, assisting to deposit monolayer of absorber dye molecules over large surface area. The efforts to replace molecular absorber dyes in DSSCs by semiconductor nano absorbers resulted in the development of Quantum Dot Sensitized Solar Cells (QDSSCs). The schematic diagrams for a dye sensitized solar cell (DSSC) and quantum dot sensitized solar cell (QDSSC) are shown in Fig. 2(a) and (b), respectively. These solar cells are quite similar in geometrical architecture with a difference that semiconductor QDs are used as excitonic absorber in QDSSCs in contrast to the molecular dyes as excitonic absorber used in DSSCs. A nanostructured, large surface area, wide band gap semiconductor electrode is used as the electron transport material (ETM) in both the cells. Here, large surface area of the electrodes provides possibility to deposit sufficient amount of excitonic sensitizer to absorb incident solar radiation. Titanium dioxide (TiO₂) is one of the most widely investigated and used electron transport material among other wide bandgap semiconductors such as ZnO, SnO₂, which are also explored as ETM in both DSSCs and QDSSCs (Jose et al., 2009). A redox couple is used as a hole transport material (HTM) in both DSSC and QDSSC, as explained in Fig. 2. Iodide redox system is the most common in DSSCs, whereas polysulfide is used as a redox system in QDSSCs (Rühle et al., 2010). An excitonic absorber absorbs incident solar radiation, leading to the excitons generation in absorber. This photogenerated exciton is dissociated at ETM/absorber interface and

electron is transferred to ETM, while hole is transferred to HTM from excitonic absorber, relatively at a later time.

Quantum dots are also integrated in different geometrical solar cell configurations in addition to the widely explored quantum dot sensitized solar cells. These architectures include Schottky quantum dot solar cells (Johnston et al., 2008; Koleilat et al., 2008), depleted heterojunction solar cell (Pattantyus-abraham et al., 2010), extremely thin absorber solar cell (Ernst et al., 2003), hybrid polymer solar Cell (Günes et al., 2007; Günes et al., 2007; Yun et al., 2009) and organic-inorganic heterojunction solar cell (Chang et al., 2010; Leschklies et al., 2007). These QDs derived architectures are shown schematically in Fig. 3. Fig. 3(a) shows the a schematic diagram for Schottky quantum dot solar cell in conjunction with respective energy levels alignment, explaining the open circuit voltage of the cell. Schottky QD solar cell works with band bending at the metal and p-type semiconductor interface as shown in Fig. 3(a), which results in a depletion region for the device. This band bending favours the extraction of electrons and simultaneously works as the barrier for hole extraction at metal contact, which are collected at high work function transparent conducting oxide (TCO) back electrode. Fig. 3(b) shows a schematic diagram for depleted heterojunction solar cell with respective energy levels and their alignment. In depleted heterojunction solar cell, semiconductor QDs layer is deposited between an electron acceptor material like TiO₂ and metal contact. The photogenerated electrons are collected efficiently by TiO₂ due to a suitable band offset between TiO₂ and quantum dots and holes are extracted at a high work function metal like Au contacts. Fig. 3(c) shows a schematic diagram of quantum dot sensitized solar cells, similar to Fig. 2(b), with respective energy levels and their alignments. The photogenerated electrons from excitonic absorber are accepted at ETM like TiO₂ and QDs are regenerated by redox electrolyte. Catalytic counter electrodes like Cu₂S are used to catalyse regeneration of redox electrolyte (Yeh et al., 2011). Fig. 3(d) shows a schematic diagram for a hybrid polymer solar cell with energy levels and their alignments. These hybrid polymer solar cells make use of electron donating or hole accepting polymers like Poly[2,6-(4,4'-bis-(2-ethylhexyl)-4H-cyclopenta [2,1-b;3,4-b']dithiophene)-alt-4,7(2,1,3-benzothiadiazole)] (PCPDTB) and electron accepting fullerene or polymer like Poly(2,3-dihydrothieno-1,4-dioxin)-poly(styrenesulfonate) (PEDOT:PSS). QDs are added in a polymer fullerene composite as the solar absorber (Emin et al., 2011). Fig. 3(e) shows a schematic diagram for hybrid polymer solar cell in conjunction with respective energy levels and their alignments. In this type of solar cells, incident photons are absorbed by QDs and excitons are accepted by electron conductor like TiO₂, while holes are accepted by the organic polymer hole transport material. Fig. 3(f) shows a schematic diagram of an extremely thin absorber cell along with energy levels and their alignments. In extremely thin absorber (ETA) solar cells, intrinsic QDs layer with high extinction coefficient is sandwiched between two transparent high bandgap electron transport and hole material materials. In such devices, carriers are generated in

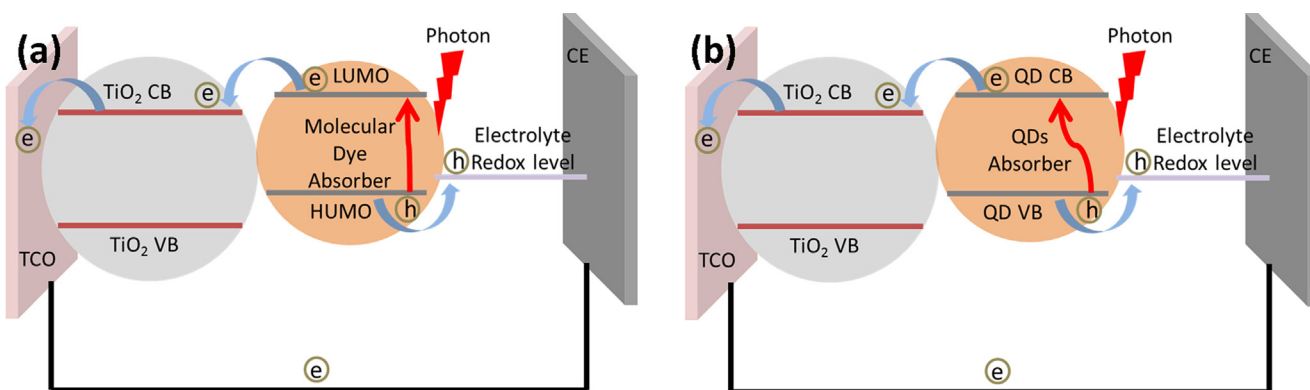


Fig. 2. Schematic diagrams for (a) Dye Sensitized solar cells (DSSCs) and (b) Quantum Dot Sensitized Solar Cells (QDSSCs).

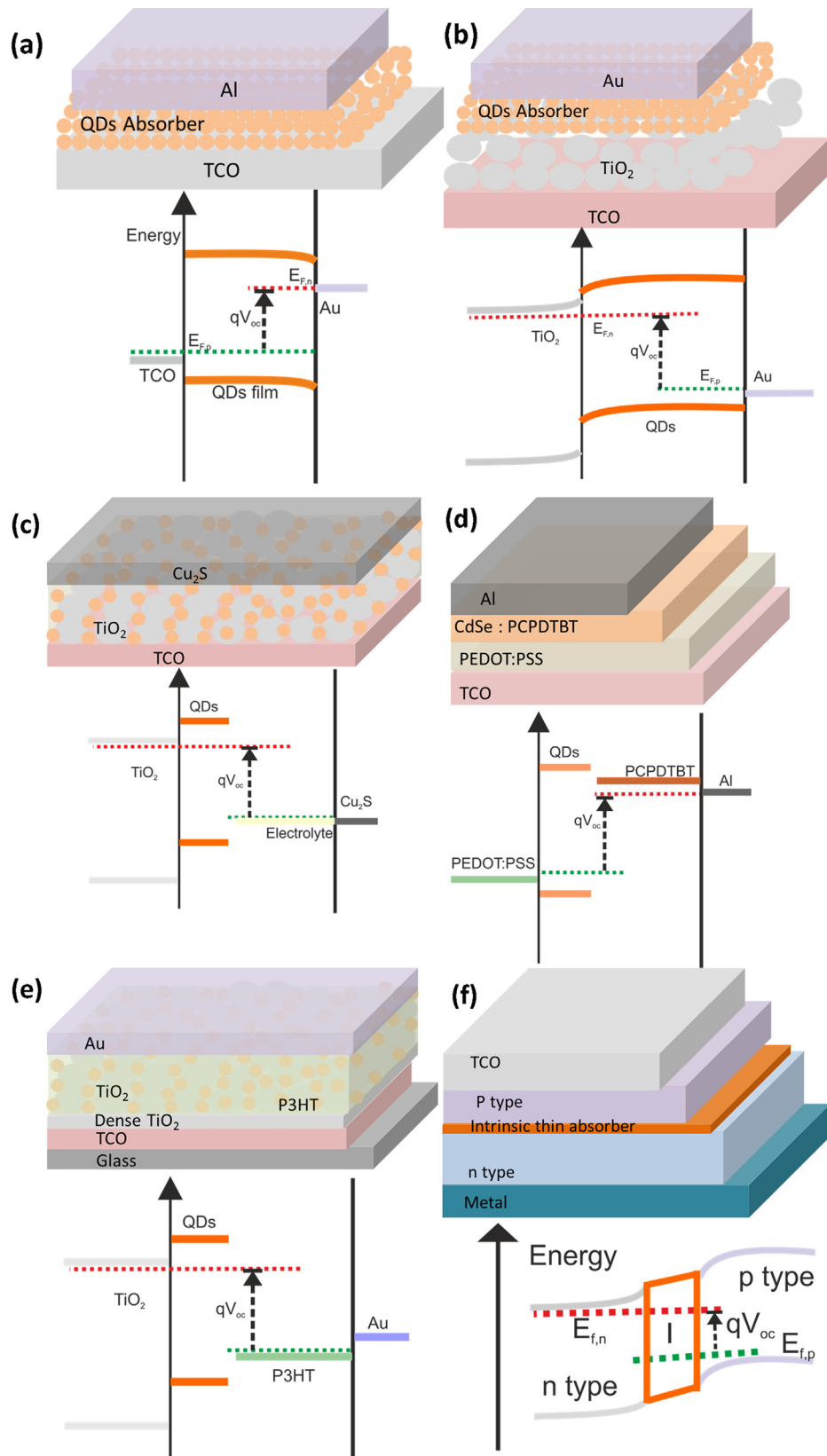


Fig. 3. Schematic diagram showing few popular architecture and energy level alignment of QDSCs: (a) Schottky Quantum Dot Solar Cell, (b) Depleted heterojunction solar cell, (c) Quantum Dot sensitized solar cell, (d) Hybrid polymer solar cell, (e) Organic-inorganic heterojunction solar cell and (f) Extremely thin absorber solar cell.

intrinsic QD absorber layer and separated due to the large electric field present at ETM/Intrinsic absorber/HTM interfaces. ETA and organic-inorganic heterojunction solar cells are similar in configurations. However, the difference lies in fact that organic HTM is used in case of organic-inorganic heterojunction solar cells, whereas inorganic HTM is utilized for ETA cells. Further, the present review will focus on QDSSCs, emphasizing the possibility of carrier multiplication towards realizing higher quantum efficiencies.

QDs as excitonic absorber make QDSSCs very exciting not only in the context of next generation photovoltaic devices for harnessing solar energy but also offering challenges to understand the fundamental concepts such as multiple exciton generation at the cost of single photon absorption. QDs are very small in geometrical size, confined in three dimensions with their sizes comparable to the excitonic radius (Memming, 2000). These offer high extinction coefficient (Yu et al., 2003) and their optoelectronic properties make them as the potential candidate from photovoltaic devices. Additionally, QDs show tunable bandgap by manipulating their sizes or alloying with suitable systems (Haram et al., 2011). This size tunable bandgap also results in the quantum confinement effects, leading the relatively larger bandgap values as compared to their bulk counterpart and is explained in term of size quantization effect (Brus, 1983; Brus, 1984; Steigerwald and Brus, 1989; Steigerwald and Brus, 1990). Further, QDs also exhibit efficient multiple exciton generation, even after absorbing the single photon. This can enhance QDSSCs performance, when compared to the conventional solid state solar cells (Schaller and Klimov, 2004). Recently, the detailed balance calculations suggested that QDSSCs can overcome the detailed balance limit of conventional single junction solar cells after considering the possibility of multiple exciton generation (MEG) in such devices (Klimov, 2006). The multiple exciton generation in QDs also provide the possibility of utilizing hot carriers in photovoltaic response. A thermodynamic limit with hot carriers can be up to 66% (Nozik, 2002). The hot carriers in QDSSCs can be utilized for MEG to realize such high photovoltaic efficiencies, yet the offset for MEG may limit the maximum thermodynamic efficiency.

There are several reviews on QDSSCs (Kamat, 2013; Bang and Kamat, 2009; Carey et al., 2015; Rajendra Prasad et al., 2017) however, only few reports provide potential and limitations for QDSSCs, correlating with their respective working mechanism in the light of multiple exciton generation (MEG) in conjunction with the progress in respective building blocks for QDSSCs. This QDSSCs review will be complementing the available reports by considering these aspects in detail. In this review, we will cover the early developments together with the understanding of the microscopic working mechanisms. The review will also cover individual QDSSCs building blocks and their development over time towards efficient QDSSCs. We will also focus on multiple exciton generation (MEG) studies related to colloidal QDs and their implications in photovoltaic conversion efficiencies.

2. Quantum dot sensitized solar cells

2.1. Initial developments

The process of wide band gap semiconductor sensitization is a topic of active research from sixties (Kallmann and Pope, 1959; Tollin et al., 1960). The molecular dyes are studied extensively for sensitization of DSSCs over the last several years (Oregan and Gratzel, 1991; Hagfeldt and Grätzel, 2000; Kong et al., 2007). These dyes can absorb incident photons and inject photogenerated electrons to the wide bandgap semiconductor while positive holes are scavenged by the liquid redox couple (Cahen et al., 2000). These dyes led to the relatively good quantum efficiencies for a monolayer covering of molecular dyes to the mesoporous electrode materials. The quantum efficiency starts reducing for more than a monolayer thick dyes on mesoporous electrodes and is attributed to the lower electron injection to mesoporous electron transport materials (ETM) (Vogel et al., 1994). The amount of solar flux

absorbed by monolayer dye is relatively small and that's why the application of these dyes was not feasible to realize enhanced absorption and efficient electron injection to the mesoporous electrode materials (Vogel et al., 1990; Weller, 1991). In 1991, Gratzel et al. developed nanostructured, high surface area, mesoporous wide band gap semiconductor electrode and coated those mesoporous electrodes with monolayer of dye molecules (Oregan and Gratzel, 1991). Gratzel photovoltaic cell showed a quantum jump in efficiency with the highest conversion efficiency for such dye sensitized or excitonic solar cells.

Vogel et al reported the sensitization of mesoporous TiO_2 by depositing in-situ cadmium sulphide (CdS) quantum dots for the first time in 1990 (Schaller and Klimov, 2004). Anatase TiO_2 is grown on Ti foil using hydrolysis and CdS quantum dots are used for sensitization of TiO_2 electrode using successive ionic layer adsorption and reaction (SILAR) method. A three electrode configuration is used for evaluating the performance of these solar cells and about 6% efficiency was recorded (Vogel et al., 1990). However, this efficiency value was not considered as the power conversion efficiency as the devices investigated were measured in the three electrode configuration (Hodes, 2012). In 1991, Weller et al reported sensitization of TiO_2 electrode by PbS QDs using SILAR and measured current spectra in the three electrode configuration. A reduction in photoconversion efficiency (PCE) was observed for more than five SILAR cycles of PbS QDs sensitization. The observed reduction in PCE is attributed to the quantization effect for PbS QDs. Weller et al proposed that bulk PbS is not suitable for injecting electrons into TiO_2 electrode due to the lower level of conduction band minima as compared to that of TiO_2 and also suggested that a band offset of 0.25 eV as the driving force was necessary to inject electrons to TiO_2 efficiently (Weller, 1991).

In 1992, Kamat et al. reported ZnO/CdS film over conducting glass and its sensitization with chlorophyll was done using electrodeposition. Photocurrent measurements were conducted in the three electrode configuration and the maximum photovoltage of ~ 135 mV was noticed (Hotchandani and Kamat, 1992). In 1994, R Vogel et al. reported sensitization of various nano porous wide band gap semiconductors with PbS , CdS , Ag_2S , Sb_2S_3 and Bi_2S_3 quantum dots using SILAR and also reported post preparative surface treatment for the first time that enhanced the photostability of sensitized quantum dots significantly (Vogel et al., 1994). O'Regan et al. prepared mesoporous TiO_2 electrode using colloidal solution (O'Regan et al., 1990), somewhat different from their earlier work, where Ti foil was used to prepare TiO_2 electrode (Vogel et al., 1990). SnO_2 nano particle were prepared using method reported by Meisel et al. (Mulvaney et al., 1990). Nb_2O_5 , Ta_2O_5 and ZnO nano particles were prepared in diameter range of 5–6 nm for their use as mesoporous electrode. The mesoporous electrodes based on these binary oxide nanoparticles were prepared by spin coating of respective colloidal solution on ITO glass and subsequently heated to 420 °C before sensitization. SILAR method was used to sensitize these electrodes with PbS , CdS , Ag_2S , Sb_2S_3 and Bi_2S_3 quantum dots. The electrochemical measurements were done in 3 electrode configuration with different electrolytes. The estimated quantum yields are $\sim 88\%$ for CdS and Sb_2S_3 , 64% for PbS , 50% for Bi_2S_3 and 15% for Ag_2S quantum dots. Among these, Sb_2S_3 and Bi_2S_3 quantum dots were reported to decompose under light while Ag_2S was showing poor quantum yield, and were intentionally ignored for future investigations. The order for quantum yield was $\text{TiO}_2 > \text{ZnO} > \text{Nb}_2\text{O}_5 > \text{SnO}_2 > \text{Ta}_2\text{O}_5$ and the quantum yield showed reduction with increasing particle size. These studies suggested that photovoltage was not determined only by conduction level of TiO_2 and redox level but also dependent on sensitizer. The enhanced stability of PbS coated TiO_2 electrode was noticed after coating sensitized electrode with a wide band gap material like TiO_2 or CdS for hole blocking (Spanhel et al., 1987).

In 1997, Jinghuai et al. reported first time cosensitization of TiO_2 mesoporous electrode with CdSe QDs and dye molecule. In this work, CdSe QDs were deposited by chemical bath deposition (CBD) method and later CdSe sensitized electrode was sensitized by molecular dyes for

evaluating photovoltaic response in 2 electrode electrochemical cell. They reported coalescence of TiO_2 particle to larger particles due to the annealing (Fang et al., 1997). They suggested growth by chemical bath deposition involves aggregation of colloids in contrast to atom by atom deposition as suggested in earlier studies (Cachet et al., 1995; Ortega-Borges, 1993).

In 1998, A. Zaban et al. for the first time reported the sensitization of mesoporous TiO_2 by pre synthesized InP QDs (Zaban et al., 1998). Trioctylphosphine oxide (TOPO)/ trioctylphosphine (TAP) capping agents over InP QDs were replaced by 4-*tert*-butylpyridine (TBP) using ligand exchange approach. Further, the studies emphasized that the presence of excess free stabilizer is hindering the adsorption of QDs in mesoporous TiO_2 . These studies concluded that the better adsorption will take place with shorter capping ligands. The photovoltaic conversion efficiency was recorded in sandwich type configuration where Teflon tape was used as spacer against Pt counter electrode and observed linear increase in photocurrent with light intensity. The important and interesting outcome from these studies suggested that traps do not play a significant role in electron transportation. The short circuit current density of $\sim 150 \mu\text{A}/\text{cm}^2$ and open circuit voltage of $\sim 0.6 \text{ V}$ are reported for these devices.

With these initial reports, sensitization of wide band gap semiconductor with short band gap semiconductor was probed further for QDSSCs application by various research groups. Two strategies became quite prominent in sensitization of wide band gap semiconductor. In one case, QDs were directly grown in wideband gap semiconductor (in-situ sensitization) and in other approach pre-synthesized QDs were deposited inside mesoporous wideband gap semiconductor (ex-situ sensitization). Various surface treatments were developed to improve power conversion efficiencies of QDSSCs further and those will be discussed in following subsections.

2.2. Basic building blocks of QDSSCs

A QDSSC consists of several components, which need to be carefully selected and engineered to design for enhanced photovoltaic response.

2.2.1. Excitonic absorber (QDs)

The selection of appropriate absorber for designing an efficient solar cell is very important. Shockley and Queisser calculated the detailed balance limit for solar conversion efficiency of a single junction solar cell (Shockley and Queisser, 1961). This detailed balance conversion efficiency depends strongly on the band gap of absorbing material. In 2006, V. I. Klimov calculated detailed balance efficiency for quantum dot absorber based solar cells (Klimov, 2006) and is shown in Fig. 4. Here also a strong dependence on band gap of absorbing quantum dot material is observed for detailed balance efficiency. Thus, the bandgap

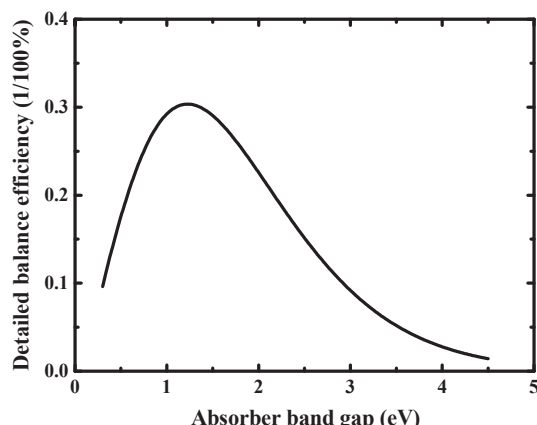


Fig. 4. Dependence of detailed balance efficiency over quantum dot absorber band gap regenerated by (Klimov, 2006).

of absorbing material is of paramount importance for design of an efficient solar cell as the photons above bandgap energy of absorbing material will be harvested to electrical energy and photons having energy below band gap will not be absorbed. Klimov et al showed that 1.2 eV is the optimum band gap of a solar absorber, Fig. 4.

In QDSSCs additional constraints are placed over absorber bandgap because QDs excitonic absorber should be able to inject electrons to the electron transport material and hole should be accepted by hole transport material (Mora-Seró and Bisquert, 2010). So there is a restriction on the bandgap of QD absorbers. The bandgap of Quantum Dots should be higher than the difference between conduction level of electron transport material and redox potential of electrolyte (Mora-Seró and Bisquert, 2010). There are reports suggesting that a driving force of 0.25 eV should be sufficient for the good rate of electron injection into electron transport material (Weller, 1991). For efficient injection of photoexcited electron to electron transport material, conduction level of QDs absorber should be 0.25 eV or more higher than the conduction level of electron transport material for efficient exciton dissociation and valence level of QDs should be lower than redox level of hole transport material. Thermodynamic limit for exciton dissociation at interface is that the band offset should be higher than the exciton binding energy (Gregg et al., 1990; Geacintov et al., 1966). Thus, the optimum bandgap of QDs absorber should be 0.25 eV higher than difference between conduction level of electron transport material and redox level of electrolyte. Fig. 5 shows the schematic diagram for energy level alignments required in quantum dot sensitized solar cell, together with showing the minimum required band gap for quantum dot absorber in QDSSCs.

Energy level in QDs can be manipulated by doping by the foreign atoms, designing core-shell structure or alloying of different QDs materials for required energy level alignment to have efficient photovoltaic performance. For doping of QDs, several studies for optically active transition metal doping in QDSSCs are carried out and improvement in conversion efficiency is reported (Santra and Kamat, 2012; Huang et al., 2013; Luo et al., 2013; Halder and Bhattacharyya, 2015). The dopant materials result in creation of mid-band states and charge dynamics of photo-excited carriers in QDs will be different from non-doped QDs (Sato, 1998). For example, improvement in photovoltaic efficiency with Mn transition metal doping, is attributed to the creation of mid band states resulting in higher lifetime states for charge carriers (Santra and Kamat, 2012). Fig. 6 shows schematically the creation of mid-gap states in QDs as reported by Kamat et al. (Santra and Kamat, 2012).

Cation and anion alloyed QDs band gap can also be tailored by their constituent materials (Yang and Li, 2008; Smith et al., 2011). Fig. 7 shows variation in energy level of alloyed CdSeTe by allowing CdTe and CdSe QDs materials. The bandgap and mole fraction of the constituent materials exhibit a non-linear relationship, which depends on the bowing parameter (Van Vechten and Bergstresser, 1970). QDSSCs with alloyed QDs have been reported to produce fairly good photovoltaic efficiency (Pan et al., 2013; Du et al., 2016).

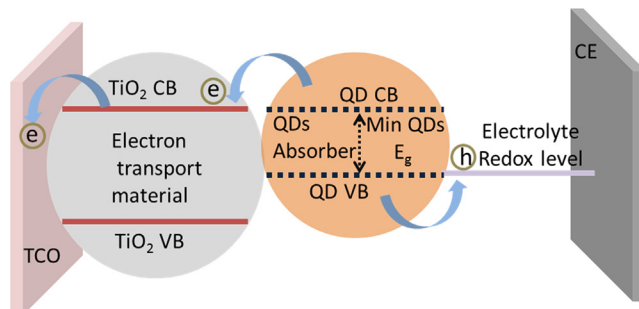


Fig. 5. A schematic diagram showing minimum QDs band gap required for QDSSCs based on ETM and HTM material energy levels.

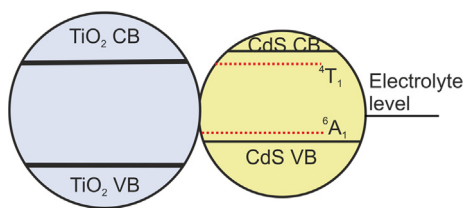


Fig. 6. Creation of mid-gap states in QDs with Mn doping. Reprinted (adapted) with permission from (Santra and Kamat, 2012).

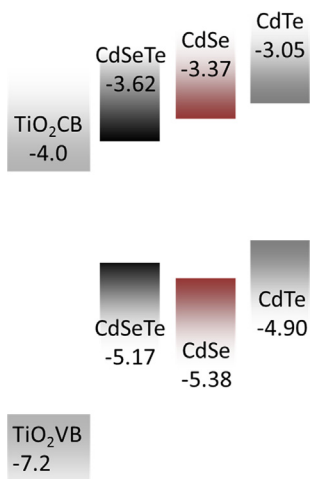


Fig. 7. Schematic diagram showing manipulation of QDs energy level by alloying different QDs material. Reprinted (adapted) with permission from (Pan et al., 2013).

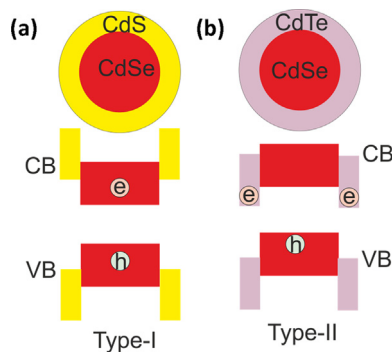


Fig. 8. (a) Schematic diagram of type - I core-shell Quantum dot with conduction and valence band alignment (b) Schematic diagram of type – II core-shell quantum dot with their conduction and valence band alignment.

The improvement in energy conversion efficiency is also reported for core-shell or multi-shell quantum dots based QDSSCs (Shalom et al., 2009; Lai et al., 2014; Ning et al., 2011). The core-shell quantum dots are normally prepared separately and sensitization of wide band gap semiconductor is done using post synthesis approaches. These core-shell QDs normally consist of different material as the core and shell of a QD. The core-shell QDs will provide additional degree of freedom in manipulating the band offset between core and shell materials. This suitable band offset is required for efficient collection of carriers by electron transport material (ETM) and also to minimise the lattice mismatch between them. The collection of photogenerated electron and hole can be controlled by the energy level alignments of core and shell material. The core-shell QDs are divided in two categories based on position of the respective positions of core and shell energy levels, type-I and type -II QDs (Hatami et al., 1998). Fig. 8 shows schematic diagram of energy level alignment in type I and type II core-shell QDs. Type-I core-shell QDs are formed by coating low bandgap core material by a high band gap shell material and photo-generated electron-hole are confined in core region in such QDs. The conduction band alignment in type I core-shell QDs is well type structure as shown in Fig. 8(a). Further, the band alignment in type II core-shell QDs is staggered as shown in Fig. 8(b). It is designed in such way that either shell conduction level or valence level reside in core band gap. This assists in retaining photogenerated carriers in separate regions in such type II QDs, as shown in Fig. 8(b). The exciplex QDs were designed using type II QDs, and reported to have band gap lower than that of individual bandgap of core or shell material (Wang et al., 2013; Jiao et al., 2015). The thickness of shell needs to be small for tunnelling of photogenerated carrier to electron transport material for electron injection or tunnelling of hole to hole transport material for hole extraction as the one of the charge carrier resides in core region (Zhao et al., 2014).

Several types and different materials based QDs are prepared over the years and utilized in QDSSCs. We have summarized some of the QDs sensitizer along with employed solar cell configuration from photo-electrode side to counter electrode side. Table 2 shows efficiencies demonstrated for different QDs absorbers together with respective photovoltaic parameters. However, photovoltaic performance does not represent the best efficiencies achieved with a particular QDs absorber considering large number of component involved in the design of QDSSCs.

Adhering of QDs on wide band gap semiconductor is referred as sensitization of mesoporous electrodes. This can be achieved by several methods, which are broadly classified into two categories, as discussed below:

(a) In-situ sensitization – In this process, QDs are grown directly inside the pores of mesoporous wide band gap semiconductor electrodes. Several approaches are explored for in-situ sensitization. Commonly utilized approaches are:

(i) Successive Ionic Layer Adsorption and Reaction (SILAR) – SILAR is a very fast and simple QDs deposition technique over mesoporous electrode. First report by Vogel et al used SILAR technique for sensitization of CdS QDs (Vogel et al., 1990). As the name suggest, this

Table 2

Performance of some QDs absorber with efficiencies among best performing devices with respective QDs. Although, they do not represent highest photo-voltaic performance for respective QDs system.(FTO = Florine doped Tin oxide, S^{2-} - S_n^{2-} represents polysulfide electrolyte).

QDs absorber	Cell Configuration	J_{SC} (mA/cm ²)	V_{OC} (volt)	FF	Efficiency (%)
CdS (Santra and Kamat, 2012)	FTO/TiO ₂ /CdS/ZnS/ S^{2-} - S_n^{2-} /FGO-Cu ₂ S/FTO	7.2	0.496	0.46	1.63
CdS-Mn (Santra and Kamat, 2012)	FTO/TiO ₂ /CdS-Mn/ZnS/ S^{2-} - S_n^{2-} /FGO-Cu ₂ S/FTO	8.9	0.583	0.49	2.52
CdSe (Zhang et al., 2012)	TiO ₂ /CdSe-MPA/ZnS/ S^{2-} - S_n^{2-} /Cu ₂ S/Brass	16.96	0.561	0.566	5.42
CdS/CdSe (Yu et al., 2011)	TiO ₂ /CdS/CdSe/ZnS/ S^{2-} - S_n^{2-} /Pt/FTO	18.23	0.489	0.54	4.81
CdTe/CdSe (Wang et al., 2013)	TiO ₂ /CdTe/CdSe/ZnS/ S^{2-} - S_n^{2-} /Cu ₂ S/Brass	19.59	0.606	0.569	6.76
CdSeTe (Ren et al., 2015)	TiO ₂ /CdSeTe/TiCl ₄ /ZnS/ S^{2-} - S_n^{2-} /Cu _{2-x} S/Brass	20.69	0.700	0.622	9.01
ZnTe/CdSe (Jiao et al., 2015)	TiO ₂ /ZnTe/CdSe/ZnS/ S^{2-} - S_n^{2-} /Cu _{2-x} S/Brass	19.35	0.646	0.551	6.89
Zn-Cu-In-Se (Du et al., 2016)	TiO ₂ /Zn-Cu-In-Se/ZnS/ S^{2-} - S_n^{2-} /MC/Ti	25.18	0.742	0.624	11.66

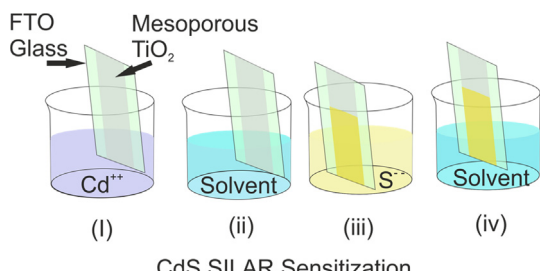


Fig. 9. Schematic representation of SILAR sensitization of mesoporous electrode by CdS QDs. (I) adsorption of Cd^{++} ions over mesoporous, (II) removal of excess Cd^{++} ions, (III) adsorption of $\text{S}^{- -}$ ions and (IV) removal of excess $\text{S}^{- -}$ ions.

technique works with layer by layer adsorption of ionic species and their reaction results in QDs formation. In this technique, cationic and anionic precursors are dissolved separately in suitable solvents. Mesoporous electrode is dipped in one precursor solution and ionic species are adsorbed over surface of mesoporous electrode. This dipped mesoporous electrode is washed by solvent to remove any excess ionic precursor that is not adsorbed on mesoporous electrode surface and further dipped in another precursor solution. Adsorbed surface ionic species reacts with another precursor and after subsequent washing with solvent, one SILAR cycle is completed. The number of SILAR cycles and dipping duration in ionic precursor solution is optimized to control QDs coverage and size (Lee et al., 2009). Fig. 9 shows schematic diagram for SILAR technique. SILAR normally results in good surface coverage of mesoporous electrode by quantum dots but the control of optoelectronic property of sensitized QDs is difficult (Lee et al., 2009). Various types of QDs are deposited using SILAR such as CdS, CdSe (Zhang et al., 2012), CdTe (Lee et al., 2009), PbS (Lee et al., 2009), CdSe_xS_{1-x} (Shu et al., 2012).

(ii) Chemical Bath Deposition – Chemical Bath Deposition (CBD) is also very simple process for the deposition of QDs over mesoporous electrode. In this process, both cationic and anionic precursors are dissolved separately in suitable solvent and mixed together to prepare a chemical bath of ionic species. Ionic precursor reacts slowly in chemical bath and gets deposited over electrode surface (Hodes and Gorer, 1994). The dipping time for electrode, precursor concentration, pH of solution and temperature of the chemical bath can be controlled to regulate size of sensitized QDs and surface coverage inside mesoporous electrode. Normally, CBD results in good surface coverage but the control of optoelectronic properties of sensitized QDs is difficult. Fig. 10 shows schematic diagram of CBD process. QDs like CdS, CdSe are deposited by CBD process successfully (Niitsoo et al., 2006; Toyoda et al., 2008; Okazaki et al., 2007).

(b) Post-synthesis sensitization – In post synthesis or ex-situ sensitization techniques, first QDs are synthesized separately for desired optoelectronic properties and then deposited over surface of wide band gap mesoporous semiconductor using different methods.

The synthesis process for QDs is discussed briefly first before discussing ex-situ deposition processes. Typically synthesis of QDs involves two stages, nucleation of ionic species followed by growth of quantum dots. Nucleation stage is controlled by temperature of precursors, pH, interfacial surface tension, and solution concentration (Kumar and Nann, 2006). After nucleation, growth takes place by adding atoms/molecules from the remaining precursor in solution by dissolving smaller QDs to form bigger QDs by Ostwald ripening mechanism (Vengrenovitch, 1982). Focusing (Reiss, 1951) and defocusing (Ostwald ripening) (De Smet et al., 1997) growth mechanism governs the growth of QDs particles. Surfactant or capping agents are also used to control the QDs properties. Growth rate (García-Rodríguez et al., 2013), phase (Huang et al., 2010), morphology, (Manna et al., 2000) and optical properties (Qu and Peng, 2002) can be controlled by capping agents. Thermal decomposition method is normally used for synthesis of QDs in chemical route. Nucleation and growth steps in thermal decomposition method can be separated by hot injection or heat-up methods. In hot injection method, precursors are injected to a hot surfactant rapidly. The saturation is induced because of injection, which promotes the onset of nucleation. Further, with injection of room temperature solution, nucleation stops and growth takes place (Murray et al., 1993). In heat up method, both stages are achieved by continuous heating of ligand and precursors (Park et al., 2007). A variation in these steps is also possible to get desired growth rate and optoelectronic properties. For example, heat-up method can be modified to the hydrothermal route to prepare water soluble QDs. In a typical hydrothermal synthesis, a mixture of capping agent like N-Acetylcysteine (NAC) and cationic precursor like cadmium oxide (CdO) is prepared in one flask. The temperature and pH of this solution are adjusted to control the nucleation stage. In a separate mixture anionic precursor like Se is dissolved by some reducing agent like NaBH_4 . Anionic precursor is injected rapidly in the cationic mixture. Injection temperature can be controlled to regulate nucleation rate and initial growth. After injection, mixture is transferred to a hydrothermal cell or autoclave for growth of quantum dots (Adegoke and Park, 2016). The duration of heating and heating temperature can be tailored to optimize the growth of QDs. Fig. 11 shows schematic diagram of hydrothermal preparation of CdSe QDs.

In ex-situ depositions methods, size and composition of QDs are normally not affected during the depositions process, and thus, the optoelectronic properties of pre-synthesized QDs are preserved. Commonly utilized approaches for ex-situ sensitization are discussed below:

(i) Direct adsorption – In direct adsorption, mesoporous electrodes are simply dipped in prepared dispersed QDs solution. QDs can easily penetrate through pores of mesoporous electrode because of their smaller size and gets deposited inside mesoporous electrode. The dipping time for QDs dispersion, size of dispersed QDs, type of QDs ligands, and concentration of QDs in solution are controlled for the optimum coverage of mesoporous electrode (Giménez et al., 2009; Zaban et al., 1998). Fig. 12 shows schematic representation of host wide band gap semiconductor sensitized with QDs sensitizer using direct adsorption. The direct adsorption process showed higher IPCE values compared to linker assisted adsorption for similar loading over mesoporous electrode (Lana-villarreal and Bisquert, 2009). The observed higher IPCE values are associated with direct contact of prepared QDs with wide band gap semiconductor electrode, exhibiting the better injection rate of photogenerated electrons to mesoporous electrode. Thus, relatively efficiencies are recorded with direct adsorption using suitable QDs having good optoelectronic properties and better injection rates, however achieving good surface coverage is a challenge with this method.

(ii) Linker assisted direct adsorption – Linker assisted direct adsorption is similar to the direct adsorption except that here mesoporous electrode is treated initially with some linker molecules to assist in QDs adsorption over mesoporous electrode. Linker molecules have normally

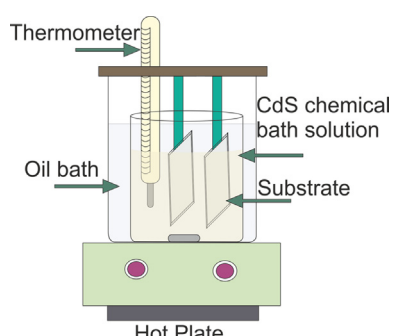


Fig. 10. Schematic diagram of sensitization of mesoporous electrode by CdS QDs using Chemical bath deposition (CBD).

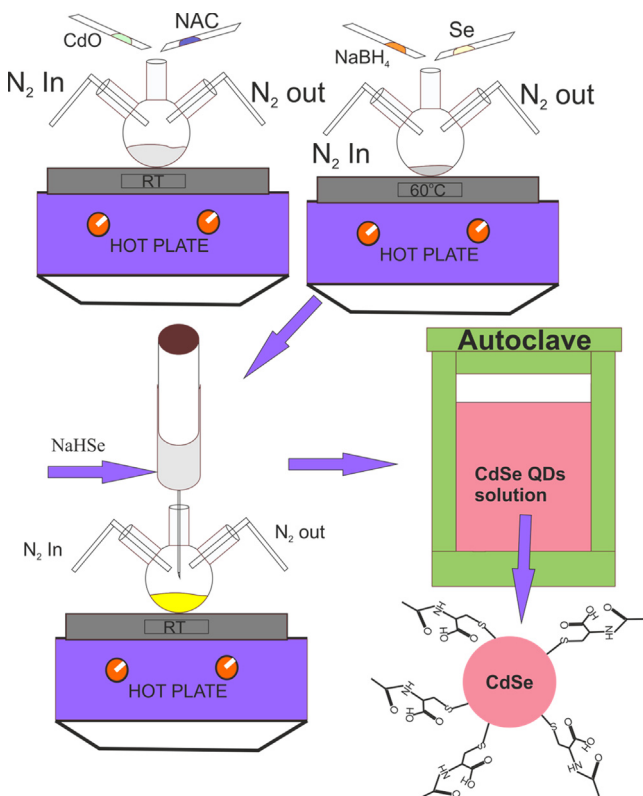


Fig. 11. Schematic diagram for synthesis of CdSe QDs using hydrothermal route, explaining the preparation of precursors followed by hydrothermal process and finally the schematic image of capped CdSe QD.

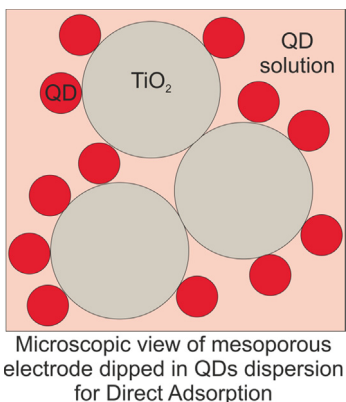


Fig. 12. Schematic diagram showing the direct adsorption of QDs over wide band gap host semiconductors.

one functional group that attach to QDs surface and other functional group attach to the host semiconductor surface (Rühle et al., 2010; Robel et al., 2006). The surface coverage depends on dipping time, temperature, QDs size, ligand type, concentration of QDs solution, and linker molecule (Peter et al., 2002; Yang and Chang, 2010; Watson, 2010). Linker molecules affect charge transfer mechanism between quantum dots and host wide band gap semiconductor. Thus, electron injection is also affected by the linker molecules. Hence, QDSSCs efficiency will depend on the choice of linker molecule having suitable electronic properties (Dibbell and Watson, 2009; Baker and Kamat, 2010; Tagliazucchi et al., 2011). That's why the choice of linker molecule is important for better photogenerated charge transfer. Fig. 13 shows schematically host semiconductor sensitized with linker assisted direct adsorption method. In this method, the optoelectronic properties of QDs are preserved, however, additional linker molecules affects

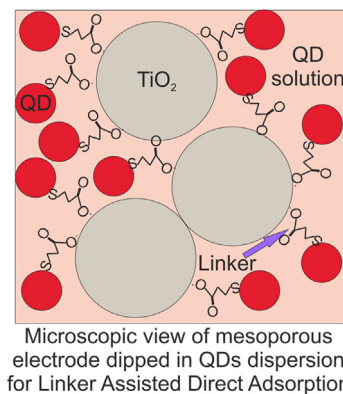


Fig. 13. Schematic diagram of wide band gap semiconductor sensitized with QDs using Linker assisted direct adsorption.

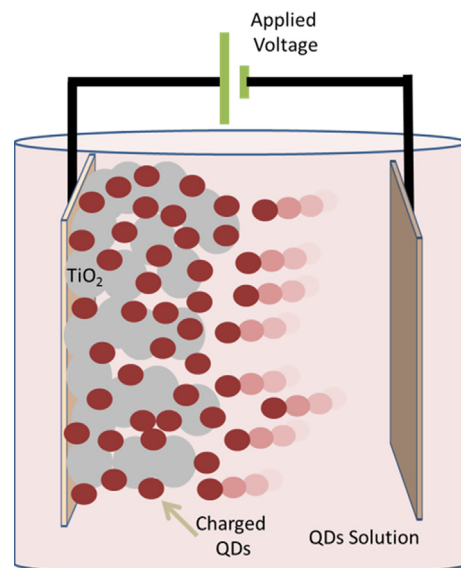


Fig. 14. Schematic diagram for QDs sensitization of mesoporous electrode using electrophoretic deposition.

charge the transfer between QDs and semiconductor.

(iii) **Electrophoretic deposition** – In this method QDs are deposited by applying strong electric field (as high as 1000 V/cm). Fig. 14 shows schematically electrophoretic deposition of QDs on mesoporous electrode. Normally, a mixed polar or non-polar solvent like toluene, acetonitrile etc. are used to disperse the prepared QDs. The mesoporous electrodes are dipped in QDs solution and a strong electric field is applied between mesoporous electrodes charge on QDs cannot be determined to be positive or negative so both mesoporous electrode are used and depending on charge on q one is sensitized]. Under the influence of electric field, charged QDs moves towards mesoporous electrode and gets deposited inside pores of mesoporous electrodes. The surface coverage depends on time duration for which electric field is applied, intensity of applied field, and concentration of dispersed QDs (Santra et al., 2013; Brown and Kamat, 2008; Salant et al., 2010). There are several constraints in electrophoretic deposition method such as (i) QDs should be dispersed in solutions, which can sustain very high fields, and (ii) QDs should be charged for its easy movement in the presence of electric field. The charge on QDs is determined by capping ligand and thus, a suitable capping ligand is another essential step for this process (Ning et al., 2014; Zhitomirsky et al., 2012; Milliron, 2014).

Initial deposition results in QDs penetration in pores of mesoporous electrode but later surface pores are blocked and QDs are stacked on surface only. The optoelectronic properties of deposited QDs are

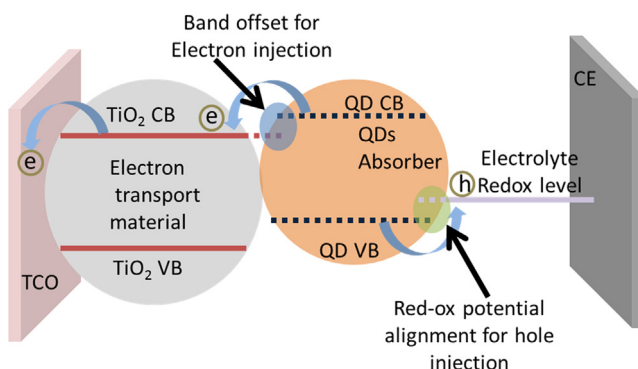


Fig. 15. Schematic diagram showing requirement of band offset for photo-excited electron transfer from QDs to the wide bandgap semiconductor and requirement of respective alignment of QDs VB level with redox level of electrolyte for hole extraction.

conserved in electrophoretic deposition but achieving the uniform distribution and high surface coverage are still issues with this process. Thus, all type of QDs cannot be deposited on mesoporous electrodes with this process because of such limitations.

(iv) Pipetting- Pipetting is very simple and new technique reported by Jin Wang et al. (Wang et al., 2013). This technique is very similar to direct adsorption. In this technique, QDs dispersion with suitable ligand is pipetted over mesoporous electrode and later pipetted electrodes are washed with solvent. This results in sufficient surface coverage of mesoporous electrode and fairly good efficiencies are recorded (Jiao et al., 2015). This technique also preserves optoelectronic properties of QDs.

2.2.2. Electron transport material (ETM)

Electron transport material plays the key role in functioning of QDSSCs. ETM accepts photogenerated electrons from QDs absorber and transport these photogenerated electrons to TCO contact. For efficient acceptance of electrons from QDs absorber, a suitable band offset between ETM and QDs absorber is required. Fig. 15 shows schematic representation of band offset requirement at ETM/QDs interface. The conduction level of ETM should be lower than that of QDs for efficient electron acceptance, as explained in Fig. 15 (Chakrapani et al., 2010). Further, the injection rate increases till band offset of 1 eV and becomes almost constant after that, which can be understood by Marcus theory of interfacial charge transfer (She et al., 2005).

Fig. 15 shows necessary energy levels alignment between ETM with QDs conduction level for electron acceptance and the redox level alignment for hole transport material with QDs valence level for efficient hole extraction. Further, ETM should be photostable and have high bandgap value. Photostability of electron transport material ensures the long term stability of QDSSCs under illumination and wide band gap ensures that most photons in solar spectrum are absorbed by QDs absorber and not by ETM. The photons' absorption in electron transport material is undesirable as it will promote recombination between electron transport material and redox hole conductor. The electrons' conductivity in electron transport material is another crucial parameter for efficient QDSSCs as the injected photocarriers are collected at contact through diffusion (González-Pedro et al., 2010). The injected photoelectrons should be collected at contact before they recombine to achieve the maximum photovoltaic response. Thus, the poor conductivity may result in loss of photogenerated electron through recombination and leading to the poor photovoltaic response. Several wide band gap semiconductor are explored in past with varying morphology and architecture to achieve efficient QDSSCs. Table 3 reviews some of electron transport materials explored in QDSSCs and their respective performance along with their morphology and QDs absorber. However, these values do not represent the highest photovoltaic performance reported for particular electron transport material.

Some of the popular electron transport materials utilized for QDSSCs are summarized here:

(a) Titanium oxide (TiO_2) - TiO_2 is one of the most widely used electron transport material for excitonic solar cells like DSSCs, QDSSCs etc. Favourable properties of TiO_2 like cheap, abundance, and non-toxicity makes it a suitable electron transport material. TiO_2 is a 'd' block binary metal oxide with dissimilarity in orbitals contribution to conduction and valence band. These dissimilarities in orbitals contributions reduce recombination probabilities and increasing the carrier lifetimes (Jose et al., 2009). TiO_2 exists in three phase namely anatase (3.23 eV band gap), rutile (3.05 eV band gap) and brookite (3.26 band gap). Fig. 16 shows crystal structures of all three crystallographic phases of TiO_2 . These structures are generated using respective crystallographic information files (CIFs), retrieved from Crystallographic Open Database (COD) (Murphy et al., 2006) and VESTA visualization software. (Murphy et al., 2006). Among these rutile phase is the most stable and widely used phase of TiO_2 for different applications. The rutile and anatase both are tetragonal and the respective lattice parameters are: $a = b = 0.458887 \text{ nm}$, $c = 0.295756 \text{ nm}$ for rutile, Fig. 16(b) (Dorolti et al., 2010) and $a = b = 0.3785 \text{ nm}$, $c = 0.95196 \text{ nm}$ for anatase, Fig. 16(a) (Rezaee et al., 2011). Brookite phase is orthorhombic with $a = 0.5463 \text{ nm}$, $b = 0.9191 \text{ nm}$ and $c = 0.5157 \text{ nm}$, Fig. 16(c) (Arroyo-De Dompablo et al., 2011). TiO_2 is normally n-type semiconductor due to the oxygen vacancies and Ti interstitial, although Ti vacancies can cause p-type conductivity as well (Nowotny et al., 2008). The Fermi level of anatase is ~0.1 eV higher than that of rutile phase, and that's why anatase phase is preferred as a photoelectrode material as it can provide higher photovoltage (Park et al., 2000). TiO_2 electrodes are explored in different nano-structures like nano-rods (Wang et al., 2012), nano-particles (Yang et al., 2013), beads (Zhou et al., 2014), nano tube (Lai et al., 2012) for preparation of photoelectrode to have efficient QDs adsorption and carrier injection for efficient QDSSCs. The different sized TiO_2 nano-particles are used in layered form; namely smaller particle (~25 nm) for transparent layer and larger particle (~200 nm) for layers with, large scattering centers rather than transparent, to have sufficient porosity for QDs adsorption and scattering property for efficient light adsorption in QDSSC (Wang et al., 2006).

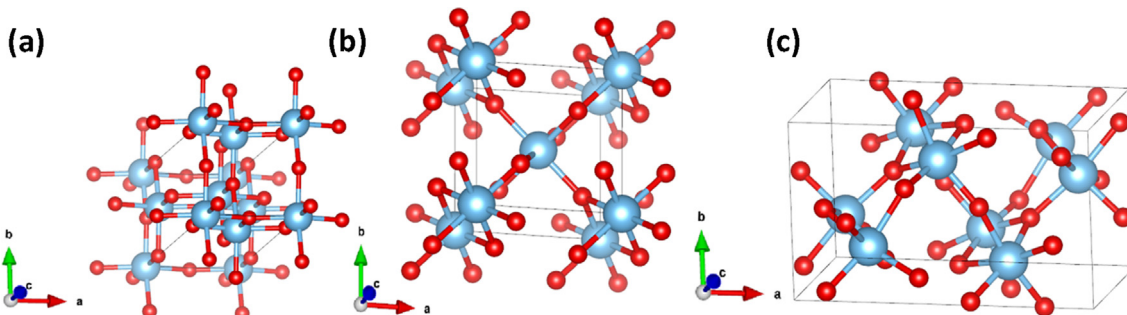
(b) Zinc oxide (ZnO) - Zinc oxide is another widely explored alternative to TiO_2 as photoanode material. Zinc oxide is a wide band gap semiconductor from II to VI group family. It has wurtzite crystal structure, with lattice parameter $a = 0.32494 \text{ nm}$ and $c = 0.51876 \text{ nm}$, Fig. 17(a) (Sowa and Ahsbahs, 2006). It also exists in cubic zinc blende structure with lattice parameter 0.46 nm, Fig. 17(b) (Bragg and Darbyshire, 1930). Zinc oxide is native n-type doped semiconductor due to the oxygen vacancies or Zn interstitials (Albrecht et al., 1999). Zinc oxide has better electron mobility as compared to TiO_2 due to its lower density of trap states and similar band structure (Solbrand et al., 2000). In 1994, Redmond first time reported sensitization of transparent ZnO nanostructured electrode with Dyes (Redmond et al., 1994). Initially, ZnO was reported to be unstable in acidic electrolyte but later with addition of KOH, with basic condition it showed stability (Bian et al., 2011). ZnO is prepared in different nano structures like nanoparticle (Tian et al., 2013), nano-rod (Tian et al., 2014), nano wire (Jean et al., 2013), and nano flower (Chen et al., 2009) for photoelectrode application. The change in electrodes' nano structure resulted in efficient adsorption of QDs absorber and good conductivity that translated into directly enhanced photovoltaic efficiency. In addition to electron transport material, ZnO is also employed in numerous electronic applications such as imaging and enhancing LED efficiencies. (Zang and Tang, 2015; Zang et al., 2016)

(c) Tin oxide (SnO_2) - SnO_2 is also utilized as a photoelectrode

Table 3

Summary of some of the electrode material utilized as electron transport material for QDSSCs.

ETM electrode material	Morphology of electron transport material	Quantum Dot used	Photo-voltaic performance			
			Current density (mA/cm ²)	Open circuit voltage (volt)	Fill factor	Efficiency (%)
TiO ₂	Nano particle mesoporous layer and scattering layer (Du et al., 2016)	Zn-Cu-In-Se	25.25	0.739	0.622	11.61
	Nanotube (Yu et al., 2017)	CdS	12.64	0.41	0.42	2.16
ZnO	Nano-rods (Zhang et al., 2017)	PbS	12.94	0.43	0.56	3.11
	Nano beads (Zhou et al., 2014)	CdS/CdSe	13.85	0.54	0.54	4.05
SnO ₂	Nano particle (Tian et al., 2013)	CdS/CdSe	15.42	0.62	0.49	4.68
	Nano flower (Tian et al., 2014)	CdS/CdSe	10.74	0.61	0.5	3.28
Zn ₂ SnO ₄	Nano-rod (Hou et al., 2016)	Mn-CdSe	12.6	0.74	0.44	4.64
	Nano wire (Jean et al., 2013)	PbS	17.9	0.6	0.40	4.3
Zinc titanate	Nano particle (Hossain et al., 2011)	CdS/CdSe	17.40	0.48	0.44	3.68
	Nano flower (Lan et al., 2015)	CdS	11.56	0.6	0.43	3
Stransium titanate	Nano-rods					
	Nano particle (Li et al., 2011)	CdS	0.5	0.5	0.36	0.1
Nanotube						
	Nano-rods (Bin Li et al., 2013)	CdS/CdSe	11.32	0.49	0.37	2.08
Zinc titanate	Nano particle (Yu et al., 2016)	CdS/CdSe	5.96	0.59	0.56	1.95
	Nano particle (Chen et al., 2015)	CdS	1.53	0.76	0.67	0.78

Fig. 16. Crystal structure of TiO₂ anatase in (a) rutile, (b) brookite, and (c) columbite crystallographic structures.

material for QDSSCs. This is similar to ZnO and TiO₂, binary oxides and offers two benefits as compared to TiO₂: (i) relatively higher mobility, which provides faster injection of photogenerated electrons together with reducing the probability of recombination (Gubbala et al., 2008), and (ii) more negative conduction level as compared to TiO₂, so lower band gap sensitizer like PbS QDs can inject electron to SnO₂, exhibiting higher photocurrents (Vogel et al., 1994). SnO₂ is also explored as electrodes in different morphology like nano particle (Hossain et al., 2011), and nano-flower (Lan et al., 2015) for QDSSCs application. However, with such favourable properties, QDSSCs efficiencies reported using SnO₂ are lower as compared to TiO₂ based QDSSCs. Further, it is reported that because of two orders of higher electron diffusion constant in SnO₂ with respect to other binary oxide

semiconductors, electron recombination dynamics in SnO₂ is much faster (Green et al., 2005). Such higher recombination dynamics will result in lower photocurrents and that's why SnO₂ based systems usually exhibit lower photovoltaic efficiencies with respect to other photonanode materials such as TiO₂ and ZnO (Green et al., 2005).

(d) Zinc stannate (Zn₂SnO₄) – Zinc stannate is a ternary oxide material, explored as a photoanode material for QDSSCs application (Dai et al., 2012). It is an inverse spinel structure with relatively larger band gap 3.6 eV (Alpuche-Aviles and Wu, 2009). It has good electron mobility (10^{-15} cm²/Vs), superior to that of TiO₂ (0.1–1 cm²/Vs) (Coutts and Young, 2000). The first use of Zn₂SnO₄ as photo anode material is reported in DSSC around 2007 (Tan et al., 2007). Zn₂SnO₄ can be prepared in different morphologies such as nano-particle (Li

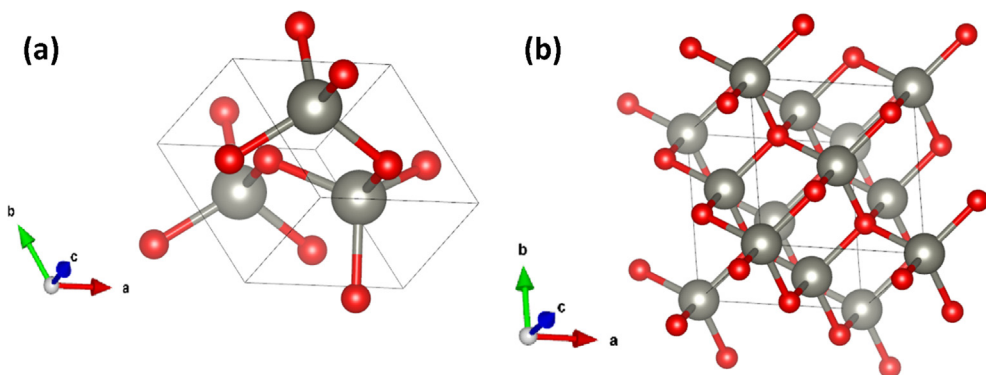


Fig. 17. Crystal structures of Zinc oxide in (a) wurtzite, and (b) zinc blende crystallographic geometries.

et al., 2011), nano-rod (Bin Li et al., 2013), octahedral (Li et al., 2012) for photoanode application. Long-Bin Li et al. used zinc stannate together with ZnO nanorods as photoanode material for CdS/CdSe based QDSSC and reported ~1.68% photovoltaic efficiency (Bin Li et al., 2013). QDSSCs photovoltaic efficiencies reported with zinc stannate are promising but still lag behind the conventional TiO₂ photoanode material.

(e) Zinc titanate – Zinc titanate is a ternary oxide material, showing three crystallographic phases. The six fold octahedral coordination in zinc titanate is very similar to Ti arrangement in anatase TiO₂. Three crystallographic phases of zinc titanate are (i) zinc metatitanate in rombohedral ilmenite crystal structure, (ii) zinc orthotitanate in cubic spinel structure, and (iii) Zn₂Ti₃O₈ in cubic defect spinel structure (Liu et al., 2009). There are few reports on zinc titanate as photoanode material in QDSSCs and rombohedral zinc titanate is reported to exhibit relatively large carrier mobility as compared to TiO₂ (Yu et al., 2016; Habibi et al., 2012). In some reports, zinc titanate is reported to perform better than TiO₂ as photoanode material (Yu et al., 2016).

(f) Strontium titanate (SrTiO₃) – Strontium titanate is a ternary oxide material similar to zinc titanate. It also has six fold octahedral coordination for Ti, similar to that in anatase TiO₂. Its band gap is nearly same as that of titanium oxide but it has higher flat band potential as compared to TiO₂, which results in a higher open circuit voltage. The higher open circuit voltage is observed for strontium titanate based QDSSCs (Chakrapani et al., 2010; Wang et al., 2006). Further, the higher carrier mobility in strontium titanate is also reported in several studies (Burnside et al., 1999; Moos et al., 1995).

Few other wide band gaps semiconductors like Nb₂O₅, Ta₂O₅ are also explored as electron transport material in QDSSCs but their photovoltaic performance was poorer to TiO₂ (Vogel et al., 1994). Thus, TiO₂ is one of the most efficient photoanode material and is widely used. Further, nanopowder of TiO₂ is commercially available to fabricate the photoanode sensitized solar cells such as DSSCs and QDSSCs. However, considering the scope for manipulation of conduction energy levels of QDs absorber by using the size variation or suitable doping, other wide band gap semiconductors may also serve as good photoanode materials in QDSSCs apart from TiO₂ for better photovoltaic efficiencies.

2.2.3. Hole transport material

Hole transport material or hole conductor is also an important part of QDSSCs. After absorbing solar flux, excitons are generated in QDs and electrons are injected to electron transport material and thus, QDs get oxidized. The role of hole transport material is to accept hole from oxidized QDs. If hole extraction rate from QDs is slow or hole conductor is having the poor hole mobility, then it will increase the recombination in QDSSCs, lowering the photovoltaic response. Hole transport materials can be utilized in liquid form like redox electrolyte, quasi-solid electrolyte, and solid hole conductor like spiro-MeOTAD. Several hole transport materials are explored for QDSSCs and few of them are described here under liquid, quasi-solid and solid hole conductor subsection further.

(a) Liquid Hole conductor- Liquid hole conductor has been traditionally used in DSSCs in form of redox electrolyte and further, followed in QDSSCs. The major redox electrolytes explored for QDSSCs are discussed below:

(i) Iodide electrolyte – Iodide electrolyte (I⁻/I³⁻) is the most efficient and widely used liquid electrolyte for DSSCs. After realizing the initial higher efficiencies in DSSCs with iodide electrolyte, it is also tried in QDSSCs. However, cadmium chalcogenide QDs are unstable in iodide electrolyte because of their photo-corrosion in the presence of iodine (Hod and Zaban, 2014). Cadmium chalcogenide QDs are the most studied QDs for QDSSCs applications. Even though iodide electrolyte exhibits slow recombination

kinetics in DSSCs, together with larger carrier lifetime and higher photovoltage due to more negative redox potential, it cannot be used in case of QDSSCs efficiently because of the poor stability of cadmium chalcogenide QDs (Ogermann et al., 2012; Samadpour et al., 2011). However, QDSSCs are not limited to cadmium chalcogenide QDs, so if compatible potential QDs materials, which are stable in iodide electrolyte, this electrolyte can be used in QDSSCs to realize higher efficiencies.

- (ii) Polysulfide electrolyte**- Polysulfide electrolyte (S²⁻/S_x) is the most widely explored electrolyte in QDSSCs. Cadmium chalcogenide QDs are reasonably stable in this electrolyte (Chakrapani et al., 2011). It is made of sodium sulfide (Na₂S) and additional sulphur together with few additives like KCl and NaOH (Lee and Chang, 2008; Jovanovski et al., 2011). Initially, the low fill factor was recorded with polysulfide electrolyte together with Pt as the counter electrode (Mora-Seró et al., 2009). Here Pt was an obvious choice for counter as used in DSSCs with iodide electrolyte. Later, high electron transfer resistance was observed at Pt counter electrode and attributed to the observed poor fill factor for QDSSCs with polysulfide electrolyte and Pt counter electrodes (Mora-Seró et al., 2008). Later with the use of more catalytic counter electrode like Cu₂S, fill factor and efficiency are improved considerably for polysulfide electrolyte. A suitable solvent was also explored for this electrolyte and a mixture of water and organic solvent like methanol was found more appropriate for high efficiency of QDSSCs (Lee and Chang, 2008). Polysulfide electrolyte showed more positive redox potential as compared to iodide electrolyte, which resulted in lower photovoltage in QDSSCs (Chakrapani et al., 2011). The recombination kinetics of polysulfide electrolyte is relatively faster than iodide electrolyte, still, it is considered as an efficient electrolyte for QDSSCs at the moment. It works well in QDSSCs but it is not as efficient as iodide in DSSCs as pointed out in several earlier reviews (Hodes, 2008; Rühle et al., 2010; Emin et al., 2011; Hod and Zaban, 2014).
- (iii) Ferrocene electrolyte** – Few studies on QDSSCs also employed ferrocene (Fe(CN)₆³⁻/Fe(CN)₆⁴⁻) electrolyte and observed that the recombination kinetics was more prominent at TCO/electrolyte interface with ferrocene electrolyte (Tachibana et al., 2008). A blocking layer at TCO/electrolyte interface was introduced to slow down the recombination kinetics at this interface, which assisted in enhanced photovoltaic performance with this electrolyte.
- (iv) Cobalt based electrolyte**- Cobalt based electrolyte is also explored for QDSSCs application in few studies. Although this electrolyte works well with Pt counter electrode, but suffers from slow ionic conductivity (Lee et al., 2009). This low ionic conductivity results in poor performance under higher illumination while works well under low illumination (0.1 Sun) (Lee et al., 2008; Rühle et al., 2010).

(b) Solid hole transport material – The solid hole transport materials are also explored for QDSSCs to overcome the leakage problem with liquid redox electrolytes. The penetration of hole conductor in sensitized mesoporous electrode is a challenge with solid hole transport material. Few reports demonstrated the use of Spiro-MeOTAD as solid hole conductor in QDSSCs (Lee et al., 2009; Lee et al., 2009). In DSSC, a higher photovoltage is observed with Spiro-MeOTAD (Chen et al., 2009). The efficiencies about 4% are recorded using Spiro-MeOTAD hole conductor in case of QDSSCs (Chang et al., 2016).

(c) Gel electrolyte (quasi-solid) – In this approach, some gelating agent is used to convert liquid polysulfide electrolyte into gel form. This gel based electrolyte is like quasi-solid QDSSCs and is characterized by a specific temperature ‘T_{gel}’ over which gel electrolyte is converted into liquid electrolyte. This parameter is used to reflect the gelation strength and intrinsic stability of the quasi solid electrolyte (Mohmeyer et al., 2004; Mohmeyer et al., 2006). These gel type electrolytes result in improved stability of QDSSCs, however with slightly lower performance

Table 4

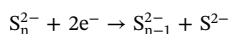
Performance of some QDSSCs with different hole conductor utilized and their respective photo-voltaic performance.

Hole Conductor	Cell configuration	Photo-voltaic performance			
		Current density (mA/cm ²)	Open circuit voltage (volt)	Fill factor	Efficiency (%)
Iodine/Iodide electrolyte (Ogermann et al., 2012)	TiO ₂ /CdS _x Se _{1-x} /S ²⁻ -S _n ²⁻ /Pt/FTO	1.38	0.565	0.34	0.32
Cobalt electrolyte (Lee et al., 2009)	TiO ₂ /CdSe ₅ Te ₁ /cobalt electrolyte /Pt/FTO	4.94	0.67	0.54	4.18
Polysulfide electrolyte (Du et al., 2016)	TiO ₂ /Zn-Cu-In-Se/ZnS/S ²⁻ -S _n ²⁻ /MC/Ti	25.18	0.742	62.4	11.66
Ferrocene electrolyte (Tachibana et al., 2008)	TiO ₂ /CdS/ZnS/Ferrocene/Pt/FTO	2.45	0.68	0.60	1.0
Spiro-MeOTAD (Lee et al., 2009)	TiO ₂ /CdSe ₅ Te ₁ /spiro-MeOTAD /Pt/FTO	2.15	0.70	0.55	0.84
Poly 3-hexylthiophene (Qian et al., 2011)	TiO ₂ /CdS/P3HT /Au/Polymer	4.31	0.67	0.55	1.42
Dextran-polysulfide gel (Chen et al., 2013)	TiO ₂ /CdS/CdSe/ZnS/dextran-S ²⁻ -S _n ²⁻ /Pyrolized-Pt	15.86	0.466	0.44	3.23

with respect to the pristine liquid polysulfide electrolyte (Hu et al., 2015). Few reports demonstrated the use of gel electrolyte in QDSSCs using gelating agents such as dextran (Chen et al., 2013), poly (poly-propylene glycol) (Karageorgopoulos et al., 2012), konjac glucomannan (Wang et al., 2013), poly acrylamide-bis-acrylamide (Yu et al., 2010), and 12-hydroxysteric acid (Hu et al., 2015). Table 4 summarizes some of the hole conductor explored in QDSSCs together with respective photovoltaic performance parameters, although the values may not reflect the highest efficiencies for QDSSCs with respective electrolyte.

2.2.4. Counter electrode

The role of counter electrode is to provide catalytic activity for efficient reduction of liquid electrolyte (hole conductor) at electrode. If counter electrode is not catalytic enough, it will hamper electron transfer, giving rise to the resistance at electrolyte/counter electrode interface. A general polysulfide reaction is expressed as



This resistance at electrolyte/counter electrode interface results in low fill factor and poor efficiency (Mora-Seró et al., 2009). It can be measured using impedance spectroscopy (Mora-Seró et al., 2008). Pt counter electrode was highly catalytic for regeneration of iodide electrolyte in DSSCs and that's why adopted in QDSSCs during initial studies (Kong et al., 2007). Later, it was observed that Pt counter electrode was not showing efficient catalytic characteristics for polysulfide electrolyte and relatively large charge transfer resistance was noticed at counter electrode/electrolyte interface, leading to poor photovoltaic efficiencies (Mora-Seró et al., 2009). Various materials are explored as counter electrode to achieve the enhanced photovoltaic efficiencies. Hodes et al. investigated metal sulfides as counter electrode materials for polysulfide electrolyte and observed that Cu₂S, and CoS are relatively better alternative catalysts for polysulfide electrolyte (Hodes and Manassen, 1980). Shen et al. prepared Cu₂S using brass sheet and used as the efficient low cost counter electrode for polysulfide electrolyte (Shen et al., 2010). Tachan et al. reported that PbS is a highly catalytic and efficient counter electrode for polysulfide electrolyte in QDSSCs application (Tachan et al., 2011). A nanostructured counter electrode is preferred over flat counter electrodes as it provides high surface area for the reduction of electrolyte, leading to enhanced charge regeneration. There are other nanostructured materials such as Cu₂S/Carbon composite (Radisch et al., 2011), graphene (Dao et al., 2015), carbon (Fan et al., 2010), PEDOT (Yeh et al., 2011) and even Au (Lee and Lo, 2009), which are explored for counter electrodes. However, the choice of counter electrode is not limited to these materials and there are continuous efforts to find a more suitable counter electrode. The choice of a counter electrode material depends on the redox electrolyte used, and thus, if more efficient electrolyte as compared to polysulfide is investigated, a suitable counter electrode should also be changed to achieve the optimal photovoltaic performance. Table 5 summarises some of the common counter electrode materials explored in QDSSCs

and their respective photovoltaic performance together with cell configurations. However, the efficiencies reported are not representing the maximum efficiency for respective counter electrode materials and cell configurations.

2.3. Development of microscopic working mechanism of QDSSCs

There are continuous efforts towards establishing working mechanism of QDSSC (i.e. excitonic solar cell) since 1990 when photovoltaic effect was measured in an organic film during its conductivity measurement (Gregg et al., 1990). In such measurements, an organic layer was positioned between two symmetrical electrodes (ITO) and photovoltaic effect was observed. Here, the illumination side became negative and other side as positive electrodes and contacts were reversed when illumination side was changed. Interestingly, illumination from both sides resulted in no photovoltaic effect. A kinetic model was proposed to explain this behaviour. Fig. 18 summarizes the proposed kinetic model (Gregg et al., 1990). In this model, excitons are produced in the organic film under illumination, and photo-excitons dissociated at the electrode interface. The electron injection rate to ITO was higher as compared to the hole injection rate. This difference in injection rates resulted in photoinduced voltage, showing photovoltaic response.

A more simplified and efficient example of excitonic solar cell came into picture with Gratzel's dye sensitized solar cell in 1991 (Oregan and Gratzel, 1991). In this solar cells, interface for exciton dissociation was distributed due to nanostructured nature of electrode. The maximum efficiency of about 7% was recorded with nanostructured TiO₂ electrode, sensitized with trimeric ruthenium complex (molecule area of 1 nm²). The open circuit voltage is demonstrated to be the difference between quasi Fermi level of TiO₂ and redox level, as shown schematically in Fig. 19 (Oregan and Gratzel, 1991).

The working mechanism of DSSCs is explained using two models (a) junction model, and (b) interface model (Gregg, 2003). The junction model has been discussed comprehensively by Klaus Schwarzburg and Frank Willig (Schwarzburg and Willig, 1999). They showed that in dark, electric field will exist to over few multiple of 10 nm from the contact of TiO₂ and FTO. They hypothesized that injected electron will diffuse in TiO₂ nano-porous interconnected network together with its charge screening due to electrolyte. This movement of injected electron along with image charge is represented schematically in Fig. 20 (Schwarzburg and Willig, 1999).

The diffused electrons are collected at FTO due to the built-in field similar to the p-n junction solar cells. The observed relatively slow transportation/diffusion time scale for photo-injected charge carriers was associated with trapping and de-trapping events (Willig et al., 1997; Schwarzburg and Willig, 1991). Further, a photopotential is developed in cell due to the spatial separation of screened injected electrons and their screening charge (hole). An upper limit of photopotential to equilibrium potential is established in such devices under dark conditions. Schwarzburg et al also proposed a p-n junction type

Table 5

Performance of some QDSSCs prepared with different counter electrode material and their respective photo-voltaic efficiencies.

Counter electrode	Cell configuration	Photo-voltaic performance			
		Current density (mA/cm ²)	Open circuit voltage (volt)	Fill factor	Efficiency (%)
Cu ₂ S/Brass (Ren et al., 2015)	TiO ₂ /CdSeTe/TiCl ₄ /ZnS/S ²⁻ -S _n ²⁻ /Cu _{2-x} S/Brass	20.69	0.700	62.2	9.01
Pt (Lee et al., 2009)	TiO ₂ /CdSe ₅ Te ₁ /cobalt electrolyte /Pt/FTO	4.94	0.67	0.54	4.18
Au (Lee and Lo, 2009)	TiO ₂ /CdS(3)/CdSe(4)/ZnS/S ²⁻ -S _n ²⁻ /Au	16.8	0.5137	0.49	4.22
PbS (Tachan et al., 2011)	TiO ₂ /CdS/CdSe/ZnS/S ²⁻ -S _n ²⁻ /PbS/Pb	9.28	0.554	0.588	3.01
Graphene (Dao et al., 2015)	ZnO-NW/CdS/CdSe/S ²⁻ -S _n ²⁻ /Au NP-Pt NP -Graphene nano platelets -grade C	15.2	0.720	0.409	4.5
Carbon (Fan et al., 2010)	TiO ₂ /CdSe/ZnS/S ²⁻ -S _n ²⁻ /activated-Carbon/FTO	11.47	0.60	0.47	3.34
Poly (3,4 ethylenedioxythiophene) (Yeh et al., 2011)	TiO ₂ /CdS/ZnS/S ²⁻ -S _n ²⁻ /PEDOT/FTO	5.66	0.435	0.47	1.16

band bending at FTO electrode and electrolyte interface and attributed this band bending for the charge collection at FTO (Lee et al., 2008). This complete process is represented schematically in Fig. 21. This band bending is also responsible for an upper limit to the open circuit potential (i.e. difference between work function of FTO substrate and electrochemical potential of electrolyte).

Another model that explains the working mechanism of DSSCs is the interface model or kinetic model, and is described in detail by B. A. Gregg (Pichot and Gregg, 2000). This model was established over the years by different researchers (Kalyanasundaram, 1998; Soedergren et al., 1994; Hagfeldt et al., 1994; Cao et al., 1996; Ferrere et al., 1997; Boschloo et al., 1997; Ferber, 1998; Enright and Fitzmaurice, 1996; Kamat et al., 1996; Zaban et al., 1998; Franco et al., 1999). Gregg pointed out that photoinduced generation of carrier and their separation is identical in excitonic cells while in conventional cells, generation and separation is spatially and temporally different [3]. The identical generation and separation of carries in excitonic solar cell imply that excitons are generated and instantly transferred to the electron transport material via rapid electron injection. Here, TiO₂ conduction and valence bands remain flat under dark or illumination conditions, implying that no electric field exists due to presence of highly conducting electrolyte and charge transfer is taking place because of carrier diffusion. Further, rapid field neutralization by mobile ions and interfacial chemical potential gradient are responsible for charge separation in DSSC as opposed to built-in field in conventional solar cells. The electrochemical energy, sum of chemical potential energy (diffusion component) and electrical potential energy (drift component), is responsible for charge flux in DSSCs. This model sets difference between photo-induced difference between quasi-fermi level of conduction

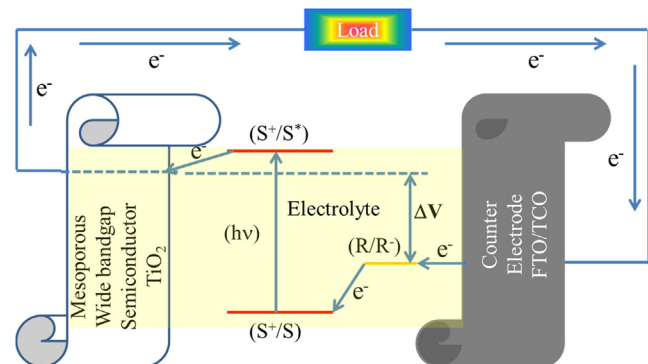


Fig. 19. Schematic representation of origin of open circuit potential in DSSC as suggested by Gratzel.

electrons in TiO₂ and electrochemical potential of electrolyte sets as upper limit to the open circuit potential rather than equilibrium electric field at TiO₂/Electrolyte, Fig. 22.

In 1999, Gratzel et al. proposed that maximum open circuit potential that can be achieved in DSSCs is the difference between conduction level of TiO₂ and redox level of electrolyte as the Fermi-level of TiO₂ will not go beyond TiO₂ conduction level under normal working conditions (Cahen et al., 2000). Fig. 23 shows energy level conditions in a DSSCs under dark and illumination conditions. Here, the maximum photovoltage that can be achieved, will be equal to difference between conduction level of TiO₂ and redox level of electrolyte.

QDSSCs also got attention during the same time as DSSCs, where for

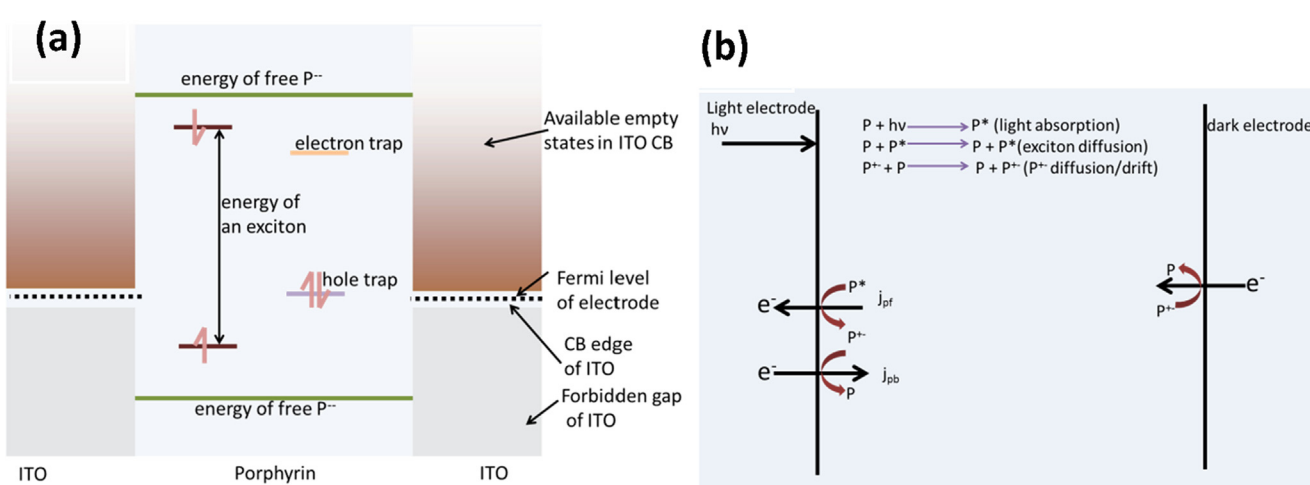


Fig. 18. (a) Energy level alignment if Porphyrin sandwiched between TCO under illumination and (b) Kinetic model proposed for generation of photo-voltage in Porphyrin film sandwiched between TCO. Reprinted (adapted) with permission from (Shockley and Queisser, 1961).

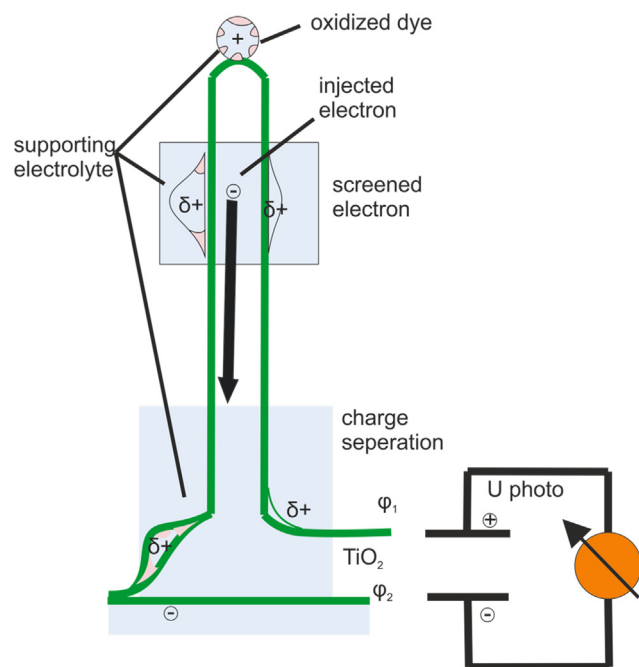


Fig. 20. Schematic representation of diffusion of injected electron along with screened charge. Reprinted (adapted) with permission from (Schwarzburg and Willig, 1999).

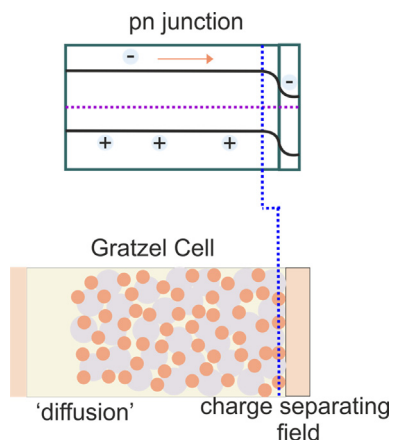


Fig. 21. Schematic diagram of Junction Model proposed by Schwarzburg and Frank Willing (Schwarzburg and Willig, 1999).

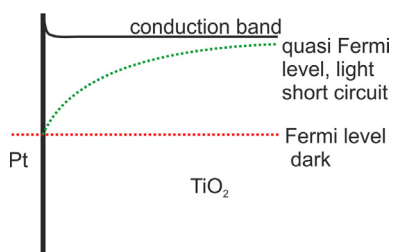


Fig. 22. Diagram showing the quasi fermi level under dark and illumination (Pichot and Gregg, 2000).

the first time in 1990, Vogel et al showed sensitization of wide band gap TiO₂ with CdS quantum dots and evaluated the photo-electrochemical response (Vogel et al., 1990). Later in 1993, Liu et al explored photochemical behaviour of TiO₂/CdSe film in an electrochemical cell, and the kinetic mechanism was proposed for understanding the response (Liu and Kamat, 1993). The proposed kinetic mechanism is

schematically presented in Fig. 24. Here, also the photovoltage is accounted because of the different transfer rate for electrons and holes at interface.

In 1994, Vogel et al studied various QDs sensitizers together with metal oxide substrates and concluded that photovoltage should not be considered as the difference between conduction level of metal oxide and redox potential of electrolyte rather. This is attributed to the contribution of defect states i.e. trap states in QDs and metal oxides will also affect the photovoltage (Vogel et al., 1994).

Zaban et al. used pre-synthesized QDs to prepare QDSSCs and suggested that the energy offset difference between conduction level of QDs and TiO₂ conduction level is main driving force for electron injection in TiO₂ electrode. Fig. 25 shows schematically the energy level offset between InP QDs sensitizer and TiO₂ conduction level. The photoelectrochemical performance was carried out to probe electron injection in TiO₂ from QDs (Zaban et al., 1998). Recently, Klimov explored the thermodynamic detailed balance efficiency for QDSSCs assuming ideal electron transport material and hole conductor. Here the detailed balance efficiency is also computed in presence of carrier multiplication under the kinetic model to explain the working mechanism of QDSSCs and estimating the photovoltaic response (Klimov, 2006).

Further, Hodes et al. reviewed the differences between DSSCs and QDSSCs to understand the associated challenges in QDSSCs (Hodes, 2008). In this review, QDSSCs are proposed to be advantageous over DSSCs because of higher absorption by QDs as compared to the monolayer of Dyes. Further, inorganic semiconductor based QDs offer better stability with respect to that of organometallic or organic dyes. Fig. 26 shows differences in carrier dynamics processes in DSSCs and QDSSCs together with their respective rates (Hodes, 2008). The position of conduction level of semiconductor should be higher to the conduction level of electron accepting semiconducting species. Further, the rate of electron injection increases according to Marcus theory till difference is equal to organization energy (injection rate increases linearly till difference in energy of 0.4 eV) (Robel et al., 2007). Here, the rate of electron flow will be determined by difference in relative energy levels rather than band bending at the interface (negligible due to electrolyte screening), similar to proposed kinetic model for DSSCs.

Thus, Hodes concluded that if charge transfer is faster with respect to recombination rate in solar cell, then further increase in charge transfer will not improve performance, which is based on the observation of Haque et al [2016] that the relative rate of charge transfer and recombination is important, Fig. 27. The relatively higher electron injection rate of ~100 ps for 3 nm CdSe and 100 ns for 7.5 nm CdSe should be sufficient and any further increase in injection rate will not affect performance (Robel et al., 2006; Robel et al., 2007). Additionally, the recombination in QDs can be band to band or trap mediated while trap mediated recombination is not present in Dye molecules utilized in DSSCs. Also the passivation on QDs will affect the carrier recombination in QDs and for some QDs, it can be fairly high, competing with electron injection rates. The hole transfer from semiconductor to electrolyte may also be taking place through the trap states together with electron transfer from QDs to electrolyte may lead to the major loss pathways in QDSSCs, Fig. 27. That's why the thicker layer of QDs absorber will exhibit poor electron injection probability, something similar to DSSCs where more than monolayer of dye results in quenching the injection of photoexcited electrons to TiO₂. Thus, we can see that rapid injection is possible by QDs absorber to the wide band gap host semiconductor however more recombination pathways are present in QDSSCs with respect to DSSCs.

In 2009, Bisquert group reported the signature of deep mono-energetic surface states of TiO₂ in photovoltaic response under illumination showing "S" shaped current voltage curve (IVC) under illumination and an intrinsic recombination pathway to CBD deposited QDs. The kinetic model of DSSCs is applicable to QDSSCs with some additional recombination pathways present in QDSSCs because of the semi-conducting nature QDs (Mora-Seró et al., 2009). Later, Bisquert group

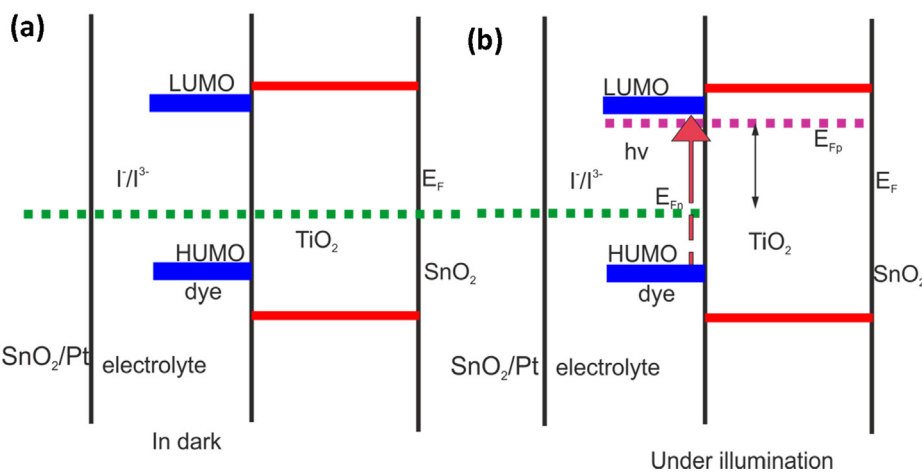


Fig. 23. (a) Alignment of energy level in DSSCs under dark and (b) alignment of energy level alignment under illumination (Pichot and Gregg, 2000).

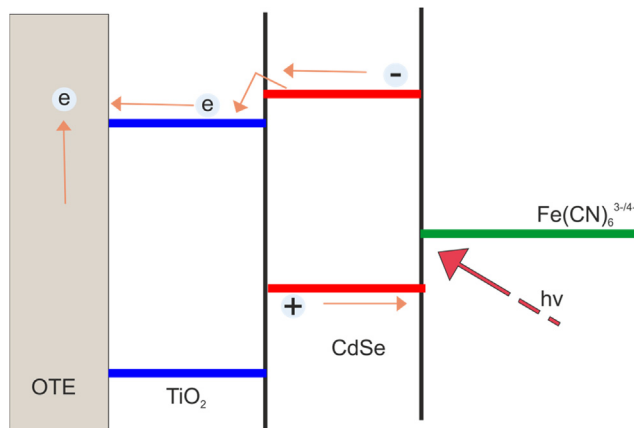


Fig. 24. Kinetic model proposed by Kamat et al. to explain photo-voltaic action (Liu and Kamat, 1993).

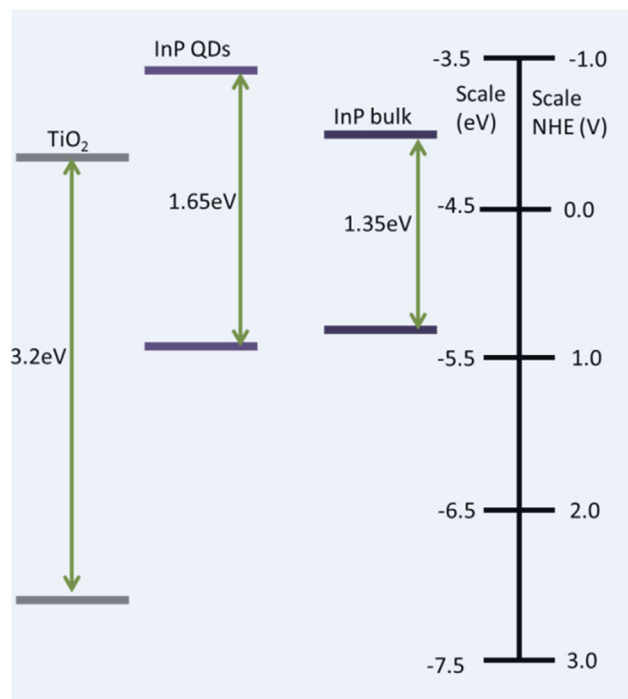


Fig. 25. Energy level positions of sensitized and TiO₂ to explain electron injection form InP QDs to TiO₂ mesoporous electrode (Vogel et al., 1994).

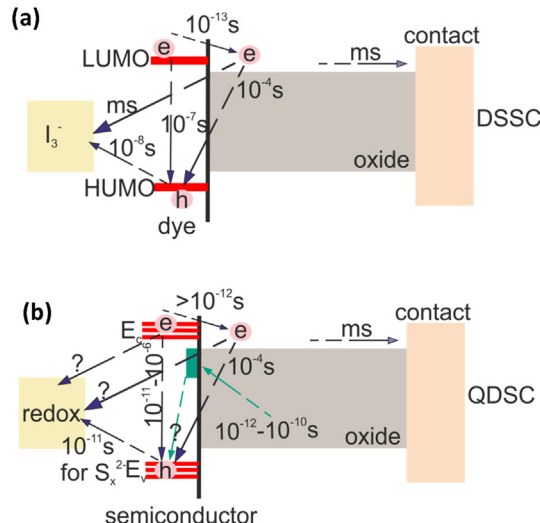


Fig. 26. (a) Process in DSSCs and their time scale and (b) Processes in QDSSCs and their time scale presented by Hodes et al. Reprinted (adapted) with permission from (Hodes, 2008).

reported modelling procedure for high efficiency QDSSCs making clear the working mechanism in QDSSCs (González-Pedro et al., 2010). The kinetic model of DSSCs was extended for QDSSCs to fit the impedance spectroscopy data by IS model such as diffusion and recombination model similar to DSSCs. Bisquert group demonstrated that QDs surface states play an active role in recombination under illumination, a recombination pathway that is not present in DSSCs.

In 2010, Zaban et al reviewed QDSSCs work and emphasized that that QDSSC working mechanism is similar to that of DSSCs apart from few differences (Rühle et al., 2010). First difference is the pH of aqueous electrolyte, which can affect the band edge position of oxide semiconductor and thus, photoinduced band changes can take place. This is not possible in DSSCs because of the organic electrolyte containing Iodide. Further, the presence of QDs may also affect recombination in QDSSCs.

Thus, we noticed that the commonly used DSSCs' kinetic model is also widely applied in QDSSCs explaining the charge generation and separation and the onset of photovoltage. However, QDSSCs suffer from the active participation of QDs surface states in recombination under illumination. QDSSCs also suffer from additional limitations in terms of additional recombination pathways as compared to that of DSSCs due to presence of surface trap states of QDs absorber and multiexciton generation, and suggested to be the key driver in next generation

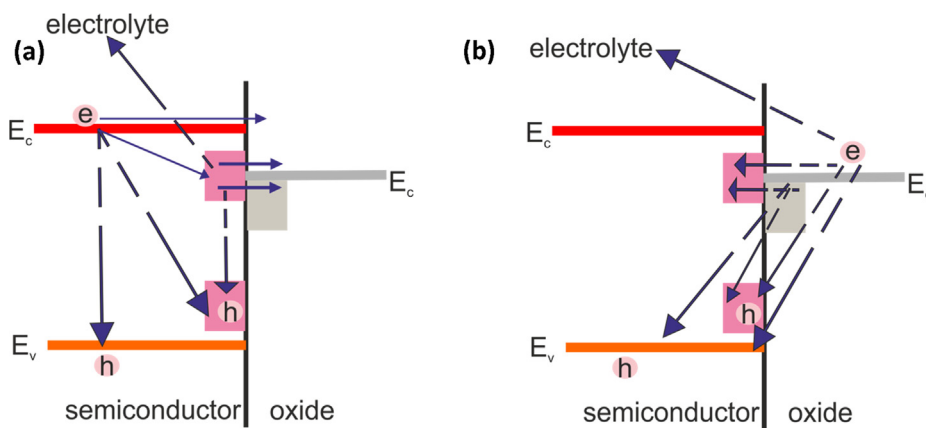


Fig. 27. (a) Various charge transfer pathway from sensitizer QDs to wide band gap host semiconductor and (b) charge transfer pathways from wide band gap host semiconductor to sensitizer QDs. Reprinted (adapted) with permission from (Hodes, 2008).

QDSSCs to achieve higher performance. However, there are various limitations in practices to realize the carrier multiplication in QDSSCs as the QDs band gap cannot be lowered to that of the difference between TiO_2 conduction level and redox level for electrolyte, which is the main outcome of DSSCs kinetic model.

2.4. Interfaces in QDSSCs

Nanostructured design of QDSSCs results in several interfaces between different layers in the device. These interfaces play a critical role in ensuring efficient operation of QDSSCs. The suitable alignment of the band offsets at these interfaces is very critical and passivation, thus, becomes important to realize efficient QDSSCs. These interfaces are described in following sub sections, together with associated critical issues for QDSSCs.

(i) Transparent conducting oxide (TCO)/Electron transport material (ETM) interface- Transparent conducting oxide (TCO)/Electron transport material(ETM) interface is the interface where photogenerated electrons are transferred to TCO by ETM. The recombination takes place at this interface by the back transfer of electrons from TCO to electrolyte because of simultaneous presence of a tri-interface i.e. TCO/ETM/Electrolyte interface. This recombination is termed as back electron transfer (BET) (Cameron and Peter, 2005; Meng and Li, 2011). At lower voltage, BET at TiO_2 /Electrolyte interface is dominant while at higher voltage BET at TCO/electrolyte is dominant (Guijarro et al., 2011). In QDSSCs, a mesoporous ETM is normally utilized, which provides the high surface area for the deposition of QDs. The partial surface of TCO is not covered by mesoporous ETM, deposited on TCO. This uncovered part of TCO will be exposed to the hole conductor or redox electrolyte. At this interface, electrons in TCO or ETM recombine to redox electrolyte. A thin dense blocking layer is deposited on TCO to eliminate possibility of electrons' recombination with electrolyte at TCO/ETM interface and thus, the direct contact of electrolyte with TCO can be avoided (Ruhle et al., 2012). Fig. 28 shows the alignment of energy levels and electron recombination pathways at TCO/ETM interface with and without blocking layer. Fig. 28(a) represents energy level alignment and recombination pathways in absence of blocking layer. Here, electrons from TCO can recombine to electrolyte (Meng and Li, 2011). Fig. 28(b) shows energy level alignment and recombination pathways in presence of blocking layer and here, electron transfer from TCO to electrolyte is absent as represented schematically. This blocking layer is normally a dense electron transport material thin film of 10–100 nm thickness (Ruhle et al., 2012). A good thin dense blocking layer avoids the recombination of electron from TCO to electrolyte, however, it may give rise to resistance for electron acceptance from nano structured ETM to TCO. So, an optimum thickness of blocking layer is very important (Ruhle et al., 2012).

(ii) Electron transport material (ETM)/QD interface- Electron transport material (ETM)/(QD) quantum dots interface is very critical interface for QDSSCs operation. This interface is responsible for exciton dissociation and in process photo-generated electrons from QDs are transferred to ETM while hole remains in QDs. The critical aspect of this interface is band offset between conduction level of ETM and conduction level of QDs absorber. Fig. 29 shows the possible band offset conditions at this interface. As discussed earlier in Section 2.3, for efficient photoelectron injection the conduction level of ETM should lie below QDs by 0.4 eV (Robel et al., 2007). Fig. 29(b) represent a suitable band offset at TCO/QD interface. The optimum band offset ensures after rapid exciton dissociation over the time scale of femto second ($\sim 10^{-15}$ s), photogenerated carriers are transferred to ETM with unity quantum efficiency (Robel et al., 2007). If the band offset at this interface is more than optimum level, that is conduction level of ETM is situated at much lower to that of QDs absorber, Fig. 29(a), then the rapid injections will not be beneficial, as discussed in Section 2.3. However, the higher position of QDs conduction level will result in higher band gap requirement of QDs and photon absorption is compromised, resulting in lower photovoltaic performance. Fig. 29(c) represents the situation where QDs conduction level is below the ETM, suggesting the very poor exciton dissociation because of respective negative band offset. The quantum efficiency of photogenerated electron transfer to ETM will be very low in this situation. For example, conduction level in bulk PbS is situated below the conduction level of TiO_2 and if the size of PbS QDs is large where energy levels are close to that of bulk energy levels, there will be no electron transfer from PbS QDs to TiO_2 , and thus, exhibiting very poor QDSSCs operation (Hyun et al., 2008).

The electron injection rate at this interface also depends on the mode of QDs attachment to the wide band gap host semiconductor. The direct attachment of QDs to host semiconductor and QDs attachment to host semiconductor through linker molecules are two strategies widely followed. The direct attachment usually provides higher electron injection rate as compared to linker assisted attachment (Pernik et al., 2011).

(iii) Red-ox/ (CE) counter electrode interface- Red-ox electrolyte/ (CE) counter electrode interface is important from electrolyte regeneration perspective. Iodide electrolyte was used in DSSCs and a highly catalytic Pt was used as counter electrode together with this electrolyte (Kong et al., 2007). In QDSSCs, polysulfide electrolyte is normally used and Pt is not a suitable counter electrode because of its relatively poor catalytic response to the polysulfide electrolyte (Mora-Seró et al., 2008). If charge carriers experience a higher interfacial resistance at this interface, then fill factor of QDSSCs is reduced, showing lower photovoltaic response (Mora-Seró et al., 2009). To ensure minimal interfacial charge transfer resistance, a highly catalytic counter

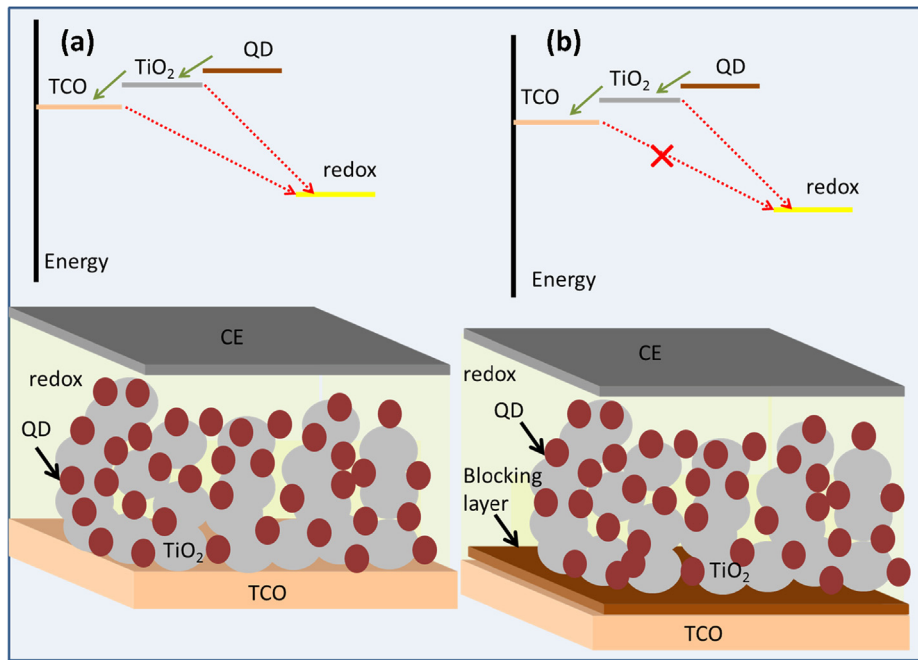


Fig. 28. (a) Schematic diagram of QDSSCs without blocking layer on TCO at bottom along recombination pathways represented in top and (b) Schematic diagram of QDSSCs with blocking layer on TCO at bottom along with recombination pathways in top. Eliminated recombination pathway is represented by cross marked arrow.

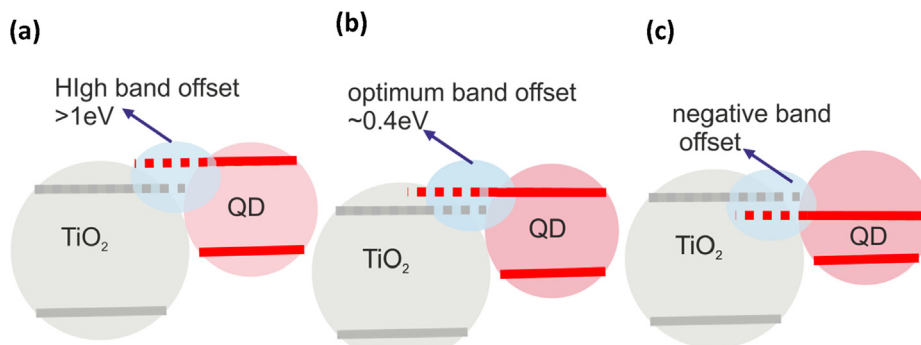


Fig. 29. Possible band offset conditions at ETM/QD interface (a) high band offset condition, (b) optimum band offset and (c) negative band offset.

electrodes made of Co, Cu, and Pb based sulphides are used (Tachan et al., 2011; Yang et al., 2010; Yang et al., 2011; Radisch et al., 2011). The low interfacial resistance has been demonstrated with these counter electrodes. While these counter electrodes remove limitation of costly Pt counter electrode with polysulfide electrolyte and showing better fill factor. However, there are also certain limitations such as durability and strength for these metal sulphide based counter electrodes. The interfacial resistance at counter electrode/electrolyte interface can be estimated from impedance spectroscopy measurements (Mora-Seró et al., 2008).

(iv) Electron transport material (ETM)/QD/Electrolyte interface- ETM/QD/Electrolyte interface, referred as triple interface, is the most critical interface in QDSSCs. This interface governs the exciton dissociation and recombination rates in QDSSCs. Fig. 30 shows the schematic representation of this triple interface. A suitable energy level alignment is required at this interface for efficient photo-carrier collection in QDSSCs. This interface directs dissociation of exciton in electron and hole, followed by the injection of such photogenerated electrons to electron transport material and acceptance of hole by hole transport material. This interface is present throughout the mesoporous ETM electrode in QDSSCs for redox liquid electrolyte. However, in case of solid hole conductor, its presence is limited due to limited penetration of solid hole conductor inside mesoporous electrode. Fig. 30 shows

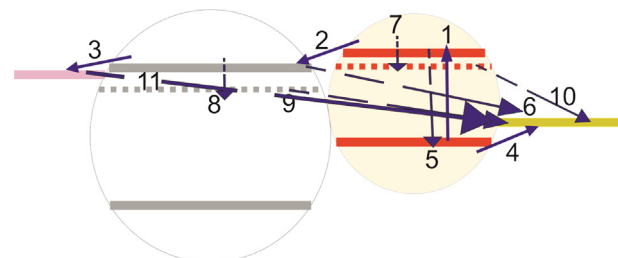


Fig. 30. Schematic representation of Energy level alignment at ETM/QD/Electrolyte interface along with photo-generation, collection and recombination pathways. Photo-generation and collection pathways are represented by solid arrows and recombination pathways are represented by dotted arrows. Energy level position of different material is represented by thick solid lines and traps states associated with ETM and QDs are shown by dotted thinner lines.

essential carrier generation and collection pathways along with recombination pathways at this triple interface. The nano structured nature materials in QDSSCs also gives rise to the trap states, affecting energy level alignment at this interface. These trap states also participate actively in recombination process. Fig. 30 also shows such possible traps states and respective recombination pathways

(Mora-Seró et al., 2009). The effective passivation of these trap states and protective covering to reduce some recombination pathways is very crucial for efficient operation of QDSSCs.

2.5. Control of charge dynamics at QDSSCs interfaces

Interfaces are very critical in QDSSCs for controlling recombination and manipulating photo-carriers' transport. A careful modification of these interfaces can result in control of certain recombination pathways, leading to the improved photo-voltaic efficiency. Various surface treatments are utilized to modify these interfaces to realize the reduce recombination in QDSSCs. Some of those common surface treatments at these interfaces are summarized in following sub sections.

(i) TCO/Electrolyte interface treatment – To control the undesired recombinations at this interface, a thin dense blocking layer is deposited on TCO before the deposition of mesoporous ETM. The blocking layer at this interface ensures that TCO is not directly exposed to hole conductor (redox electrolyte) and thus, assisting in reducing the back recombination (Ruhle et al., 2012). Fig. 26 shows schematically the elimination of recombination pathways by blocking layer deposition. TiCl₄ treatment of FTO is widely used for blocking layer deposition in case of TiO₂ electron transport material. In this method, TCO is dipped in 30% HCl solution of TiCl₄ for 30 min to 1 h at 70 °C and washed with the solvent. After that TiCl₄ treated TCO is annealed at 450 °C for 30 min to 1 h before the deposition of mesoporous TiO₂ using doctor blade or screen printing or other suitable techniques. This process results in a thin dense TiO₂ layer on TCO. The time duration and solution concentration can be optimized to control thickness of blocking layer (Salaramoli et al., 2013). Spray pyrolysis can be also used for blocking layer deposition (Liu et al., 2013). Other thin film deposition techniques like sputtering and e-beam evaporation can also be explored for depositing a very thin and uniform blocking layer films.

(ii) Electron transport material (TiO₂)/QD/Electrolyte interface surface treatment- The proper band alignment is required at TiO₂/QD/Electrolyte interface for the efficient collection of photogenerated carriers as shown in Fig. 31, where, the essential charge dynamics for functioning of QDSSCs is represented by solid arrows. The processes 1, 2, 3 and 4 are essential in QDSSCs. Here, process 1 represents photo-excitation of exciton after absorption of incident solar radiation, process 2 shows electron injection from QDs absorber to ETM (electron transport material) TiO₂, diffusion of electrons in electron transport material and collection at TCO is represented as process 3, and the acceptance of hole from QDs absorber by electrolyte as process 4.

Further, the recombination pathways are represented by dotted arrows. There are certain intrinsic recombination pathways, which cannot be completely eliminated. The processes 5, 6 show intrinsic recombination pathways. Process 5 is showing intrinsic recombination in QDs absorber by radiative recombination and process 6 corresponds

to the recombination from electron transport material to red-ox electrolyte due to presence of this interface throughout mesoporous electrode. Processes 7, 8, 9, 10, and 11 are representing recombination pathways, which are appearing because of defect states in nanostructured electron transport material and QDs absorber. So, these processes i.e. 7, 8, 9, 10, and 11 could be controlled by passivating the defect states at triple interface. Process 7 and 10 shows recombination due to defect states of QDs and 8 and 9 processes represent the recombination due to defect states of TiO₂. Process 11 corresponds to the recombination due to back electron transfer. This shows that TiO₂/QD/Electrolyte interface is very important to control recombination. The surface treatments are required to passivate defect states to control recombination at the triple interface. Surface treatments are also utilized to reduce the back electron transfer. The defect states of TiO₂ nano structures are usually passivated by a thin TiO₂ covering over mesoporous electrode. This covering can be obtained by TiCl₄ treatment (Pan et al., 2013). A thin shell covering is also deposited over QDs to reduce defect states. The defect states of QDs are also passivated by surface treatment with a suitable wide band gap semiconductor like ZnS and Al₂O₃ (Liu et al., 2013; Guijarro et al., 2011; Ren et al., 2015). ZnS and Al₂O₃ also act as barrier layer that prohibits QDs from injecting electrons to electrolyte (back recombination). ZnS and Al₂O₃ covering is normally carried out using SILAR process. The conduction level of such wide band semiconductor is normally above the conduction level of QDs and act as barrier for charge transfer between QDs and electrolyte. The barrier function for these passivation layers is shown schematically in Fig. 32. Sometimes QDs are not stable in electrolyte and thus, a protective covering on QDs can help to address the stability issues as well. The thickness of these passivation layers is also critical as too thick passivation layers will hamper charge transfer into nanostructured ETM electrode. The aluminium oxide covering of ZnS QDs i.e. ZnS/Al₂O₃ may stop the recombination process labelled as 12, Fig. 32.

(iii) Transition metal treatment – The doping with transition metal of QDs can change the carrier dynamics in QDs, as demonstrated by Kamat et al. (Santra and Kamat, 2012). Such doping of foreign atoms will create mid gap states, as shown schematically in Fig. 6 and discussed in Section 2.2.1. However, few reports show that the incorporation of transition elements during surface passivation process like ZnS treatment may also results in improved QDSSCs photovoltaic performance (Gopi et al., 2015). Such improvement in performance is usually attributed to the onset of mid gap states close to ETM conduction level, which assists in charge transport.

3. Multiple exciton generation in quantum dot sensitized solar cells

Generation of more than one electron and hole pairs at the cost of one photon absorption is called “multiple exciton generation (MEG)”. MEG was predicted and experimentally demonstrated for Quantum Dots using spectroscopic techniques. Here, hot carriers are produced after absorbing the high energy photons and these hot carriers can produce more than one electron and hole pairs at the cost of one photon

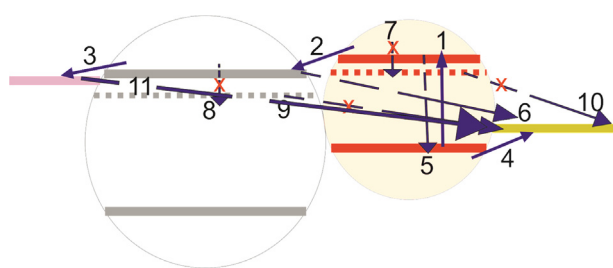


Fig. 31. Schematic representation of energy level alignment at ETM(TiO₂)/QD/Electrolyte interface and control of recombination pathways. Photo-generation and collection is represented by solid arrows and recombination pathways are represented by dotted arrows. Energy level position of different material is represented by thick solid lines and traps states associated with ETM and QDs are shown by dotted thinner lines. Eliminated recombination pathways are shown by cross marked dotted arrow.

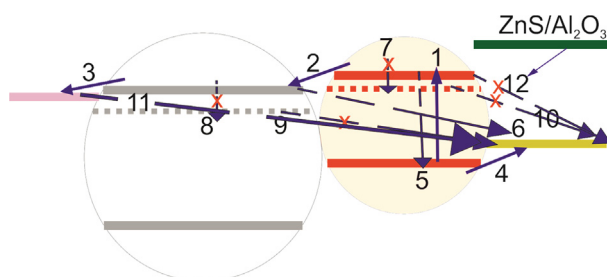


Fig. 32. Impact of passivation layer on QDs to reduce the back recombination process 12, as marked by cross for Al₂O₃ passivated ZnS QDs.

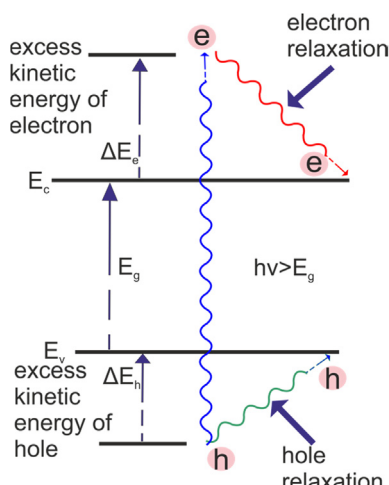


Fig. 33. Schematic diagram showing the generation of hot carrier and its relaxation mediated by phonon scattering Reprinted (adopted) with permission from (Yang et al., 2011).

absorption and thus, may exhibit more than 100% internal quantum efficiency. The impact of hot carriers in QDs is described below.

3.1. Hot carrier in QDs

The absorption of photons above band gap energy in a semiconductor results in electron and hole pairs generation (hot carriers) with excess thermal energy $\Delta E = h\nu - E_g$, which are not in equilibrium (Schaller and Klimov, 2004). Fig. 33 shows schematically the generation of hot carriers and their relaxation (Steigerwald and Brus, 1989; Yang et al., 2011). The excess energy is distributed between electron and hole according to their effective masses (Nozik, 2001). The higher energy fraction will be available to the lower effective mass carriers. These hot carriers with excess thermal energy will return back to the equilibrium via thermalization by means of carrier scattering, phonon emission, radiative, and non-radiative recombination. When a semiconductor is confined spatially like in case of Quantum Dots, the carrier dynamics is different from their bulk counterparts. The change in dynamics of photoexcited carriers is very important for QDSCCs application and is investigated widely to predict their suitability for different applications. If photon energy is greater than band gap then the excess energy is associated with electron and hole as kinetic energy depending upon their effective masses. Under continuous illumination, as the case for a solar cell, a steady state condition with excited carriers is reached, where kinetics of different pathways are under equilibrium. The carriers i.e. electrons and holes interact separately among themselves to form two Boltzmann distributions of carrier population, respectively. Each Boltzmann distribution can be assigned to a temperature, which is greater than the lattice temperature, and thus, the term hot carrier is used. This initial relaxation occurs very fast over time scale of 100 fs, known as thermalization process (i.e. the formation of thermal distribution described by Boltzmann statistics) (Pelouch et al., 1992; Pelouch et al., 1992). After that, carriers are in equilibrium with lattice by carrier-phonon interaction. Here, phonons involved in this process are longitudinal optical (LO) phonons. This process is termed as carrier cooling by carrier-phonon interaction. Final stage of equilibrium is achieved by carrier recombination or carrier separation. If hot carriers are utilized before interaction with phonons, then thermodynamic limit for radiation energy conversion can be extended to 66% from 32% (Ross and Nozik, 1982; Boudreux et al., 1980).

Hot carriers can be utilized in two ways: in one case these can be collected before relaxation, and in second case, these can be utilized for another electron and hole pair generation via impact ionization. This second process is known as multiple exciton generation (MEG) or

impact ionization in bulk materials (Landsberg et al., 1993; Kolodinski et al., 1993). The rate of impact ionization should be greater than rate of carrier cooling (relaxation of carrier with phonon interaction) for realizing MEG. In Quantum dots, the competition between impact ionization and carrier cooling is important for MEG. It is observed that the quantum confinement in QDs can reduce the carrier cooling rate, making impact ionization more probable with respect to the carrier cooling, leading to enhanced MEG.

3.2. MEG in quantum structures

For quantum structures such as quantum wells and superlattices, the relatively slower hot carrier cooling takes place through hot phonons bottleneck, however the photogenerated carrier density required is of the order of $10^{18} / \text{cm}^3$. Such carrier density is not possible from solar radiation, however it can be produced by shining intense laser beams (Rosenwaks et al., 1993). For example, an optical concentration of 10^4 will be required to achieve such high carrier density, which is a non-practical constraint. However in case of quantum dots, slow carrier cooling is possible at lower light intensity by means of phonon bottleneck, assisting in thermalization process. This can be easily be achieved from the normal Sun solar radiation for QDs (Guyot-Sionnest et al., 1999; Klimov et al., 2000).

In 1980, Boudreux predicted the slower carrier cooling in quantum confined structures for the first time. Here, it was suggested that carrier will require multi-phonon for cooling when energy levels are separated more than the phonon energy in quantized systems (Boudreux et al., 1980). Later, Benisty proposed the mechanism, suggesting that the cooling of hot electrons in QDs can take place by means of longitudinal acoustic (LA) phonons only (Benisty et al., 1991; Benisty, 1995). Additionally, there are other mechanisms proposing to bypass the phonon bottleneck like Auger recombination (Efros et al., 1995), electron-hole scattering (Klimov et al., 2000), deep-level trapping (Sercel, 1995) and

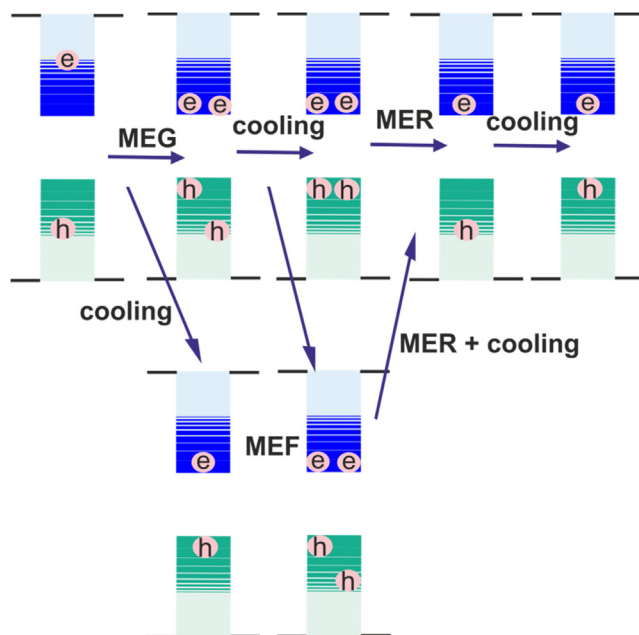


Fig. 34. Schematic diagram representing the hot carrier dynamics. Here, an initially excited electron hole pair of high energy can generate another electron and hole pair i.e. MEG. MEG competes with charge-phonon non-radiative recombination, converting exciton energy to heat. The generated multiple electron and hole pairs diphase into independent single electron and hole pair by coupling to phonons i.e. MEF. The lower energy multiple exciton states undergo MER. Ultimately, all processes leads to a long lived electron and hole pair at band gap energy Reprinted (adopted) with permission from (Sambur et al., 2010).

acoustic-phonon interaction (Inoshita and Sakaki, 1992; Inoshita and Sakaki, 1997).

Fig. 34 shows the schematic diagram representing all possible dynamics for hot carriers including MEG, MEF and MER, as marked by the respective arrows (Qu and Peng, 2002; Park et al., 2000). Several researchers have explored the experimental investigations for slower hot carrier cooling in QDs and found contradicting results. Some of the results are in support of phonon bottleneck (Murdin et al., 1999; Heitz et al., 1997; Adler et al., 1998), whereas some contradict or oppose it (Lowisch et al., 1999; Klimov and McBranch, 1998). Further, Nozik reviewed these experimental investigations in 2001 (Nozik, 2001) and noticed that cancelling or negating the phonon bottleneck also observed the slower carrier cooling but still the process of cooling was not very long enough (tens of pico seconds), as evident from the respective photoluminescence studies (Heitz et al., 1998; Li and Arakawa, 1998; Sosnowski et al., 1998). Here, it was interesting to note that the carrier transfer from bulk semiconductor to redox was sub-pico second level, and thus, it was possible to utilize hot carrier before carriers' cooling (Meier et al., 1999; Meier et al., 1997).

3.3. MEG in colloidal QDs

QDSSCs make use of colloidal QDs, thus, it becomes important to review the multi-exciton studies for colloidal QDs. There are two kinds of experiments, proposed and utilized to measure the efficiency of multi-exciton generation. In one case, THz spectroscopy is used while in other the measurement of transient current to probe generation of multi-excitons is investigated.

Spectroscopic studies involve the investigation of dynamics of multi-excitons, where multi-excitons are distinguished from single exciton based upon time scale of respective dynamics. In such cases, two types of dynamics are observed: (i) the fast dynamics is attributed to Auger recombination, which bypasses the phonon bottleneck and thus, indicating bi-exciton or multi-exciton generation, and (ii) the slower dynamics is attributed to the single exciton along with hole trapping kinetics of the capping agents. These spectroscopic studies normally involve the generation of exciton using a fast laser pulse, as shown in Fig. 35 with blue color pulse, and probing their dynamics using a probe pulse, purple color in Fig. 35, using Tera Hertz (THz) spectroscopy. The dynamics of carrier is measured by varying energy of laser pulses to generate excitons in colloidal QDs. Such spectroscopic studies also report the generation of multi-excitons on absorption of two photons where each photon does not carry enough thermodynamic energy to generate multi-exciton individually (Schaller and Klimov, 2004).

In 2004 Schaller et al demonstrated very fast and efficient multi-

exciton generation in PbSe QDs for the first time (Schaller and Klimov, 2004). A very efficient bi-exciton generation is observed in these experiments together with a very fast Auger recombination at picosecond (ps) scale while a slow exciton recombination time scale, somewhere close to micro second time scale (Wehrenberg et al., 2002). For pump energy greater than $3E_g$, bi-exciton dynamics is observed. These bi-exciton components could be separated into single exciton component and fitted with the exponential decay (Klimov, 2000). Here, even one carrier with excess energy equal to E_g was sufficient to drive energy conservation mechanism for multi-exciton generation. Further, Schaller et al also concluded that multi-exciton generation is not instantaneous due to the build-up time for carrier population, and its competition with intra-band relaxation similar to that in bulk material.

In 2005, Ellingson et al. observed multiple exciton in PbS and PbSe QDs and claimed that the threshold for multiple exciton generation is $2E_g$ not $3E_g$ as claimed by Schaller et al (Ellingson et al., 2005). Here, it was observed that the exciton lifetime is around 6000 ps and bi-exciton lifetime is around 100 ps. Further, Ellingson et al pointed out that a photon with energy greater than $2E_g$ will create a superposition of various single and multi-exciton states, which are coupled with multi-electron Coulomb interaction (Shabaev et al., 2006). Thus, with photon energy between $2E_g$ and $3E_g$, the direct Coulombic interaction couples a symmetric electron and hole pair to an asymmetric pair where total kinetic energy is residing on one electron carrier and is sufficient to create multi carriers. The difference between non-coherent theoretical model of impact ionization and quantum mechanical theoretical model of coherent impact ionization is pointed out by Ellingson et al (Wehrenberg et al., 2002). Further, MEG is not limited to PbS and PbSe QDs but also observed in other colloidal QDs like PbTe (Murphy et al., 2006), CdSe (Schaller et al., 2005), InAs (Pijpers et al., 2007; Schaller et al., 2007), and even in Si QDs (Beard et al., 2007).

Another approach for observing the multi-exciton generation includes probing of transient current dynamics (Gao et al., 2015). Here, MEG efficiency is determined in electronically coupled quantum dot films. In 2015, Gao et al. reported the detection of carrier multiplication using ultrafast transient photo-current technique (TPC) (Gao et al., 2015). Here, early time electron dynamics is investigated in device grade QDs coupled films. QDs are incorporated in fast electro-optical switches and monitored the photo-generated multicarrier dynamics with 40 ps resolution to resolve Auger decay for multicarrier states. The process is represented schematically, showing a photo-conductive setup and switch in Fig. 36. Here, PbSe QDs are coupled in thin films with electro-optical switches with a 20 GHz sampling oscilloscope to record the decay response after shining with a femtosecond laser pulse.

There are also reports of non-Poissonian formation of multi-exciton

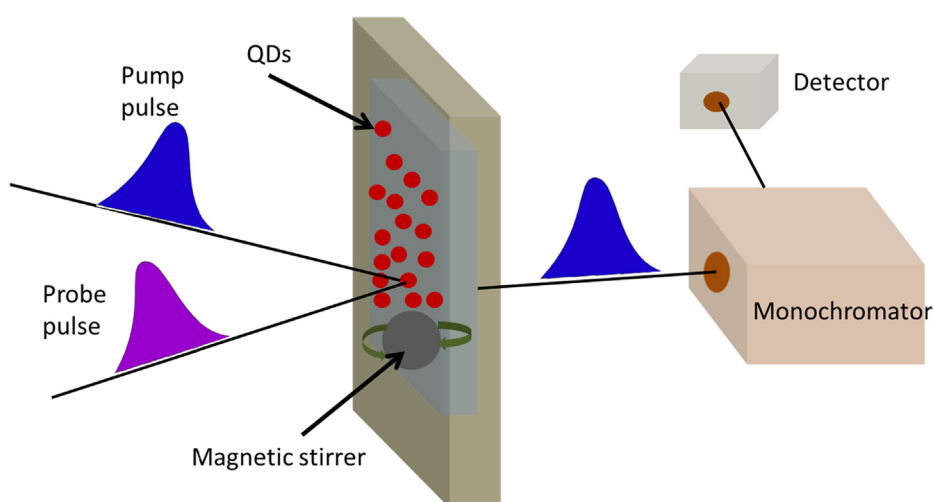


Fig. 35. Schematic diagram for Setup of spectroscopic determination of multi-exciton dynamics (Li and Arakawa, 1998).

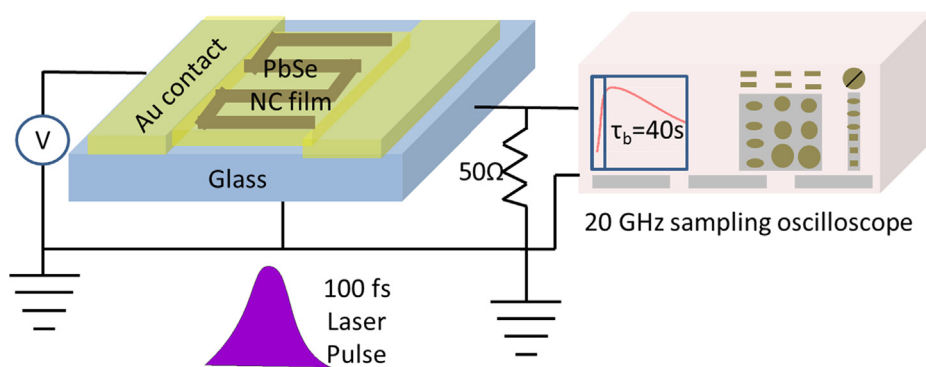


Fig. 36. Schematic diagram for detection of multi-exciton using ultrafast transient photo-current (TPC) (Gao et al., 2015).

at the cost of two non-resonant photons' absorption. In 2013, Gandman et al. reported non-Poissonian formation of multiple excitons by absorption of femtosecond non-resonant two photons absorption process in semiconductor QDs using direct multi-exciton spectroscopy for the first time (Gandman et al., 2013). This is considered as non-quadratic dependence of the pulse intensity on the average number of excitons per QDs. Further, Gandman et al also explained the observation by multi-exciton formation model, which is based on the phenomenon of intrapulse state filling of the few quantum electronic states retrieved by two photon transitions.

3.4. Multi-Exciton Generation- a theoretical view

In general, two models are considered for multiple-exciton generation findings in the literature. One is based on non-coherent impact ionization,

Fig. 37, and other is based on quantum mechanical treatment of coherent impact ionization, Fig. 38. The threshold for impact ionization is observed to be $3E_g$ for non-coherent impact ionization and $2E_g$ for coherent impact ionization model (Beard et al., 2007)

Fig. 37 shows schematically the non-coherent model of multi-exciton generation (Beard et al., 2007). According to non-coherent model or classical impact ionization, the hot carriers are generated after absorption of photons with energy higher than the band gap of QDs. The excess energy is distributed among carriers according to their effective masses (Nozik, 2001). One of the carrier should have energy greater than band gap to generate the additional electron and hole pairs (Landsberg et al., 1993; Kolodinski et al., 1993). In case of similar electron and hole effective masses, threshold for MEG is about $3E_g$ while if one of the carrier has lower effective mass, MEG threshold can be closed to $2E_g$ (Schaller, 2005), Fig. 39. In this scenario, the impact ionization starts competing with intra-band relaxation.

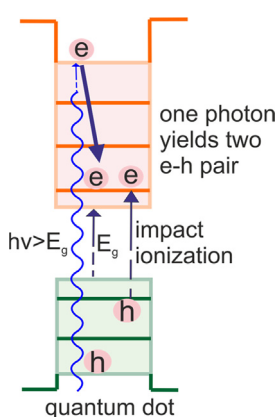


Fig. 37. Schematic representation of non-coherent model of multi-exciton generation, Reprinted (adapted) with permission from (Beard et al., 2007).

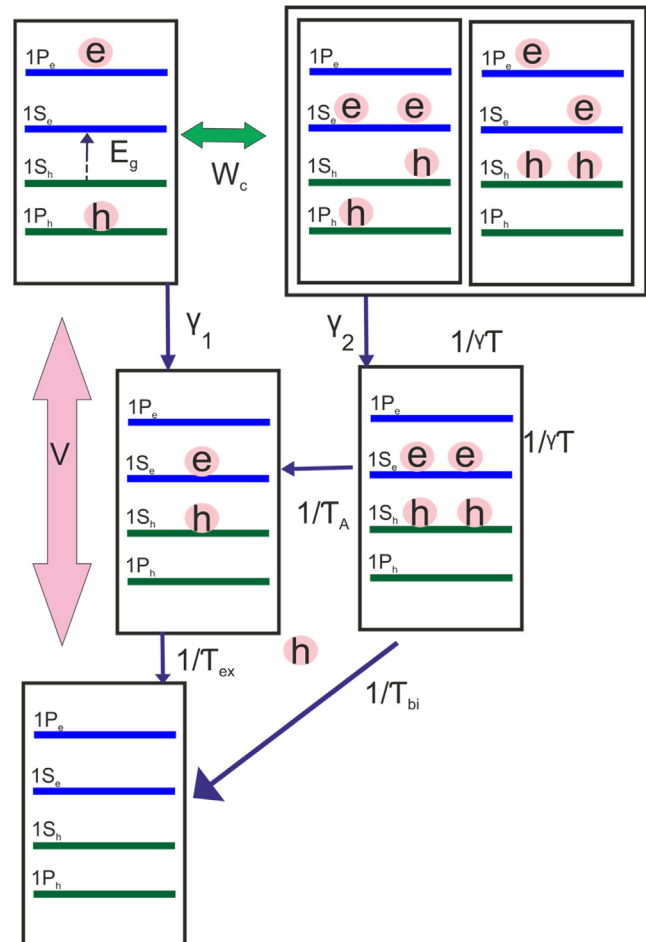


Fig. 38. Schematic representation of coherent impact ionization model proposed by Shabaev et al Reprinted (adapted) with permission from (Wehrenberg et al., 2002).

The second model describes MEG using the coherent superposition of multi-exciton and single exciton states. This model uses the time-dependent density matrix approach, which allows the simultaneous consideration of an arbitrary strength coupling between single and multi-exciton states, different dephasing rates for these states and short pulse excitation of NCs. The steady state solution of density matrix provides restrictive conditions for efficient MEG. Energy relaxation rate for the single exciton initiated by light γ_1 must be slower than both energy relaxation rate for multi-exciton γ_2 and the rate for Coulomb coupling between the two states W_c/\hbar where W_c is matrix element of Coulombic interaction between single and multi-exciton states

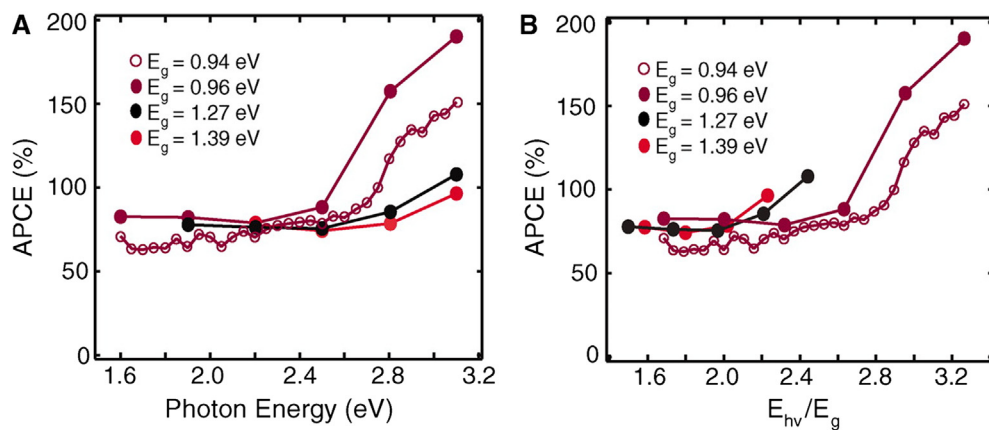


Fig. 39. APCE values as a function of illumination energy (a) APCE values vs absolute incident photon energy and (b) APCE values versus incident photon energy divided by band gap. Reprinted (adopted) with permission from (Schaller, 2005).

(Shabaev et al., 2006).

In 2008, Nozik reviewed enhanced multi-exciton generation in QDs with respect to bulk semiconductor (Nozik, 2008). He pointed out that $2E_g$ constraint is the threshold for MEG in terms of energy conservation based on earlier reports. He also emphasized that electronic coupling in QDs film, should not reduce MEG efficiency, as one might expect it (to reduce) with reduction in quantum confinement during QDs film preparation (Murphy et al., 2006).

3.5. Multi-Exciton generation (MEG) at device level

Sambur et al. reported the effect on MEG at device level in PbS/TiO₂ sensitized electrode (Sambur et al., 2010). Here, atomically flat anatase TiO₂ electrode was prepared, and sensitized with MPA capped PbS QDs. The photocurrent spectroscopy is used to resolve the sensitized photocurrents as a function of incident photon energy. The recorded adsorbed photon to current efficiency (APCE) is greater than 100% and attributed this to the multi-exciton collection (MEC) as opposed to term multi exciton generation, Fig. 39.

Further, Semonin et al. observed more than 100% peak external photocurrent efficiency (PEPC), substantiating MEG in device for the first time (Semonin et al., 2011). As shown in Fig. 40, about 130% internal quantum efficiency (IQE) is recorded with PbSe QDs based QDSSCs. Here a 40–50 nm thick ZnO porous electrode is used to deposit PbSe QDs which are treated with 1,2-ethanedithiol (EDT)-hydrazine using layer by layer deposition process. QDs films thickness of 50–250 nm is deposited together with top Au contacts using thermal evaporation. The fabricated QDSSCs could show external photocurrent efficiency (EQE) more than 100% at higher energy close to 3.4 eV, Fig. 40. Further, for higher energy photons, the drop in photoconversion efficiency is recorded as glass, ITO and ZnO start absorbing beyond 3.5 eV.

These reports showed effect of MEG on carefully deposited electronically coupled QDs film with sophisticated ligand treatment over atomically flat planer electrode. However, in case of conventional QDSSCs, still there are no reports, demonstrating MEG effect explicitly.

3.6. QDSSCs from MEG perspective

There are two possibilities for multiple exciton generation in quantum dot sensitized solar cells utilizing the hot electrons. In one case, cooling of hot carriers needs to be prolonged enough e.g. more than 10 ps to utilize hot carrier using interfacial carrier transfer. Thus, hot electrons are reinjected across the interface before cooling, and thus, it will be difficult for these electrons to reach selective contacts before cooling in electron transport material (ETM). Even in an ideal case, collection of hot carrier in the device is expected to produce

higher photovoltage but following the discussion in Section 3.2, photovoltage is limited by conduction level of electron transport material and redox potential of electrolyte. Thus, in this situation, prolonged lifetime of hot carriers is not supposed to exhibit any real effect on photovoltaic performance of QDSSCs. In second case, if hot carrier cooling is slow enough and multi-excitons can be generated before electron injection across interface then one photon can effectively inject multi-electron in electron transport material. In this case, hot carriers can have meaningful effect over photovoltaic efficiency of QDSSCs. Although, there are no reports for more than 100% IPCE in quantum dot sensitized solar cell till present to the authors' knowledge, yet there is a possibility of exceeding IPCE more than 100% in principle.

If we consider widely used electron transport material TiO₂, and polysulfide redox electrolyte then the minimum band gap for QDs, which can be used for MEG, should lie in range of 0.8–1 eV. Further, a band offset of 0.4 eV is required to realize very fast electron injection since multi-excitons need to be collected before they are lost via Auger recombination. Thus, the requirement for the minimum band gap of QDs absorber increases by this offset i.e. in the range of 1.2–1.4 eV. Following the discussion in Section 3.2, thermodynamic energy offset for bi-exciton generation in quantum dot absorber is $2E_g$, and very low carrier multiplication (CM) efficiency is observed at $2E_g$. Similarly, the thermodynamic limit for tri-exciton generation will be $3E_g$ making incident photon energy offset for tri-exciton to 3.6–4.2 eV. Since a very small or even negligible fraction of such high energy (3.6–4.2 eV) photons are available in the incident solar flux (in far UV region), the only contribution from bi-excitons can be expected to have any impact on the photovoltaic performance. As per thermodynamic limit for bi-exciton, the incident photons having energy higher than 2.4–2.8 eV can contribute efficiently on the photovoltaic performance. This suggests that the incident solar photons with energy in 2.4–2.8 eV range will be able to produce bi-excitons. Although following discussion in Section 3.2, even though thermodynamic limit for bi-exciton is $2E_g$ but meaningful MEG efficiencies are observed close to $3E_g$. Thus, the incident photons having energy higher than 3.6–4.2 eV can have impact on photovoltaic performance, and thus not significant photons will be available in solar flux in this energy range, showing any meaningful impact of MEG on the overall photovoltaic performance. Although photovoltaic efficiency utilizing hot carriers can push the thermodynamic energy conversion limit to 66%, MEG will have limited effect on QDSSCs's photovoltaic performance.

In 2006, Klimov calculated the detailed balance efficiency of QDSSC for the absorber bandgap, Fig. 41. The hot carrier cooling and interfacial charge transfer may exhibit < 5% enhancement in QDSSCs photovoltaic efficiency assuming ideal conditions for MEG with absorber band gap in range of 1.2–1.4 eV. In addition, to realize any improvement in real device, the ideal energy levels should lie near the

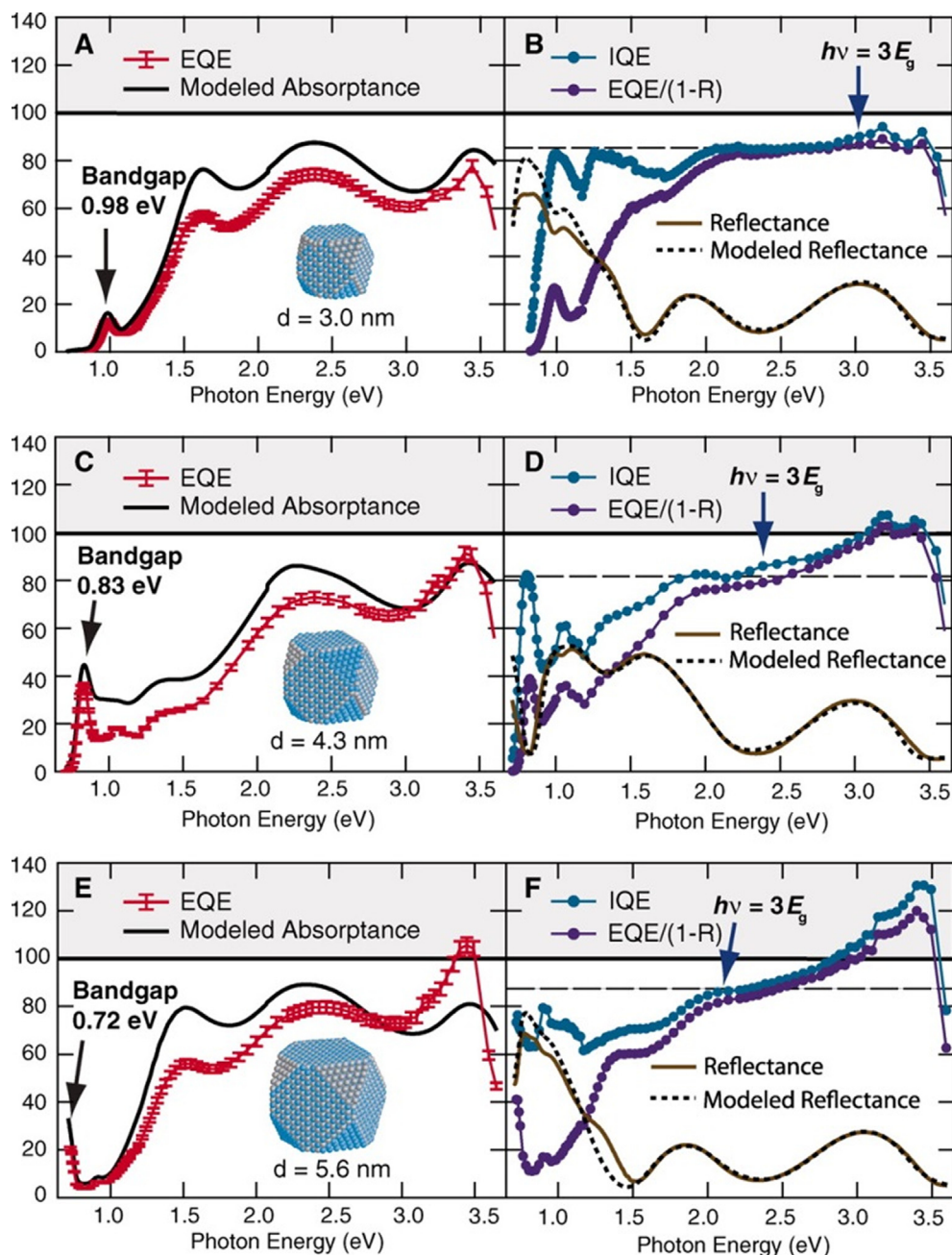


Fig. 40. Red curve are measured EQE for three representative QD solar cells made from PbSe QDs with indicated diameters and associated bandgaps of (A and B) 0.98 eV, (C and D) 0.83 eV and (E and F) 0.72 eV. Estimate of uncertainty of EQE curve is 3%. modelled plot of absorptance of QDs and ZnO layers [A,C and E solid black] and measured reflectance [B,D and F brown], Reprinted (adopted) with permission from ([Nozik, 2008](#)).

triple interface. Thus, we see that even though MEG is highly exciting and theoretically demonstrated to have effect at device level in photovoltaic performance, the overall impact on performance of QDSSCs seems to be limited.

4. Future directions and limitations for QDSSCs

Quantum dot sensitized solar cells have already made progress in photovoltaic efficiency from less than 1% to 12% or more over the years. The efficient redox hole conductors such as poly sulphide electrolyte and highly catalytic counter electrode like Cu_2S together with carefully designed core-shell quantum dots resulted in highly efficient QDSSCs, exhibiting about 12% photovoltaic efficiency. The advancement in surface treatments, used for passivating defects states in

nanostructured electrode and QDs absorber, resulted in enhanced efficiencies. Further, multiple exciton generation is demonstrated in colloidal quantum dots together with theoretical framework, explaining the experimental findings. There are possibilities that colloidal QDs may show more than 100% internal quantum efficiencies because of efficient MEG possibilities. The theoretical threshold for observing MEG is $2E_g$, however in practice threshold is observed at much higher energies $\sim 3E_g$ in QDs. The improvement in QDSSCs photovoltaic performance can be realized provided hot carrier cooling is slow enough to achieve MEG before electron injection in electron transport material is really taking place. Thus, after MEG, there will be multiple electron injection even after the absorption of one photon only. Further, meeting the minimum bandgap requirement for QDs absorber with widely used electron transport material TiO_2 , and polysulfide redox electrolyte hole

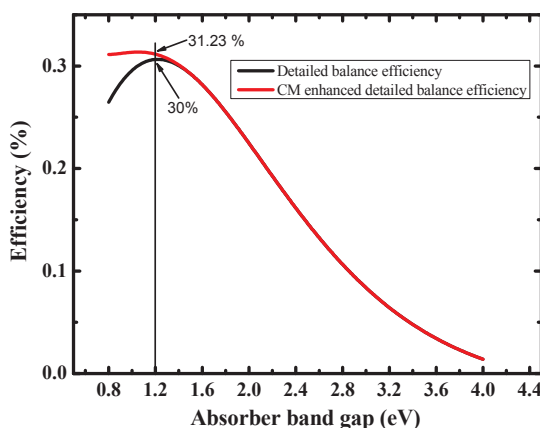


Fig. 41. Effect over detailed balance efficiency in QDSSCs with required absorber band gap calculated by V. I. klimov (Steigerwald and Brus, 1990) and efficiency marked at 1.2 eV absorber band gap.

conductor, less than 5% improvement is predicted in detailed balance efficiency (Steigerwald and Brus, 1990). This improvement can be even more than 5% if one can design suitable electron transport materials, QDs absorbers, redox hole conductor, and counter electrode material. Without finding suitable substitute for commonly used TiO_2 , polysulfide electrolyte, any significant jump beyond Shockley-Queisser efficiency limit in QDSSCs seems difficult.

5. Conclusion

A large jump in photovoltaic efficiency is made for quantum dot sensitized solar cells and the maximum of about 12% photovoltaic efficiency is demonstrated. However, there is a need to develop right bandgap absorbers and respective electron and hole transport materials together with highly stable electrolyte to realize the enhanced efficiency by aligning their energy levels more appropriately. Further, the concept of MEG seems very promising, which may provide the way to overcome the Shockley-Queisser limits in next generation QDSSCs. However, the experimental realization of MEG effectively in QDSSCs is still a challenge and will require designing and developing new QDs with suitable bandgap values together with slow carrier dynamics and longer carrier lifetimes. Thus, QDSSCs seems very promising, however, overcoming the issues and challenges associated with the development of efficient QDSSCs will require both experimental and theoretical understanding of the materials properties, their integration in device configurations, interface issues, and associated carrier dynamics.

Acknowledgement

Author Ambesh Dixit acknowledges Department of Science and Technology, Gov. of India, through project # DST/INT/Mexico/P-20/2016 for this work.

References

- Adegoke, O., Park, E.Y., 2016. Size-confined fixed-composition and composition-dependent engineered band gap alloying induces different internal structures in L-cysteine-capped alloyed quaternary CdZnTeS quantum dots. *Sci Rep.* 6, 27288. <https://doi.org/10.1038/srep27288>.
- Adler, F., Geiger, M., Bauknecht, A., Haase, D., Ernst, P., Dörnen, A., Scholz, F., Schweizer, H., 1998. Self-assembled InAs/GaAs quantum dots under resonant excitation. *J. Appl. Phys.* 83, 1631–1636. <https://doi.org/10.1063/1.366876>.
- Albrecht, J.D., Ruden, P.P., Limpijumpong, S., Lambrecht, W.R.L., Brennan, K.F., 1999. High field electron transport properties of bulk ZnO . *J. Appl. Phys.* 86, 6864–6867. <https://doi.org/10.1063/1.371764>.
- Alpuche-Aviles, M.A., Wu, Y., 2009. Photoelectrochemical study of the band structure of Zn_2SnO_4 prepared by the hydrothermal method. *J. Am. Chem. Soc.* 131, 3216–3224. <https://doi.org/10.1021/ja806719x>.
- Arroyo-De Dompablo, M.E., Morales-Garcia, A., Taravillo, M., 2011. DFTU calculations of crystal lattice, electronic structure, and phase stability under pressure of TiO_2 polymorphs. *J. Chem. Phys.* 135. <https://doi.org/10.1063/1.3617244>.
- Baker, D.R., Kamat, P.V., 2010. Tuning the emission of CdSe quantum dots by controlled trap enhancement. *Langmuir* 26, 11272–11276. <https://doi.org/10.1021/la100580g>.
- Bang, J.H., Kamat, P.V., 2009. Quantum dot sensitized solar cells. A tale of two semiconductor nanocrystals: CdSe and CdTe , *ACS Nano*. 3, 143–154. <https://doi.org/10.1021/nm090324q>.
- Bauhuis, G.J.Å., Mulder, P., Haverkamp, E.J., Huijben, J.C.C.M., Schermer, J.J., 2009. Solar Energy Materials & Solar Cells 26. 1% thin-film GaAs solar cell using epitaxial lift-off. *Sol. Energy Mater. Sol. Cells.* 93, 1488–1491. <https://doi.org/10.1016/j.solmat.2009.03.027>.
- Beard, M.C., Knutson, K.P., Yu, P., Luther, J.M., Song, Q., Metzger, W.K., Ellingson, R.J., Nozik, A.J., 2007. Multiple exciton generation in colloidal silicon nanocrystals. *Nano Lett.* 7, 2506–2512. <https://doi.org/10.1021/nl071486l>.
- Benick, J., Richter, A., Müller, R., Hauser, H., Feldmann, F., Krenkel, P., Riepe, S., Schindler, F., Schubert, M.C., Hermle, M., Bett, A.W., Glunz, S.W., 2017. High-Efficiency n-Type HP mc Silicon Solar Cells. *IEEE J. Photovoltaics*. 7, 1171–1175. <https://doi.org/10.1109/JPHOTOV.2017.2714139>.
- Benisty, H., 1995. Reduced electron-phonon relaxation rates in quantum-box systems: Theoretical analysis. *Phys. Rev. B*. 51, 13281–13293. <https://doi.org/10.1103/PhysRevB.51.13281>.
- Benisty, H., Sotomayor-Torrès, C.M., Weisbuch, C., 1991. Intrinsic mechanism for the poor luminescence properties of quantum-box systems. *Phys. Rev. B*. 44, 10945–10948. <https://doi.org/10.1103/PhysRevB.44.10945>.
- Bian, S.W., Mudunkotuwa, I.A., Rupasinghe, T., Grassian, V.H., 2011. Aggregation and dissolution of 4 nm ZnO nanoparticles in aqueous environments: Influence of pH, ionic strength, size, and adsorption of humic acid. *Langmuir* 27, 6059–6068. <https://doi.org/10.1021/la200570n>.
- Bin Li, L., Wang, Y.F., Rao, H.S., Wu, W.Q., Li, K.N., Su, C.Y., Bin Kuang, D., 2013. Hierarchical macroporous $\text{Zn}_{2}\text{SnO}_4\text{-ZnO}$ nanorod composite photoelectrodes for efficient cds/cdse quantum dot Co-sensitized solar cells. *ACS Appl. Mater. Interfaces*. 5, 11865–11871. <https://doi.org/10.1021/am4035653>.
- Boschloo, G.K., Goossens, A., Schoonman, J., 1997. Investigation of the potential distribution in porous nanocrystalline TiO_2 electrodes by electrolyte electrorefraction. *J. Electroanal. Chem.* 428, 25–32.
- Boudreault, D.S., Williams, F., Nozik, A.J., 1980. Hot carrier injection at semiconductor-electrolyte junctions Hot carrier injection at semiconductor-electrolyte junctions. *J. Appl. Phys.* 51, 2158–2169.
- Bragg FRS, W.L., Darbshire, J.A., 1930. The structure of thin films of certain metallic oxides. *Proc. Roy. Soc. A*. 13, 522–525.
- Brown, P., Kamat, P.V., 2008. Quantum Dot Solar Cells. *Electrophoretic Deposition of CdSe - Cd₃[sub60] Composite Films and Capture of Photogenerated Electrons with nCd₃[sub60] Cluster Shell*. *J. Am. Chem. Soc.* 130, 8890–8891.
- Brus, L.E., 1983. A simple model for the ionization potential, electron affinity, and aqueous redox potentials of small semiconductor crystallites. *J. Chem. Phys.* 79, 5566–5571. <https://doi.org/10.1063/1.445676>.
- Brus, L.E., 1984. Electron-electron and electron-hole interactions in small semiconductor crystallites: The size dependence of the lowest excited electronic state. *J. Chem. Phys.* 80, 4403–4409. <https://doi.org/10.1063/1.447218>.
- Burnside, S., Moser, J.-E., Brooks, K., Grätzel, M., Cahen, D., 1999. Nanocrystalline Mesoporous Strontium Titanate as Photoelectrode Material for Photosensitized Solar Devices: Increasing Photovoltage through Flatband Potential Engineering. *J. Phys. Chem. B*. 103, 9328–9332. <https://doi.org/10.1021/jp9913867>.
- Cachet, H., Essaaidi, H., Froment, M., Maurin, G., 1995. Chemical bath deposition of CdSe layers from Cd(II)-selenosulfite solutions. *J. Electroanal. Chem.* 396, 175–182. [https://doi.org/10.1016/0022-0728\(95\)04088-6](https://doi.org/10.1016/0022-0728(95)04088-6).
- Cahen, D., Hodas, G., Grätzel, M., Guillemoles, J.F., Riess, I., 2000. Nature of Photovoltaic Action in Dye-Sensitized Solar Cells. *J. Phys. Chem. B*. 104, 2053–2059. <https://doi.org/10.1021/jp9931871>.
- Cameron, P.J., Peter, L.M., 2005. How does back-reaction at the conducting glass substrate influence the dynamic photovoltage response of nanocrystalline dye-sensitized solar cells? *J. Phys. Chem. B*. 109, 7392–7398. <https://doi.org/10.1021/jp0407270>.
- Cao, F., Oskam, G., Meyer, G.J., Searson, P.C., 1996. Electron Transport in Porous Nanocrystalline TiO_2 Photoelectrochemical Cells. *J. Phys. Chem.* 100, 17021–17027. <https://doi.org/10.1021/jp9616573>.
- Carey, G.H., Abdelhady, A.L., Ning, Z., Thon, S.M., Bakr, O.M., Sargent, E.H., Cells, Colloidal Quantum Dot Solar, 2015. *Chem. Rev.* 150624090720003. <https://doi.org/10.1021/acs.chemrev.5b00063>.
- Chakrapani, V., Tvrdy, K., Kamat, P.V., 2010. Modulation of Electron Injection in CdSe-TiO₂ System through Medium Alkalinity. *J. Am. Chem. Soc.* 132, 1228–1229. <https://doi.org/10.1021/ja909663r>.
- Chakrapani, V., Baker, D., Kamat, P.V., 2011. Understanding the Role of the Sulfide Redox Couple (S_2/Sn_2) in Quantum Dot-Sensitized Solar Cells. *J. Am. Chem. Soc.* 133, 9607–9615. <https://doi.org/10.1021/ja203131b>.
- Chang, J.A., Rhee, J.H., Im, S.H., Lee, Y.H., Kim, H.J., Il Seok, S., Nazeeruddin, M.K., Grätzel, M., 2010. High-performance nanostructured inorganic-organic heterojunction solar cells. *Nano Lett.* 10, 2609–2612. <https://doi.org/10.1021/nl101322h>.
- Chang, Y.C., Suriyawong, N., Aragaw, B.A., Bin Shi, J., Chen, P., Lee, M.W., 2016. Lead antimony sulfide ($\text{Pb}_5\text{Sb}_8\text{S}_17$) solid-state quantum dot-sensitized solar cells with an efficiency of over 4%. *J. Power Sources*. 312, 86–92. <https://doi.org/10.1016/j.jpowsour.2016.02.051>.
- Chen, C., Dai, Q., Miao, C., Xu, L., Song, H., 2015. Strontium titanate nanoparticles as the photoanode for CdS quantum dot sensitized solar cells. *RSC Adv.* 5, 4844–4852. <https://doi.org/10.1039/C4RA11960F>.
- Chen, J., Li, C., Song, J.L., Sun, X.W., Lei, W., Deng, W.Q., 2009. Bilayer ZnO nanostucture fabricated by chemical bath and its application in quantum dot sensitized

- solar cell. *Appl. Surf. Sci.* 255, 7508–7511. <https://doi.org/10.1016/j.apsusc.2009.03.091>.
- Chen, H.Y., Lin, L., Yu, X.Y., Qiu, K.Q., Lü, X.Y., Bin Kuang, D., Su, C.Y., 2013. Dextran based highly conductive hydrogel polysulfide electrolyte for efficient quasi-solid-state quantum dot-sensitized solar cells. *Electrochim. Acta*. 92 117–123. <https://doi.org/10.1016/j.electacta.2013.01.025>.
- Chen, P., Yum, J.H., De Angelis, F., Mosconi, E., Fantacci, S., Moon, S., Baker, R.H., Ko, J., Nazeeruddin, K., Gra, M., 2009. High Open-Circuit Voltage Solid-State Dye-Sensitized Solar Cells with Organic Dye 2009. *Nano Lett.* 9, 2487–2492.
- Chiu, P.T., Law, D.C., Woo, R.L., Singer, S.B., Bhusari, D., Hong, W.D., Zakaria, A., Boisvert, J., Mesropian, S., King, R.R., Karam, N.H., 2014. 35.8% space and 38.8% terrestrial 5J direct bonded cells. 2014 IEEE 40th Photovolt. Spec. Conf. PVSC 2014, pp. 11–13. doi: 10.1109/PVSC.2014.6924957.
- Contreras, M.A., Romero, M.J., To, B., Hasoon, F., Noufi, R., Ward, S., Ramanathan, K., 2002. Optimization of CBD CdS process in high-efficiency Cu (In, Ga) Se 2 -based solar cells. *Thin Solid Films* 404, 204–211.
- Coutts, T.J., Young, D.L., 2000. Characterization of Transparent Conducting Oxides. *MRS Bull.* 58–55.
- Dai, Q., Chen, J., Lu, L., Tang, J., Wang, W., 2012. Pulsed Laser Deposition of CdSe Quantum Dots on Zn 2 SnO 4 Nanowires and Their Photovoltaic Applications. *Nano Lett.* 12, 4187–4193. <https://doi.org/10.1021/nl301761w>.
- Dao, V.D., Choi, Y., Yong, K., Larina, L.L., Choi, H.S., 2015. Graphene-based nanohybrid materials as the counter electrode for highly efficient quantum-dot-sensitized solar cells. *Carbon N. Y.* 84, 383–389. <https://doi.org/10.1016/j.carbon.2014.12.014>.
- De Smet, Y., Deriemaeker, L., Finsy, R., 1997. A Simple Computer Simulation of Ostwald Ripening. *Langmuir* 13, 6884–6888. <https://doi.org/10.1021/la970379b>.
- Dibbell, R.S., Watson, D.F., 2009. Distance-Dependent Electron Transfer in Tethered Assemblies of CdS Quantum Dots and TiO 2 Nanoparticles. *J. Phys. Chem. C* 113, 13511–13519. <https://doi.org/10.1021/la702127t>.
- Dorolit, E., Cario, L., Corraze, B., Janod, E., Vaju, C., Koo, H.J., Kan, E., Whangbo, M.H., 2010. Half-metallic ferromagnetism and large negative magnetoresistance in the new lacunar spinel GaTi 3 VS 8 . *J. Am. Chem. Soc.* 132, 5704–5710. <https://doi.org/10.1021/ja908128b>.
- Du, J., Du, Z., Hu, J.-S., Pan, Z., Shen, Q., Sun, J., Long, D., Dong, H., Sun, L., Zhong, X., Wan, L.-J., 2016. Zn–Cu–In–Se Quantum Dot Solar Cells with a Certified Power Conversion Efficiency of 11.6%. *J. Am. Chem. Soc.* 138, 4201–4209. <https://doi.org/10.1021/jacs.6b00615>.
- Efros, A.L., Kharchenko, V.A., Rosen, M., 1995. Breaking the phonon bottleneck in nanometer quantum dots: Role of Auger-like processes. *Solid State Commun.* 93, 281–284. [https://doi.org/10.1016/0038-1098\(94\)00760-8](https://doi.org/10.1016/0038-1098(94)00760-8).
- Ellingson, R.J., Beard, M.C., Johnson, J.C., Yu, P., Micic, O.I., Nozik, A.J., Shabaev, A., Efros, A.L., 2005. Highly efficient multiple exciton generation in colloidal PbSe and PbS quantum dots. *Nano Lett.* 5, 865–871. <https://doi.org/10.1021/nl0502672>.
- Emin, S., Singh, S.P., Han, L., Satoh, N., Islam, A., 2011. Colloidal quantum dot solar cells. *Sol. Energy*. 85, 1264–1282. <https://doi.org/10.1016/j.solener.2011.02.005>.
- Enright, B., Fitzmaurice, D., 1996. Spectroscopic Determination of Electron and Hole Effective Masses in a Nanocrystalline Semiconductor Film. *J. Phys. Chem.* 100, 1027–1035. <https://doi.org/10.1021/jp951142w>.
- Ernst, K., Belaïdi, A., Nenkamp, R.K., 2003. Solar cell with extremely thin absorber on highly structured substrate. *Semicond. Sci. Technol.* 18, 475–479. <https://doi.org/10.1088/0268-1242/18/6/314>.
- Fan, S.Q., Fang, B., Kim, J.H., Kim, J.Y., Yu, J.S., Ko, J., 2010. Hierarchical nanostructured spherical carbon with hollow core/mesoporous shell as a highly efficient counter electrode in CdSe quantum-dot-sensitized solar cells. *Appl. Phys. Lett.* 96, 2008–2011. <https://doi.org/10.1063/1.3313948>.
- Fang, J., Wu, J., Lu, X., Shen, Y., Lu, Z., 1997. Sensitization of nanocrystalline TiO 2 electrode with quantum sized CdS and ZnTCP molecules. *Chem. Phys. Lett.* 270, 145–151. [https://doi.org/10.1016/S0009-2614\(97\)00333-3](https://doi.org/10.1016/S0009-2614(97)00333-3).
- Farber, J., 1998. An electrical model of the dye-sensitized solar cell. *Sol. Energy Mater. Sol. Cells.* 53, 29–54. [https://doi.org/10.1016/S0927-0248\(98\)00005-1](https://doi.org/10.1016/S0927-0248(98)00005-1).
- Ferrere, S., Zaban, A., Gregg, B.A., 1997. Dye sensitization of nanocrystalline TiO 2 by perylene derivatives. *J. Phys. Chem. B* 128, 299–304. [https://doi.org/10.1016/S0379-6779\(02\)00007-3](https://doi.org/10.1016/S0379-6779(02)00007-3).
- Franco, G., Gehring, J., Peter, L.M., Ponomarev, E.A., Uhlendorf, I., 1999. Frequency-resolved optical detection of photojected electrons in dye-sensitized nanocrystalline photovoltaic cells. *J. Phys. Chem. B* 103, 692–698. <https://doi.org/10.1002/chin.199917016>.
- Gandman, A., Bronstein-Tojen, M., Kloper, V., Muallem, M., Yanover, D., Lifshitz, E., Amitay, Z., 2013. Non-poissonian formation of multiple excitons in photoexcited CdTe colloidal quantum qots by femtosecond nonresonant two-photon absorption. *Opt. Express.* 21, 24300–24308. <https://doi.org/10.1364/OE.21.024300>.
- Gao, J., Fidler, A.F., Klimov, V.I., 2015. Carrier multiplication detected through transient photocurrent in device-grade films of lead selenide quantum dots. *Nat. Commun.* 6. 10. <https://doi.org/10.1038/ncomms9185>.
- García-Rodríguez, R., Hendricks, M.P., Cossairt, B.M., Liu, H., Owen, J.S., 2013. Conversion reactions of cadmium chalcogenide nanocrystal precursors. *Chem. Mater.* 25, 1233–1249. <https://doi.org/10.1021/cm3035642>.
- Geacintov, N., Pope, M., Kallmann, H., 1966. Photogeneration of Charge Carriers in Tetracene. *J. Chem. Phys.* 45, 2639–2649. <https://doi.org/10.1063/1.1727984>.
- Giménez, S., Mora-Seró, I., Macor, L., Guijarro, N., Lana-Villarreal, T., Gómez, R., Diguna, L.J., Shen, Q., Toyoda, T., Bisquert, J., 2009. Improving the performance of colloidal quantum-dot-sensitized solar cells. *Nanotechnology*. 20, 295204. <https://doi.org/10.1088/0957-4484/20/29/295204>.
- González-Pedro, V., Xu, X., Mora-Seró, I., Bisquert, J., 2010. Modeling high-efficiency quantum dot sensitized solar cells. *ACS Nano* 4, 5783–5790. <https://doi.org/10.1021/nn101534y>.
- Gopi, C.V.V.M., Venkata-Haritha, M., Kim, S.-K., Kim, H.-J., 2015. Improved photovoltaic performance and stability of quantum dot sensitized solar cells using Mn-ZnSe shell structure with enhanced light absorption and recombination control. *Nanoscale*. 7, 12552–12563. <https://doi.org/10.1039/C5NR03291A>.
- Green, M.A., Hishikawa, Y., Warta, W., Dunlop, E.D., Levi, D.H., Hohl-Ebinger, J., Hoballie, A.W.H., 2017. Solar cell efficiency tables (version 50). *Prog. Photovoltaics Res. Appl.* 25, 668–676. <https://doi.org/10.1002/pip.2909>.
- Green, A.N.M., Palomares, E., Haque, S.A., Kroon, J.M., Durrant, J.R., 2005. Charge Transport versus Recombination in Dye-Sensitized Solar Cells Employing Nanocrystalline TiO 2 and SnO 2 Films. *J. Phys. Chem. B* 109, 12525–12533.
- M.A. Green, Third Generation Photovoltaics, n.d.
- Gregg, B.A., 2003. Excitonic Solar Cells. *J. Phys. Chem. B* 107, 4688–4698. <https://doi.org/10.1021/jp022507x>.
- Gregg, B., Fox, M., Bard, A., 1990. Photovoltaic effect in symmetrical cells of a liquid crystal porphyrin. *J. Phys. Chem.* 94, 1586–1598. <https://doi.org/10.1021/j100367a068>.
- Gregg, B.A., Hanna, M.C., 2003. Comparing organic to inorganic photovoltaic cells: Theory, experiment, and simulation. *J. Appl. Phys.* 93, 3605–3614. <https://doi.org/10.1063/1.1544413>.
- Gubbala, S., Chakrapani, V., Kumar, V., Sunkara, M.K., 2008. Band-edge engineered hybrid structures for dye-sensitized solar cells based on SnO 2 nanowires. *Adv. Funct. Mater.* 18, 2411–2418. <https://doi.org/10.1002/adfm.200800099>.
- Guizarro, N., Campiña, J.M., Shen, Q., Toyoda, T., Lana-Villarreal, T., Gómez, R., 2011. Uncovering the role of the ZnS treatment in the performance of quantum dot sensitized solar cells. *Phys. Chem. Chem. Phys.* 13, 12024–12032. <https://doi.org/10.1039/c1cp20290a>.
- Günes, S., Neugebauer, H., Sariciftci, N.S., 2007. Conjugated polymer-based organic solar cells. *Chem. Rev.* 107, 1324–1338. <https://doi.org/10.1021/cr050149z>.
- Günes, S., Fritz, K.P., Neugebauer, H., Sariciftci, N.S., Kumar, S., Scholes, G.D., 2007. Hybrid solar cells using PbS nanoparticles. *Sol. Energy Mater. Sol. Cells.* 91, 420–423. <https://doi.org/10.1016/j.solmat.2006.10.016>.
- Guyot-Sionnest, P., Shim, M., Matranga, C., Hines, M., 1999. Intraband relaxation in CdSe quantum dots. *Phys. Rev. B* 60, R2181–R2184. <https://doi.org/10.1103/PhysRevB.60.R2181>.
- Habibi, M.H., Mikhak, M., Zendehdel, M., Habibi, M., 2012. Influence of nanostructured zinc titanate, zinc oxide or titanium dioxide thin film coated on fluorine doped tin oxide as working electrodes for dye-sensitized solar cell. *Int. J. Electrochem. Sci.* 7, 6787–6798.
- Hagfeldt, A., Grätzel, M., 2000. Molecular photovoltaics. *Acc. Chem. Res.* 33, 269–277. <https://doi.org/10.1021/ar980112j>.
- Hagfeldt, A., Lindquist, S.E., Grätzel, M., 1994. Charge carrier separation and charge transport in nanocrystalline junctions. *Sol. Energy Mater. Sol. Cells.* 32, 245–257. [https://doi.org/10.1016/0927-0248\(94\)90262-3](https://doi.org/10.1016/0927-0248(94)90262-3).
- Halder, G., Bhattacharyya, S., 2015. Plight of Mn doping in colloidal CdS quantum dots to boost the efficiency of solar cells. *J. Phys. Chem. C* 119, 13404–13412. <https://doi.org/10.1021/acs.jpcsc.5b01932>.
- Haram, S.K., Kshirsagar, A., Gujarathi, Y.D., Ingole, P.P., Nene, O.A., Markad, G.B., Nanavati, S.P., 2011. Quantum confinement in CdTe quantum dots: Investigation through cyclic voltammetry supported by density functional theory (DFT). *J. Phys. Chem. C* 115, 6243–6249. <https://doi.org/10.1021/jp111463f>.
- Hatami, F., Grundmann, M., Ledentsov, N.N., Heinrichsdorff, F., Heitz, R., Böhner, J., Bimberg, D., Ruvimov, S.S., Werner, P., Ustinov, V.M., Kop'ev, P.S., Alferov, Z.I., 1998. Carrier dynamics in type-II GaSb/GaAs quantum dots. *Phys. Rev. B* 57, 4635–4641. <https://doi.org/10.1103/PhysRevB.57.4635>.
- Heitz, R., Veit, M., Kalburge, A., Xie, Q., Grundmann, M., Chen, P., Ledentsov, N.N.N., Hoffmann, A., Madhukar, A., Bimberg, D., Ustinov, V.M.M., Kop'ev, P.S.S., Alferov, Z.I., 1998. Hot carrier relaxation in InAs/GaAs quantum dots. *Phys. E Low-Dimensional Syst. Nanostructures*. 2, 578–582. [https://doi.org/10.1016/S1386-9477\(98\)00118-0](https://doi.org/10.1016/S1386-9477(98)00118-0).
- Heitz, R., Kalburge, A., Xie, Q., Grundmann, M., Chen, P., Hoffmann, A., Madhukar, A., Bimberg, D., 1997. Excited states and energy relaxation in stacked InAs/GaAs quantum dots. *Phys. Rev. B* 57, 9050–9060. <https://doi.org/10.1103/PhysRevB.57.9050>.
- Hod, I., Zaban, A., 2014. Materials and interfaces in quantum dot sensitized solar cells: Challenges, advances and prospects. *Langmuir* 30, 7264–7273. <https://doi.org/10.1021/la403768j>.
- Hodes, G., 2008. Comparison of Dye- and Semiconductor-Sensitized Porous Nanocrystalline Liquid Junction. *J. Phys. Chem. B* 112, 17778–17787.
- Hodes, G., 2012. Photoelectrochemical cell measurements: Getting the basics right. *J. Phys. Chem. Lett.* 3, 1208–1213. <https://doi.org/10.1021/jz300220b>.
- Hodes, G., Gorin, S., 1994. Quantum size effects in the study of chemical solution deposition mechanisms of semiconductor films. *J. Phys. Chem.* 98, 5338–5346. <https://doi.org/10.1021/j100071a026>.
- Hodes, G., Manassen, J., 1980. Electrocatalytic Electrodes for the Polysulfide Redox System. *J. Electrochem. Soc.* 127, 544–549. <https://doi.org/10.1149/1.2129709>.
- Hoppe, H., Sariciftci, N.S., 2004. Organic solar cells: An overview. *J. Mater. Res.* 19, 1924–1945. <https://doi.org/10.1557/JMR.2004.0252>.
- Hossain, A., Jennings, J.R., Koh, Z.Y., Wang, Q., 2011. Carrier Generation and Collection in CdS/CdSe-Sensitized SnO 2 Solar Cells Exhibiting Unprecedented Photocurrent Densities. *ACS Nano* 5, 3172–3181.
- Hotchandani, S., Kamat, P.V., 1992. Modification of electrode surface with semiconductor colloids and its sensitization with chlorophyll a. *Chem. Phys. Lett.* 191, 320–326. [https://doi.org/10.1016/0009-2614\(92\)85308-W](https://doi.org/10.1016/0009-2614(92)85308-W).
- Hou, J., Zhao, H., Huang, F., Jing, Q., Cao, H., Wu, Q., Peng, S., Cao, G., 2016. High performance of Mn-doped CdSe quantum dot sensitized solar cells based on the vertical ZnO nanorod arrays. *J. Power Sources*. 325, 438–445. <https://doi.org/10.1016/j.jpowsour.2016.04.045>.

- 1016/j.jpowsour.2016.06.070.
- Huang, J., Kovalenko, M.V., Talapin, D.V., 2010. Alkyl chains of surface ligands affect polytypism of CdSe nanocrystals and play an important role in the synthesis of anisotropic nanostructures. *J. Am. Chem. Soc.* 132, 15866–15868. <https://doi.org/10.1021/ja105132u>.
- Huang, Z., Zou, X., Zhou, H., 2013. A strategy to achieve superior photocurrent by Cu-doped quantum dot sensitized solar cells. *Mater. Lett.* 95, 139–141. <https://doi.org/10.1016/j.matlet.2012.12.095>.
- Huo, Z., Tao, L., Wang, S., Wei, J., Zhu, J., Dong, W., Liu, F., Chen, S., Zhang, B., Dai, S., 2015. A novel polysulfide hydrogel electrolyte based on low molecular mass organogelators for quasi-solid-state quantum dot-sensitized solar cells. *J. Power Sources* 284, 582–587. <https://doi.org/10.1016/j.jpowsour.2015.03.049>.
- Hyun, B., Zhong, Y., Bartnik, A.C., Sun, L., Abrun, H.D., Wise, F.W., Goodreau, J.D., Matthews, J.R., Leslie, T.M., Borrelli, N.F., 2008. Electron Injection from Colloidal PbS Nanoparticles. *ACS Nano* 2, 2206–2212. <https://doi.org/10.1021/nm800336b>.
- Ichikawa, Y., Yoshida, T., Hama, T., Sakai, H., Harashima, K., 2001. Production technology for amorphous silicon-based flexible solar cells. *Sol. Energy Mater. Sol. Cells* 66, 107–115.
- Inoshita, T., Sakaki, H., 1992. Electron relaxation in a quantum dot: Significance of multiphonon processes. *Phys. Rev. B* 46, 7260–7263. <https://doi.org/10.1103/PhysRevB.46.7260>.
- Inoshita, T., Sakaki, H., 1997. Density of states and phonon-induced relaxation of electrons in semiconductor quantum dots. *Phys. Rev. B* 56, R4355–R4358. <https://doi.org/10.1103/PhysRevB.56.R4355>.
- Jean, J., Chang, S., Brown, P.R., Cheng, J.J., Rekemeyer, P.H., Bawendi, M.G., Gradečák, S., Bulovic, V., 2013. ZnO nanowire arrays for enhanced photocurrent in PbS quantum dot solar cells. *Adv. Mater.* 25, 2790–2796. <https://doi.org/10.1002/adma.201204192>.
- Jiao, S., Shen, Q., Mora-Seró, I., Wang, J., Pan, Z., Zhao, K., Kuga, Y., Zhong, X., Bisquert, J., 2015. Band Engineering in Core / Shell ZnTe / CdSe for Photovoltage and Efficiency Enhancement in Exciplex. *ACS Nano* 9, 908–915. <https://doi.org/10.1021/nm506638n>.
- Jiao, S., Shen, Q., Mora-Seró, I., Wang, J., Pan, Z., Zhao, K., Kuga, Y., Zhong, X., Bisquert, J., 2015. Band engineering in core/shell ZnTe/cdse for photovoltage and efficiency enhancement in exciplex quantum dot sensitized solar cells. *ACS Nano* 9, 908–915. <https://doi.org/10.1021/nm506638n>.
- Johnston, K.W., Pattantyus-Abraham, A.G., Clifford, J.P., Myrskog, S.H., MacNeil, D.D., Levina, L., Sargent, E.H., 2008. Schottky-quantum dot photovoltaics for efficient infrared power conversion. *Appl. Phys. Lett.* 92, 90–93. <https://doi.org/10.1063/1.2912340>.
- Jose, R., Thavasi, V., Ramakrishna, S., 2009. Metal oxides for dye-sensitized solar cells. *J. Am. Ceram. Soc.* 92, 289–301. <https://doi.org/10.1111/j.1551-2916.2008.02870.x>.
- Jovanovski, V., González-Pedro, V., Giménez, S., Azaceta, E., Cabañero, G., Grande, H., Tena-Zaera, R., Mora-Seró, I., Bisquert, J., 2011. A sulfide/polysulfide-based ionic liquid electrolyte for quantum dot-sensitized solar cells. *J. Am. Chem. Soc.* 133, 20156–20159. <https://doi.org/10.1021/ja2096865>.
- Kallmann, H., Pope, M., 1959. Photovoltaic Effect in Organic Crystals. *J. Chem. Phys.* 30, 585–586. <https://doi.org/10.1063/1.1729992>.
- Kalyanasundaram, K., 1998. Applications of functionalized transition metal complexes in photonic and optoelectronic devices. *Coord. Chem. Rev.* 177, 347–414. [https://doi.org/10.1016/S0010-8545\(98\)00189-1](https://doi.org/10.1016/S0010-8545(98)00189-1).
- Kamat, P.V., 2013. Quantum Dot Solar Cells. The Next Big Thing in Photovoltaics.
- Kamat, P.V., Bedja, I., Hotchandani, S., Patterson, L.K., 1996. Photosensitization of Nanocrystalline Semiconductor Films. Modulation of Electron Transfer between Excited Ruthenium Complex and SnO₂ Nanocrystallites with an Externally Applied Bias. *J. Phys. Chem.* 100, 4900–4908. <https://doi.org/10.1021/jp9512691>.
- Karageorgopoulos, D., Stathatos, E., Vitoratos, E., 2012. Thin ZnO nanocrystalline films for efficient quasi-solid state electrolyte quantum dot sensitized solar cells. *J. Power Sources* 219, 9–15. <https://doi.org/10.1016/j.jpowsour.2012.07.034>.
- Kato, T., Handa, A., Yagioka, T., Matsuura, T., Yamamoto, K., Higashi, S., 2017. Enhanced Efficiency of Cd-Free Cu (In, Ga)(Se, S) 2 Minimodule Via (Zn, Mg) O Second Buffer Layer and Alkali Metal Post-Treatment. *IEEE J. Photovoltaics* 7, 1173–1180. <https://doi.org/10.1109/JPHOTOV.2017.2745710>.
- Kayes, B.M., Nie, H., Twist, R., Spruytte, S.G., Reinhardt, F., Kizilyalli, I.C., Higashi, G.S., 2011. 27.6% Conversion efficiency, a new record for single-junction solar cells under 1 sun illumination. *Conf. Rec. IEEE Photovolt. Spec. Conf.* 000004–000008. <https://doi.org/10.1109/PVSC.2011.6185831>.
- Klimov, V.I., 2000. Optical Nonlinearities and Ultrafast Carrier Dynamics in Semiconductor Nanocrystals. *J. Phys. Chem. B* 104, 6112–6123. <https://doi.org/10.1021/jp9944132>.
- Klimov, V.I., 2006. Detailed-balance power conversion limits of nanocrystal-quantum-dot solar cells in the presence of carrier multiplication. *Appl. Phys. Lett.* 89, 123118. <https://doi.org/10.1016/j.12356314>.
- Klimov, V., McBranch, D., 1998. Femtosecond 1P-to-1S Electron Relaxation in Strongly Confined Semiconductor Nanocrystals. *Phys. Rev. Lett.* 80, 4028–4031. <https://doi.org/10.1103/PhysRevLett.80.4028>.
- Klimov, V.I., Mikhailovsky, A.A., McBranch, D.W., Leatherdale, C.A., Bawendi, M.G., 2000. Mechanisms for intraband energy relaxation in semiconductor quantum dots: The role of electron-hole interactions. *Phys. Rev. B* 61, R13349–R13352. <https://doi.org/10.1103/PhysRevB.61.R13349>.
- Koleilat, G.I., Levina, L., Shukla, H., Myrskog, S.H., Hinds, S., Pattantyus-abraham, A.G., Sargent, E.H., 2008. Efficient, Stable Infrared Photovoltaics Quantum Dots. *ACS Nano* 2, 833–840. <https://doi.org/10.1021/nm800093v>.
- Kolodinski, S., Werner, J.H., Wittchen, T., Queisser, H.J., Werner, J.H., Queisser, H.J., 1993. Quantum efficiencies exceeding unity due to impact ionization in silicon solar cells. Quantum efficiencies in silicon solar cells exceeding unity due to impact ionization. *J. Appl. Phys.* 63, 2405–2407. <https://doi.org/10.1063/1.110489>.
- Kong, F.-T., Dai, S.-Y., Wang, K.-J., 2007. Review of Recent Progress in Dye-Sensitized Solar Cells. *Adv. Optoelectron.* 2007, 1–13. <https://doi.org/10.1155/2007/75384>.
- Kumar, S., Nann, T., 2006. Shape control of II-VI semiconductor nanomaterials. *Small* 2, 316–329. <https://doi.org/10.1002/smll.200500357>.
- Lai, Y., Lin, Z., Zheng, D., Chi, L., Du, R., Lin, C., 2012. CdSe/CdS quantum dots co-sensitized TiO₂ nanotube array photoelectrode for highly efficient solar cells. *Electrochim. Acta* 79, 175–181. <https://doi.org/10.1016/j.electacta.2012.06.105>.
- Lai, L.-H., Protesescu, L., Kovalenko, M.V., Loi, M.A., 2014. Sensitized solar cells with colloidal PbS-CdS core-shell quantum dots. *Phys. Chem. Chem. Phys.* 16, 736–742. <https://doi.org/10.1039/C3CP54145B>.
- Lan, Z., Liu, L., Huang, M., Wu, J., Lin, J., 2015. Preparation of nano-flower-like SnO₂ particles and their applications in efficient CdS quantum dots sensitized solar cells. *J. Mater. Sci. Mater. Electron.* 26, 7914–7920. <https://doi.org/10.1007/s10854-015-3444-y>.
- Lana-villarreal, T., Bisquert, J., 2009. CdSe Quantum Dot-Sensitized TiO₂ Electrodes: Effect of Quantum Dot Coverage and Mode Ne. Society. 4208–4214.
- Landsberg, P.T., Nussbaumer, H., Willeke, G., 1993. Band-band impact ionization and solar cell efficiency. *J. Appl. Phys.* 74, 1451–1452.
- Lee, Y.L., Chang, C.H., 2008. Efficient polysulfide electrolyte for CdS quantum dot-sensitized solar cells. *J. Power Sources* 185, 584–588. <https://doi.org/10.1016/j.jpowsour.2008.07.014>.
- Lee, H.J., Chen, P., Moon, S.J., Sauvage, F., Sivula, K., Bessho, T., Gamelin, D.R., Comte, P., Zakeeruddin, S.M., Il Seok, S., Grätzel, M., Nazeeruddin, M.K., 2009. Regenerative PbS and CdS quantum dot sensitized solar cells with a cobalt complex as hole mediator. *Langmuir* 25, 7602–7608. <https://doi.org/10.1021/la900247r>.
- Lee, H., Leventis, H.C., Moon, S.-J., Chen, P., Ito, S., Haque, S.A., Torres, T., Nüesch, F., Geiger, T., Zakeeruddin, S.M., Grätzel, M., Nazeeruddin, M.K., 2009. PbS and CdS quantum dot-sensitized solid-state solar cells: "Old concepts, new results". *Adv. Funct. Mater.* 19, 2735–2742. <https://doi.org/10.1002/adfm.200900081>.
- Lee, Y.L., Lo, Y.S., 2009. Highly efficient quantum-dot-sensitized solar cell based on co-sensitization of CdS/CdSe. *Adv. Funct. Mater.* 19, 604–609. <https://doi.org/10.1002/adfm.200800940>.
- Lee, H., Wang, M., Chen, P., Gamelin, D.R., Zakeeruddin, S.M., Gra, M., 2009. Efficient CdSe Quantum Dot-Sensitized Solar Cells Prepared by an Improved Successive Ionic Layer Adsorption and Reaction Process. *NANO*.
- Lee, H., Wang, M., Chen, P., Gamelin, D.R., Zakeeruddin, S.M., Gra, M., 2009. Efficient CdSe Quantum Dot-Sensitized Solar Cells Prepared by an Improved Successive Ionic Layer Adsorption and Reaction Process. *Nano Lett.* 9, 4221–4227.
- Lee, H.J., Yun, J., Leventis, H.C., Zakeeruddin, S.M., Saif, A., Chen, P., Il Seok, S., Gra, M., Nazeeruddin, K., Haque, S.A., 2008. CdSe Quantum Dot-Sensitized Solar Cells Exceeding Efficiency 1% at Full-Sun Intensity CdSe Quantum Dot-Sensitized Solar Cells Exceeding Efficiency 1% at Full-Sun Intensity. *J. Phys. Chem. C* 112, 11600–11608. <https://doi.org/10.1021/jp802572b>.
- Leschkies, K.S., Divakar, R., Basu, J., Enache-Pommer, E., Boercker, J.E., Carter, C.B., Kortshagen, U.R., Norris, D.J., Aydin, E.S., 2007. Photosensitization of ZnO nanowires with CdSe quantum dots for photovoltaic devices. *Nano Lett.* 7, 1793–1798. <https://doi.org/10.1021/nl070430o>.
- Li, X.-Q., Arakawa, Y., 1998. Anharmonic decay of confined optical phonons in quantum dots. *Phys. Rev. B* 57, 12285. <https://doi.org/10.1103/PhysRevB.57.12285>.
- Li, Y., Pang, A., Zheng, X., Wei, M., 2011. CdS quantum-dot-sensitized Zn₂SnO₄ solar cell. *Electrochim. Acta* 56, 4902–4906. <https://doi.org/10.1016/j.electacta.2011.02.071>.
- Li, Z., Zhou, Y., Zhang, J., Tu, W., Liu, Q., Yu, T., Zou, Z., 2012. Hexagonal nanoplate-textured micro-octahedron Zn₂SnO₄: Combined effects toward enhanced efficiencies of dye-sensitized solar cell and photoreduction of CO₂ into hydrocarbon fuels. *Cryst. Growth Des.* 12, 1476–1481. <https://doi.org/10.1021/cg201568q>.
- Liu, D., Kamat, P.V., 1993. Photoelectrochemical behavior of thin cadmium selenide and coupled titania/cadmium selenide semiconductor films. *J. Phys. Chem.* 97, 10769–10773. <https://doi.org/10.1021/j100143a041>.
- Liu, C., Mu, L., Jia, J., Zhou, X., Lin, Y., 2013. Electrochimica Acta Boosting the cell efficiency of CdSe quantum dot sensitized solar cell via a modified ZnS post-treatment. *Electrochim. Acta* 111, 179–184. <https://doi.org/10.1016/j.electacta.2013.07.220>.
- Liu, Z., Zhou, D., Gong, S., Li, H., 2009. Studies on a basic question of zinc titanates. *J. Alloys Compd.* 475, 840–845. <https://doi.org/10.1016/j.jallcom.2008.08.021>.
- Lowisch, M., Rabe, M., Kreller, F., Henneberger, F., 1999. Electronic excitations and longitudinal optical phonon modes of self-assembled CdSe quantum dots revealed by microprobe studies. *Appl. Phys. Lett.* 74, 2489–2491. <https://doi.org/10.1063/1.123016>.
- Luo, J., Wei, H., Huang, Q., Hu, X., Zhao, H., Yu, R., Li, D., Luo, Y., Meng, Q., 2013. Highly efficient core-shell CuInS₂-Mn doped CdS quantum dot sensitized solar cells. *Chem. Commun. (Camb)* 49, 3881–3883. <https://doi.org/10.1039/C3CC40715B>.
- Manna, L., Scher, E.C., Alivisatos, A.P., 2000. Synthesis of Soluble and Processable Rod-, Arrow-, Teardrop-, and Tetrapod-Shaped CdSe Nanocrystals. *J. Am. Chem. Soc.* 122, 12700–12706. <https://doi.org/10.1021/ja003055+>.
- Mathew, S., Yella, A., Gao, P., Humphry-Baker, R., Curchod, B.F.E., Ashari-Astani, N., Tavernelli, I., Rothlisberger, U., Nazeeruddin, M.K., Grätzel, M., 2014. Dye-sensitized solar cells with 13% efficiency achieved through the molecular engineering of porphyrin sensitizers. *Nat. Chem.* 6, 242–247. <https://doi.org/10.1038/nchem.1861>.
- Matsui, T., Maejima, K., Bidiville, A., Sai, H., Koida, T., Suezaki, T., 2015. High-efficiency thin-film silicon solar cells realized by integrating stable a-Si:H absorbers into improved device design High-efficiency thin-film silicon solar cells realized by integrating stable a-Si:H absorbers into improved device design. *Jpn. J. Appl. Phys.* 54 08KB10. <https://doi.org/10.7567/JJP.54.08KB10>.
- Meier, A., Kocha, S.S., Hanna, M.C., Nozik, A.J., Siemonite, K., Reineke-Koch, R., Memming, R., 1997. Electron Transfer Rate Constants for Majority Electrons at GaAs

- and GaInP2 Semiconductor – Liquid Interfaces. *J. Phys. Chem. B.* 101, 7038–7042. <https://doi.org/10.1021/jp9714882>.
- Meier, A., Selmarthen, D.C., Siemoneit, K., Smith, B.B., Nozik, A.J., 1999. Fast Electron Transfer Across Semiconductor – Molecule Interfaces: GaAs/Co(Cp)2 + /O. *J. Phys. Chem. B.* 103, 2122–2141. <https://doi.org/10.1021/jp983230x>.
- Memming, R., 2000. Semiconductor Electrochemistry. <https://doi.org/10.1002/9783527613069>.
- Meng, L., Li, C., 2011. Blocking Layer Effect on Dye-Sensitized Solar Cells Assembled with TiO(2) Nanorods Prepared by dc Reactive Magnetron Sputtering. *Nanosci. Nanotechnol. Lett.* 3, 181–185. <https://doi.org/10.1166/nnl.2011.1143>.
- Milliron, D.J., 2014. Quantum dot solar cells: The surface plays a core role. *Nat. Mater.* 13, 772–773. <https://doi.org/10.1038/nmat4032>.
- Mishima, T., Taguchi, M., Sakata, H., Maruyama, E., 2011. Solar Energy Materials & Solar Cells Development status of high-efficiency HIT solar cells. *Sol. Energy Mater. Sol. Cells.* 95, 18–21. <https://doi.org/10.1016/j.solmat.2010.04.030>.
- Mohmeyer, N., Wang, P., Schmidt, H.-W.H.-W., Zakeeruddin, S.M., Grätzel, M., 2004. Quasi-solid-state dye sensitized solar cells with 1,3,2,4-di-O-benzylidene-D-sorbitol derivatives as low molecular weight organic gelators. *J. Mater. Chem.* 14, 1905–1909. <https://doi.org/10.1039/b402324b>.
- Mohmeyer, N., Kuang, D., Wang, P., Schmidt, H.-W., Zakeeruddin, S.M., Graetzel, M., 2006. An efficient organogelator for ionic liquids to prepare stable quasi-solid-state dye-sensitized solar cells. *J. Mater. Chem.* 16, 2978. <https://doi.org/10.1039/b604021g>.
- Moos, R., Meneskou, W., Härdtl, K.H., 1995. Hall mobility of undoped n-type conducting strontium titanate single crystals between 19 K and 1373 K. *Appl. Phys. A Mater. Sci. Process.* 61, 389–395. <https://doi.org/10.1007/BF01540113>.
- Mora-Seró, I., Bisquert, J., 2010. Breakthroughs in the development of semiconductor-sensitized solar cells. *J. Phys. Chem. Lett.* 1, 3046–3052. <https://doi.org/10.1021/jz100863b>.
- Mora-Seró, I., Giménez, S., Moehl, T., Fabregat-Santiago, F., Lana-Villareal, T., Gómez, R., Bisquert, J., 2008. Factors determining the photovoltaic performance of a CdSe quantum dot sensitized solar cell: the role of the linker molecule and of the counter electrode. *Nanotechnology.* 19, 424007. <https://doi.org/10.1088/0957-4448/19/42/424007>.
- Mora-Seró, I., Giménez, S., Fabregat-Santiago, F., Gómez, R., Shen, Q., Toyoda, T., Bisquert, J., 2009. Recombination in quantum dot sensitized solar cells. *Acc. Chem. Res.* 42, 1848–1857. <https://doi.org/10.1021/ar900134d>.
- Mori, S., Oh-oka, H., Nakao, H., Gotanda, T., Nakano, Y., Jung, H., Iida, A., Hayase, R., Shida, N., Saito, M., Todori, K., Asakura, T., Matsui, A., Hosoya, M., 2015. Organic photovoltaic module development with inverted device structure. *MRS Proc.* 1737. <https://doi.org/10.1557/proc.2015.540>. mrsf14-1737-u17-02.
- Mulvaney, P., Grieser, F., Meisel, D., 1990. Electron Transfer in Aqueous Colloidal SnO₂ Solutions. *Langmuir* 6, 567–572. <https://doi.org/10.1021/la00093a009>.
- Murdin, B.N., Hollingworth, A.R., Kamal-Saadi, M., Kotitschke, R.T., Ciesla, C.M., Pidgeon, C.R., Findlay, P.C., Pellemans, H.P.M., Langerak, C.J.G.M., Rowe, A.C., Stradling, R.A., Gornik, E., 1999. Suppression of LO phonon scattering in Landau quantized quantum dots. *Phys. Rev. B.* 59, 7817–7820. <https://doi.org/10.1103/PhysRevB.59.R7817>.
- Murphy, J.E., Beard, M.C., Nozik, A.J., 2006. Time-resolved photoconductivity of PbSe nanocrystal arrays. *J. Phys. Chem. B.* 110, 25455–25461. <https://doi.org/10.1021/jp0646123>.
- Murphy, J.E., Beard, M.C., Norman, A.G., Ahrenkiel, S.P., Johnson, J.C., Yu, P., Mićić, O.I., Ellingson, R.J., Nozik, A.J., 2006. PbTe colloidal nanocrystals: Synthesis, characterization, and multiple exciton generation. *J. Am. Chem. Soc.* 128, 3241–3247. <https://doi.org/10.1021/ja0574973>.
- Murray, C.B., Norris, D.J., Bawendi, M.G., 1993. Synthesis and Characterization of Nearly Monodisperse Cd_E (E = S, Se, Te) Semiconductor Nanocrystallites. *J. Am. Chem. Soc.* 115, 8706–8715. <https://doi.org/10.1021/ja00072a025>.
- Niitsoo, O., Sarkar, S.K., Pejoux, C., Rühle, S., Cahen, D., Hodas, G., 2006. Chemical bath deposited CdS/CdSe-sensitized porous TiO₂ solar cells. *J. Photochem. Photobiol. A Chem.* 181, 306–313. <https://doi.org/10.1016/j.jphotochem.2005.12.012>.
- Ning, Z., Tian, H., Yuan, C., Fu, Y., Qin, H., Sun, L., Ågren, H., 2011. Solar cells sensitized with type-II ZnSe–CdS core/shell colloidal quantum dots. *Chem. Commun.* 47, 1536–1538. <https://doi.org/10.1039/COCC03401K>.
- Ning, Z., Dong, H., Zhang, Q., Voznyy, O., Sargent, E.H., 2014. Solar cells based on inks of n-type colloidal quantum dots. *ACS Nano* 8, 10321–10327. <https://doi.org/10.1021/nm503569p>.
- Nowotny, M.K., Sheppard, L.R., Bak, T., Nowotny, J., 2008. Defect chemistry of titanium dioxide. Application of defect engineering in processing of TiO₂-based photocatalysts. *J. Phys. Chem. C.* 112, 5275–5300. <https://doi.org/10.1021/jp077275m>.
- Nozik, A.J., 2001. Spectroscopy and Hot Electron Relaxation Dynamics in Semiconductors Quantum Wells and Quantum Dots. *Annu. Rev. Phys. Chem.* 52, 193–231. <https://doi.org/10.1146/annurev.physchem.52.1.193>.
- Nozik, A.J., 2002. Quantum dot solar cells. *Phys. E Low-Dimensional Syst. Nanostructures.* 14, 115–120. [https://doi.org/10.1016/S1386-9477\(02\)00374-0](https://doi.org/10.1016/S1386-9477(02)00374-0).
- Nozik, A.J., 2008. Multiple exciton generation in semiconductor quantum dots. *Chem. Phys. Lett.* 457, 3–11. <https://doi.org/10.1016/j.cplett.2008.03.094>.
- O'Regan, B., Moser, J., Anderson, M., Graetzel, M., 1990. Vectorial electron injection into transparent semiconductor membranes and electric field effects on the dynamics of light-induced charge separation. *J. Phys. Chem.* 94, 8720–8726. <https://doi.org/10.1021/J100387a017>.
- Ogermann, D., Wilke, T., Kleinermanns, K., 2012. CdSxSe/TiO₂ Solar Cell Prepared with Sintered Mixture Deposition. *J. Phys. Chem. C.* 116, 47–57. <https://doi.org/10.4236/oipc.2012.21007>.
- Okazaki, K., Kojima, N., Tachibana, Y., Kuwabata, S., Torimoto, T., 2007. One-step Preparation and Photosensitivity of Size-quantized Cadmium Chalcogenide Nanoparticles Deposited on Porous Zinc Oxide Film Electrodes. *Chem. Lett.* 36, 712–713. <https://doi.org/10.1246/cl.2007.712>.
- Oregan, B., Grätzel, M., 1991. a Low-Cost, High-Efficiency Solar-Cell Based on Dye-Sensitized Colloidal TiO₂ Films. *Nature* 353, 737–740. <https://doi.org/10.1038/353737a0>.
- Ortega-Borges, R., 1993. Mechanism of Chemical Bath Deposition of Cadmium Sulfide Thin Films in the Ammonia-Thiourea System. *J. Electrochem. Soc.* 140, 3464. <https://doi.org/10.1149/1.2221111>.
- Pan, Z., Zhao, K., Wang, J., Zhang, H., Feng, Y., Zhong, X., 2013. Near Infrared Absorption of CdSe x Te 1-x Alloyed Quantum Dot Sensitized Solar Cells with More than 6% Efficiency and High Stability. *ACS Nano* 7, 5215–5222. <https://doi.org/10.1021/nn400947e>.
- Pandikumar, R., Ramaraj, Alagarsamy, 2018. Rational Design of Solar Cells for Efficient Solar Energy Conversion, first ed.
- Park, J., Joo, J., Soon, G.K., Jang, Y., Hyeon, T., 2007. Synthesis of monodisperse spherical nanocrystals. *Angew. Chemie - Int. Ed.* 46, 4630–4660. <https://doi.org/10.1002/anie.200603148>.
- Park, N.-G., van de Lagemaat, J., Frank, A.J., 2000. Comparison of Dye-Sensitized Rutile- and Anatase-Based TiO₂ Solar Cells. *J. Phys. Chem. B.* 104, 8989–8994. <https://doi.org/10.1021/jp994365l>.
- Pattantyus-abraham, A.G., Kramer, K.I.J., Barkhouse, K.A.R., Wang, X., Konstantatos, G., Debnath, R., Levina, L., Raabe, I., Nazeeruddin, M.K., Sargent, E.H., 2010. Depleted-Heterojunction Colloidal Quantum Dot Solar Cells. *ACS Nano* 4, 3374–3380. <https://doi.org/10.1021/mn100335g>.
- Pelouch, W.S., Ellingson, R.J., Powers, P.E., Tang, C.L., Szmyd, D.M., Nozik, A.J., 1992. Investigation of hot-carrier relaxation in quantum wells and bulk GaAs at high carrier densities. *Semicond. Sci. Technol.* 7, B337–B339. <https://doi.org/10.1103/PhysRevB.45.1450>.
- Pelouch, W.S., Ellingson, R.J., Powers, P.E., Tang, C.L., 1992. Comparison of hot-carrier relaxation in quantum wells and bulk GaAs at high carrier densities. *Phys. Rev. B.* 45, 1450–1453.
- Pernik, D.R., Tvrđ, K., Radich, J.G., Kamat, P.V., 2011. Tracking the adsorption and electron injection rates of CdSe quantum dots on TiO₂: Linked versus direct attachment. *J. Phys. Chem. C.* 115, 13511–13519. <https://doi.org/10.1021/jp203055d>.
- Peter, L.M., Riley, D.J., Tull, J., Wijayantha, K.G.U., 2002. Photosensitization of nanocrystalline TiO₂ by self-assembled layers of CdS quantum dots. *Chem. Comm.* 1030–1031. <https://doi.org/10.1039/b201661c>.
- Pichot, F., Gregg, B.A., 2000. The Photovoltage-Determining Mechanism in Dye-Sensitized Solar Cells. *J. Phys. Chem. B.* 104, 6–10. <https://doi.org/10.1021/jp993035y>.
- Pichot, F., Gregg, B.A., 2000. The Photovoltage-Determining Mechanism in Dye-Sensitized Solar Cells Franc. *J. Phys. Chem. B.* 104, 6–10.
- Pijpers, J.J.H., Hendry, E., Milder, M.T.W., Fanciulli, R., Savolainen, J., Herek, J.L., Vanmaekelbergh, D., Ruhmen, S., Mocatta, D., Oron, D., Aharoni, A., Banin, U., Bonn, M., 2007. Carrier multiplication and its reduction by photodoping in colloidal InAs quantum dots. *J. Phys. Chem. C.* 111, 4146–4152. <https://doi.org/10.1021/jp066709v>.
- Powell, R.C., Soos, Z.G., 1975. Singlet exciton energy transfer in organic solids. *J. Lumin.* 11, 1–45. [https://doi.org/10.1016/0022-2313\(75\)90077-0](https://doi.org/10.1016/0022-2313(75)90077-0).
- Qian, J., Liu, Q.-S., Li, G., Jiang, K.-J., Yang, L.-M., Song, Y., 2011. P3HT as hole transport material and assistant light absorber in CdS quantum dots-sensitized solid-state solar cells. *Chem. Commun. (Camb)* 47, 6461–6463. <https://doi.org/10.1039/c1cc11595b>.
- Qu, L., Peng, X., 2002. Control of photoluminescence properties of CdSe nanocrystals in growth. *J. Am. Chem. Soc.* 124, 2049–2055. <https://doi.org/10.1021/ja017002j>.
- Radisch, J.G., Dwyer, R., Kamat, P.V., 2011. Cu₂S Reduced Graphene Oxide Composite for High-Efficiency Quantum Dot Solar Cells: Overcoming the Redox Limitations of S₂/Sn₂- at the Counter Electrode. *J. Phys. Chem. Lett.* 2, 2453–2460.
- Rajendra Prasad, M.B., Kadam, V., Joo, O.S., Pathan, H.M., 2017. Improving the photovoltaic parameters in Quantum dot sensitized solar cells through employment of chemically deposited compact titania blocking layer. *Mater. Chem. Phys.* 194, 165–171. <https://doi.org/10.1016/j.matchemphys.2017.03.027>.
- Redmond, G., Fitzmaurice, D., Graetzel, M., 1994. Visible Light Sensitization by cis-Bis (thiocyanato)bis(2,2'-bipyridyl-4,4'-dicarboxylato)ruthenium(II) of a Transparent Nanocrystalline ZnO Film Prepared by Sol-Gel Techniques. *Chem. Mater.* 6, 686–691. <https://doi.org/10.1021/cm00041a020>.
- Reiss, H., 1951. The Growth of Uniform Colloidal Dispersions. *J. Chem. Phys.* 19, 482–487. <https://doi.org/10.1063/1.1748251>.
- Ren, Z., Wang, J., Pan, Z., Zhao, K., Zhang, H., Li, Y., Zhao, Y., Mora-Sero, I., Bisquert, J., Zhong, X., 2015. Amorphous TiO₂ Buffer Layer Boosts Efficiency of Quantum Dot Sensitized Solar Cells to over 9%. *Chem. Mater.* 27, 8398–8405. <https://doi.org/10.1021/acs.chemmater.5b03864>.
- Rezaee, Masih, Mousavi Khoie, Seyyed Mohammad, Liu, Kun Hua, 2011. The role of brookite in mechanical activation of anatase-to-rutile transformation of nanocrystalline TiO₂: An XRD and Raman spectroscopy investigation. *CrystEngComm* 13 (16), 5055. <https://doi.org/10.1039/c1ce05185g>.
- Robel, I., Subramanian, V., Kuno, M., Kamat, P.V., 2006. Quantum dot solar cells. Harvesting light energy with CdSe nanocrystals molecularly linked to mesoscopic TiO₂ films. *J. Am. Chem. Soc.* 128, 2385–2393. <https://doi.org/10.1021/ja056494n>.
- Robel, I., Kuno, M., Kamat, P.V., 2007. Size-dependent electron injection from excited CdSe quantum dots into TiO₂ nanoparticles. *J. Am. Chem. Soc.* 129, 4136–4137. <https://doi.org/10.1021/ja070099a>.
- Rosenwaks, Y., Hanna, M.C., Levi, D.H., Szmyd, D.M., Ahrenkiel, D.M., Nozik, A.J., 1993. Hot-carrier cooling in GaAs: Quantum wells versus bulk. *Phys. Rev. B.* 48, 14675–15678.
- Ross, R.T., Nozik, A.J., 1982. Efficiency of hotcarrier solar energy converters. *J. Appl.*

- Phys. 53, 3813–3818. <https://doi.org/10.1063/1.331124>.
- Rühle, S., Shalom, M., Zaban, A., 2010. Quantum-dot-sensitized solar cells. *ChemPhysChem* 11, 2290–2304. <https://doi.org/10.1002/cphc.201000069>.
- Ruhle, S., Yahav, S., Greenwald, S., Zaban, A., 2012. Importance of recombination at the TCO/electrolyte interface for high efficiency quantum dot sensitized solar cells. *J. Phys. Chem. C* 116, 17473–17478. <https://doi.org/10.1021/jp306782q>.
- Sai, H., Maejima, K., Matsui, T., Koida, T., Matsubara, K., Kondo, M., Takeuchi, Y., Sugiyama, S., Katayama, H., Yoshida, I., 2015. Effect of Front TCO Layer on Properties of Substrate-Type Thin-Film Microcrystalline Silicon Solar Cells. *IEEE J. Photovoltaics* 5, 1528–1533. <https://doi.org/10.1109/JPHOTOV.2015.2478030>.
- Salant, A., Shalom, M., Hod, I., Faust, A., Zaban, A., Banin, U., 2010. Quantum Dot Sensitized Solar Cells with Improved Efficiency Prepared Using Electrophoretic Deposition. *ACS Nano* 4, 5962–5968. <https://doi.org/10.1039/C5TA04021C>.
- Salaramoli, H., Maleki, E., Sharatinia, Z., Ranjbar, M., 2013. CdS/CdSe quantum dots co-sensitized solar cells with Cu2S counter electrode prepared by SILAR, spray pyrolysis and Zn-Cu alloy methods. *J. Photochem. Photobiol. A Chem.* 271, 56–64. <https://doi.org/10.1016/j.jphotochem.2013.08.006>.
- Samadpour, M., Iraji zad, A., Taghavinia, N., Molaei, M., 2011. A new structure to increase the photostability of CdTe quantum dot sensitized solar cells. *J. Phys. D. Appl. Phys.* 44. <https://doi.org/10.1088/0022-3727/44/4/045103>.
- Sambur, J.B., Novet, T., Parkinson, B.A., 2010. Multiple Exciton collection in a sensitized photovoltaic system. *Science* (80–) 330, 63–66. <https://doi.org/10.1126/science.1191462>.
- Santra, P.K., Kamat, P.V., 2012. Mn-doped quantum dot sensitized solar cells: A strategy to boost efficiency over 5%. *J. Am. Chem. Soc.* 134, 2508–2511. <https://doi.org/10.1021/ja211224s>.
- Santra, P.K., Nair, P.V., George Thomas, K., Kamat, P.V., 2013. CuInS2-sensitized quantum dot solar cell: electrophoretic deposition, excited-state dynamics, and photovoltaic performance. *J. Phys. Chem. Lett.* 4, 722–729. <https://doi.org/10.1021/jz400181m>.
- Sato, N., 1998. Electrochemistry at Metal and Semiconductor Electrodes, First 1998, Elsevier Science B.V. doi:10.1016/B978-044482806-4/50010-6.
- Schaller, R.D., Klimov, V.I., 2004. High efficiency carrier multiplication in PbSe nanocrystals: Implications for solar energy conversion. *Phys. Rev. Lett.* 92, 186601–186611. <https://doi.org/10.1103/PhysRevLett.92.186601>.
- Schaller, R.D., Petruska, M.A., Klimov, V.I., 2005. Effect of electronic structure on carrier multiplication efficiency: Comparative study of PbSe and CdSe nanocrystals. *Appl. Phys. Lett.* 87, 1–3. <https://doi.org/10.1063/1.2142092>.
- Schaller, R.D., Pietryga, J.M., Klimov, V.I., 2007. Carrier multiplication in InAs nanocrystal quantum dots with an onset defined by the energy conservation limit. *Nano Lett.* 7, 3469–3476. <https://doi.org/10.1021/nl072046x>.
- Schaller, R.D., Petruska, M.A., Klimov, V.I., 2005. Effect of electronic structure on carrier multiplication efficiency: Comparative study of PbSe and CdSe nanocrystals. *Appl. Phys. Lett.* 87, 1–3. <https://doi.org/10.1063/1.2142092>.
- Schwarzburg, K., Willig, F., 1991. Influence of trap filling on photocurrent transients in polycrystalline TiO₂. *Appl. Phys. Lett.* 2520, 2520–2522.
- Schwarzburg, K., Willig, F., 1999. Origin of Photovoltage and Photocurrent in the Nanoporous Dye-Sensitized Electrochemical Solar Cell. *J. Phys. Chem. B* 103, 5743–5746. <https://doi.org/10.1021/jp990312s>.
- Semonin, O.E., Luther, J.M., Choi, S., Chen, H.-Y., Gao, J., Nozik, A.J., Beard, M.C., 2011. Peak external photocurrent quantum efficiency exceeding 100% via MEG in a quantum dot solar cell. *Science* (80–) 334, 1530–1533. <https://doi.org/10.1126/science.1209845>.
- Sercel, P.C., 1995. Multiphonon-assisted tunneling through deep levels: A rapid energy-relaxation mechanism in nonideal quantum-dot heterostructures. *Phys. Rev. B* 51, 14532–14541. <https://doi.org/10.1103/PhysRevB.51.14532>.
- Shabaev, A., Efros, A.L., Nozik, A.J., 2006. Multiexciton generation by a single photon in nanocrystals. *Nano Lett.* 6, 2856–2863. <https://doi.org/10.1021/nl062059v>.
- Shalom, M., Dor, S., Rühle, S., Grinis, L., Zaban, A., 2009. Core/CdS Quantum Dot/Shell Mesoporous Solar Cells with Improved Stability and Efficiency Using an Amorphous TiO₂ Coating. *J. Phys. Chem. C* 113, 3895–3898. <https://doi.org/10.1021/jp8108682>.
- She, C., Anderson, N.A., Guo, J., Liu, F., Goh, W.H., Chen, D.T., Mohler, D.L., Tian, Z.Q., Hupp, J.T., Lian, T., 2005. PH-dependent electron transfer from re-bipyridyl complexes to metal oxide nanocrystalline thin films. *J. Phys. Chem. B* 109, 19345–19355. <https://doi.org/10.1021/jp053948u>.
- Shen, Q., Yamada, A., Tamura, S., Toyoda, T., 2010. CdSe quantum dot-sensitized solar cell employing TiO₂ nanotube working-electrode and Cu2 S counter-electrode. *Appl. Phys. Lett.* 97, 5–7. <https://doi.org/10.1063/1.3491245>.
- Shockley, W., Queisser, H.J., 1961. Detailed balance limit of efficiency of p-n junction solar cells. *J. Appl. Phys.* 32, 510–519. <https://doi.org/10.1063/1.1736034>.
- Shu, T., Zhou, Z., Wang, H., Liu, G., Xiang, P., Rong, Y., Han, H., Zhao, Y., 2012. Efficient quantum dot-sensitized solar cell with tunable energy band CdSexS(1-x) quantum dots. *J. Mater. Chem.* 22, 10525. <https://doi.org/10.1039/c2jm31177a>.
- Smith, D.K., Luther, J.M., Semonin, O.E., Nozik, A.J., Beard, M.C., 2011. Tuning the synthesis of ternary lead chalcogenide quantum dots by balancing precursor reactivity. *ACS Nano* 5, 183–190. <https://doi.org/10.1021/nm102878u>.
- Soedergren, S., Hagfeldt, A., Ollsson, J., Lindquist, S.-E., 1994. Theoretical Models for the Action Spectrum and the Current-Voltage Characteristics of Microporous Semiconductor Films in Photoelectrochemical Cells. *J. Phys. Chem.* 98, 5552–5556. <https://doi.org/10.1021/j100072a023>.
- Solbrand, A., Keis, K., So, S., Lindstro, H., Lindquist, S., Hagfeldt, A., 2000. Charge transport properties in the nanostructured ZnO thin {Im electrode} electrolyte system studied with time resolved photocurrents. *Sol. Energy Mater.* 60, 181–193. [https://doi.org/10.1016/S0927-0248\(99\)00083-5](https://doi.org/10.1016/S0927-0248(99)00083-5).
- Sosnowski, T., Norris, T., Jiang, H., Singh, J., Kamath, K., Bhattacharya, P., 1998. Rapid carrier relaxation in In0.4Ga0.6As/GaAs quantum dots characterized by differential transmission spectroscopy. *Phys. Rev. B* 57 R9423–R9426. <https://doi.org/10.1103/PhysRevB.57.R9423>.
- Sowa, H., Ahhsbahs, H., 2006. High-pressure X-ray investigation of zincite ZnO single crystals using diamond anvils with an improved shape. *J. Appl. Crystallogr.* 39, 169–175. <https://doi.org/10.1107/S0021889805042457>.
- Spanhel, Y., Haase, M., Weller, H., Henglein, A., 1987. Photochemistry of Colloidal Semiconductors. 20. Surface Modification and Stability of Strong Luminescing CdS Particles. *J. Am. Chem. Soc.* 109, 5649–5655. <https://doi.org/10.1021/ja00253a015>.
- Steigerwald, M.L., Brus, L., 1989. Synthesis, Stabilization and Electronic structure of Quantum Semiconductor Nanoclusters. *Annu. Rev. Mater. Sci.* 19, 471–495.
- Steigerwald, M.L., Brus, L.E., 1990. Semiconductor Crystallites: A Class of Large Molecules. *Acc. Chem. Res.* 23, 183–188. <https://doi.org/10.1021/ar00174a003>.
- Sun, K., Yan, C., Liu, F., Huang, J., Zhou, F., Stride, J.A., Green, M., Hao, X., 2016. Over 9% Efficient Kesterite Cu2ZnSnS4Solar Cell Fabricated by Using Zn1-xCdx Buffer Layer. *Adv. Energy Mater.* 6, 4–9. <https://doi.org/10.1002/aenm.201600046>.
- Tachan, Z., Shalom, M., Hod, I., Rühle, S., Tirosh, S., Zaban, A., 2011. PbS as a highly catalytic counter electrode for polysulfide based quantum dot solar cells 6162–6166.
- Tachibana, Y., Umekita, K., Otsuka, Y., Kuwabata, S., 2008. Performance improvement of CdS quantum dots sensitized TiO₂ solar cells by introducing a dense TiO₂ blocking layer. *J. Phys. D. Appl. Phys.* 41, 102002. <https://doi.org/10.1088/0022-3727/41/10/102002>.
- Tagliazucchi, M., Tice, D.B., Sweeney, C.M., Morris-Cohen, A.J., Weiss, E.A., 2011. Ligand-controlled rates of photoinduced electron transfer in hybrid CdSe nanocrystal/poly(viologen) films. *ACS Nano* 5, 9907–9917. <https://doi.org/10.1021/nn1203683s>.
- Taguchi, M., Yano, A., Tohoda, S., Matsuyama, K., Nakamura, Y., Nishiaki, T., Fujita, K., Maruyama, E., 2014. 24.7% Record efficiency HIT solar cell on thin silicon wafer. *IEEE J. Photovoltaics* 4 96–99. <https://doi.org/10.1109/JPHOTOV.2013.2282737>.
- Tan, B., Toman, E., Li, Y., Wu, Y., 2007. Zinc stannate (Zn₂SnO₄) dye-sensitized solar cells. *J. Am. Chem. Soc.* 129, 4162–4163. <https://doi.org/10.1021/ja070804f>.
- Tian, J., Zhang, Q., Uchaker, E., Gao, R., Qu, X., Zhang, S., Cao, G., 2013. Architectured ZnO photoelectrode for high efficiency quantum dot sensitized solar cells. *Energy Environ. Sci.* 6, 3542. <https://doi.org/10.1039/c3ee41056k>.
- Tian, J., Uchaker, E., Zhang, Q., Cao, G., 2014. Hierarchically structured ZnO nanorods–nanosheets for improved quantum-dot-sensitized solar cells. *ACS Appl. Mater. Interfaces*. 6, 4466–4472. <https://doi.org/10.1021/am500209f>.
- Tollin, G., Kearns, D.R., Calvin, M., 1960. Electrical Properties of Organic Solids. 1. Kinetics and Mechanism of Conductivity of Metal-free Phthalocyanine. *J. Chem. Phys.* 32, 1013–1019.
- Toyoda, T., Kobayashi, J., Shen, Q., 2008. Correlation between crystal growth and photosensitization of nanostructured TiO₂ electrodes using supporting Ti substrates by self-assembled CdSe quantum dots. *Thin Solid Films* 516, 2426–2431. <https://doi.org/10.1016/j.tsf.2007.04.143>.
- Van Vechten, J.A., Bergstresser, T.K., 1970. Electronic structures of semiconductor alloys. *Phys. Rev. B* 1, 3351–3358. <https://doi.org/10.1103/PhysRevB.1.3351>.
- Vengrenovich, R.D., 1982. Overview on the owsld. *Acta Metall.* 30, 1079–1086.
- Vogel, R., Pohl, K., Weller, H., 1990. Sensitization of highly porous, polycrystalline TiO₂ electrodes by quantum sized CdS. *Chem. Phys. Lett.* 174, 241–246. [https://doi.org/10.1016/0009-2614\(90\)85339-E](https://doi.org/10.1016/0009-2614(90)85339-E).
- Vogel, R., Hoyer, P., Weller, H., 1994. Quantum-sized PbS, CdS, Ag₂S, Sb₂S₃, and Bi₂S₃ particles as sensitizers for various nanoporous wide-bandgap semiconductors. *J. Phys. Chem.* 1383–3188. <https://doi.org/10.1021/100063a022>.
- Wakisaka, K., Taguchi, M., Sawada, T., Tanaka, M., Matsuyama, T., Matsuoka, T., Tsuda, S., Nakano, S., Kishi, Y., Kuwano, Y., 1991. More than 16% solar cells with a new “HIT” (doped a-Si/nondoped a-Si/crystalline Si) structure. *Proc. 22th IEEE Photovolt. Spec. Conf. Las Vegas, NV, Oct 7–11(1991) 887–892.* <https://doi.org/10.1109/PVSC.1991.169337>.
- Wang, Q., Ito, S., Gratzel, M., Fabregat-Santiago, F., Mora-Sero, I., Bisquert, J., Bessho, T., Imai, H., 2006. Characteristics of high efficiency dye-sensitized solar cells. *J. Phys. Chem. B* 110, 25210–25221. <https://doi.org/10.1021/jp064256o>.
- Wang, C., Jiang, Z., Wei, L., Chen, Y., Jiao, J., Eastman, M., Liu, H., 2012. Photosensitization of TiO₂ nanorods with CdS quantum dots for photovoltaic applications: A wet-chemical approach. *Nano Energy* 1, 440–447. <https://doi.org/10.1016/j.nanoen.2012.02.005>.
- Wang, J., Mora-Seró, I., Pan, Z., Zhao, K., Zhang, H., Feng, Y., Yang, G., Zhong, X., Bisquert, J., 2013. Core/shell colloidal quantum dot exciplex states for the development of highly efficient quantum-dot-sensitized solar cells. *J. Am. Chem. Soc.* 135, 15913–15922. <https://doi.org/10.1021/ja4079804>.
- Wang, J., Mora-Seró, I., Pan, Z., Zhao, K., Zhang, H., Feng, Y., Yang, G., Zhong, X., Bisquert, J., 2013. Core/Shell Colloidal Quantum Dot Exciplex States for the Development of Highly Efficient Quantum-Dot-Sensitized Solar Cells. *J. Am. Chem. Soc.* 135, 15913–15922. <https://doi.org/10.1021/ja4079804>.
- Wang, T., Ren, S., Li, C., Li, W., Liu, C., Zhang, J., Wu, L., Li, B., 2018. Exploring window buffer layer technology to enhance CdTe solar cell performance Back contact Window layer 40 nm. *Sol. Energy*. 164, 180–186. <https://doi.org/10.1016/j.solener.2018.02.044>.
- Wang, M., Wang, H., Li, W., Hu, X., Sun, K., Zang, Z., 2019. Defect passivation using ultrathin PTAA layers for efficient and stable perovskite solar cells with a high fill factor and eliminated hysteresis †. *J. Mater. Chem. A*. 7, 26421–26428. <https://doi.org/10.1039/c9ta08314f>.
- Wang, S., Zhang, Q.X., Xu, Y.Z., Li, D.M., Luo, Y.H., Meng, Q.B., 2013. Single-step in-situ preparation of thin film electrolyte for quasi-solid state quantum dot-sensitized solar cells. *J. Power Sources*. 224, 152–157. <https://doi.org/10.1016/j.jpowsour.2012.09.044>.
- Watson, D.F., 2010. Linker-assisted assembly and interfacial electron-transfer reactivity of

- Quantum dot-substrate architectures. *J. Phys. Chem. Lett.* 1, 2299–2309. <https://doi.org/10.1021/jz100571u>.
- Wehrenberg, B.L., Wang, C., Guyot-Sionnest, P., 2002. Interband and intraband optical studies of PbSe colloidal quantum dots. *J. Phys. Chem. B* 106, 10634–10640. <https://doi.org/10.1021/jp021187e>.
- Weller, H., 1991. Quantum sized semiconductor particles in solution and in modified layers. *Berichte Der Bunsengesellschaft Für Phys. Chem.* 95, 1361–1365 papers3://publication/uuid/CCFBF6F6-4E7C-4AB2-AC15-177A744FCF81.
- Willig, F., Burfeindt, B., Schwarzbürg, K., Hannappel, T., Storck, W., 1997. Experimental results and basic considerations concerning injection and transport of electrons in the dye-sensitized colloidal sponge-type anatase TiO₂ electrode. *Proc. Indian Acad. Sci. - Chem. Sci.* 109, 415–428 c:/pdflib/00013490.pdf.
- Yang, Z., Chang, H.-T., 2010. CdHgTe and CdTe quantum dot solar cells displaying an energy conversion efficiency exceeding 2%. *Sol. Energy Mater. Sol. Cells.* 94, 2046–2051. <https://doi.org/10.1016/j.solmat.2010.06.013>.
- Yang, Z., Chen, C.-Y., Liu, C.-W., Chang, H.-T., 2010. Electrocatalytic sulfur electrodes for CdS/CdSe quantum dot-sensitized solar cells. *Chem. Commun.* 46, 5485. <https://doi.org/10.1039/c0cc00642d>.
- Yang, Z., Chen, C.Y., Liu, C.W., Li, C.L., Chang, H.T., 2011. Quantum dot-sensitized solar cells featuring CuS/CoS electrodes provide 4.1% efficiency. *Adv. Energy Mater.* 1, 259–264. <https://doi.org/10.1002/aenm.201000029>.
- Yang, W.S., Noh, J.H., Jeon, N.J., Kim, Y.C., Ryu, S., Seo, J., Il Seok, S., 2015. High-performance photovoltaic perovskite layers fabricated through intramolecular exchange. *Science* (80-) 348, 1234–1237. <https://doi.org/10.1126/science.aaa9272>.
- Yang, J., Kim, J.-Y., Yu, J.H., Ahn, T.-Y., Lee, H., Choi, T.-S., Kim, Y.-W., Joo, J., Ko, M.J., Hyeon, T., 2013. Copper-indium–selenide quantum dot-sensitized solar cells. *Phys. Chem. Chem. Phys.* 15, 20517. <https://doi.org/10.1039/c3cp54270j>.
- Yang, C.C., Li, S., 2008. Size, dimensionality, and constituent stoichiometry dependence of bandgap energies in semiconductor quantum dots and wires. *J. Phys. Chem. C* 112, 2851–2856. <https://doi.org/10.1021/jp076694g>.
- Yeh, M.H., Lee, C.P., Chou, C.Y., Lin, L.Y., Wei, H.Y., Chu, C.W., Vittal, R., Ho, K.C., 2011. Conducting polymer-based counter electrode for a quantum-dot-sensitized solar cell (QDSSC) with a polysulfide electrolyte. *Electrochim. Acta* 57, 277–284. <https://doi.org/10.1016/j.electacta.2011.03.097>.
- Yoshikawa, K., Kawasaki, H., Yoshida, W., Irie, T., Konishi, K., Nakano, K., Uto, T., Adachi, D., Kanematsu, M., Uzu, H., Yamamoto, K., 2017. Silicon heterojunction solar cell with interdigitated back contacts for a photoconversion efficiency over 26%. *Nat. Energy*. 2. <https://doi.org/10.1038/nenergy.2017.32>.
- Yu, J., Li, D., Zhu, L., Xu, X., 2016. Application of ZnTiO₃ in quantum-dot-sensitized solar cells and numerical simulations using first-principles theory. *J. Alloys Compd.* 681, 88–95. <https://doi.org/10.1016/j.jallcom.2016.04.224>.
- Yu, L., Li, Z., Song, H., 2017. The influence of linker molecule on photovoltaic performance of CdS quantum dots sensitized translucent TiO₂nanotube solar cells. *J. Mater. Sci. Mater. Electron.* 28, 2867–2876. <https://doi.org/10.1007/s10854-016-5871-9>.
- Yu, X.Y., Liao, J.Y., Qiu, K.Q., Bin Kuang, D., Su, C.Y., 2011. Dynamic study of highly efficient CdS/CdSe quantum dot-sensitized solar cells fabricated by electrodeposition. *ACS Nano* 5, 9494–9500. <https://doi.org/10.1021/nn203375g>.
- Yu, W.W., Qu, L., Guo, W., Peng, X., 2003. Experimental Determination of the Extinction Coefficient of CdTe, CdSe, and CdS Nanocrystals 125, 2854–2860. <https://doi.org/10.1021/cm034081k>.
- Yu, Z., Zhang, Q., Qin, D., Luo, Y., Li, D., Shen, Q., Toyoda, T., Meng, Q., 2010. Highly efficient quasi-solid-state quantum-dot-sensitized solar cell based on hydrogel electrolytes. *Electrochim. Commun.* 12, 1776–1779. <https://doi.org/10.1016/j.elecom.2010.10.022>.
- Yun, D., Feng, W., Wu, H., Yoshino, K., 2009. Efficient conjugated polymer-ZnSe and -PbSe nanocrystals hybrid photovoltaic cells through full solar spectrum utilization. *Sol. Energy Mater. Sol. Cells.* 93, 1208–1213. <https://doi.org/10.1016/j.solmat.2009.01.001>.
- Zaban, A., Micic, O., Gregg, B.A., Nozik, A.J., 1998. Photosensitization of nanoporous TiO₂ electrodes with InP quantum dots. *Langmuir*. 14, 3153–3156. <https://doi.org/10.1021/la9713863>.
- Zaban, A., Ferrere, S., Gregg, B.A., 1998. Relative energetics at the semiconductor/sensitizing dye/electrolyte interface. *J. Phys. Chem. B* 102, 452–460. <https://doi.org/10.1021/jp972924n>.
- Zang, Z., Tang, X., 2015. Enhanced fluorescence imaging performance of hydrophobic colloidal ZnO nanoparticles by a facile method. *J. Alloys Compd.* 619, 98–101. <https://doi.org/10.1016/j.jallcom.2014.09.072>.
- Zang, Z., Zeng, X., Du, J., Wang, M., Tang, X., 2016. Femtosecond laser direct writing of microholes on roughened ZnO for output power enhancement of InGaN light-emitting diodes. *Opt. Lett.* 41, 3463. <https://doi.org/10.1364/ol.41.003463>.
- Zeng, X., Zhou, T., Leng, C., Zang, Z., Wang, M., Hu, W., Tang, X., Lu, S., Fang, L., Zhou, M., 2017. Performance improvement of perovskite solar cells by employing a CdSe quantum dot/PCBM composite as an electron transport layer. *J. Mater. Chem. A*. 5, 17499–17505. <https://doi.org/10.1039/c7ta00203c>.
- Zhang, H., Cheng, K., Hou, Y.M., Fang, Z., Pan, Z.X., Wu, W.J., Hua, J.L., Zhong, X.H., 2012. Efficient CdSe quantum dot-sensitized solar cells prepared by a postsynthesis assembly approach. *Chem. Commun.* 48, 11235. <https://doi.org/10.1039/c2cc36526j>.
- Zhang, Z., Shi, C., Lv, K., Ma, C., Xiao, G., Ni, L., 2017. 200-nm long TiO₂ nanorod arrays for efficient solid-state PbS quantum dot-sensitized solar cells. *J. Energy Chem.* <https://doi.org/10.1016/j.jechem.2017.08.017>.
- Zhang, Y., Zhu, J., Yu, X., Wei, J., Hu, L., Dai, S., 2012. The optical and electrochemical properties of CdS/CdSe co-sensitized TiO₂ solar cells prepared by successive ionic layer adsorption and reaction processes. *Sol. Energy*. 86, 964–971. <https://doi.org/10.1016/j.solener.2012.01.006>.
- Zhao, H., Fan, Z., Liang, H., Selopal, G.S., Gonfa, B.A., Jin, L., Soudi, A., Cui, D., Enrichi, F., Natile, M.M., Concina, I., Ma, D., Govorov, A.O., Rosei, F., Vomiero, A., 2014. Controlling photoinduced electron transfer from PbS@CdS core@shell quantum dots to metal oxide nanostructured thin films. *Nanoscale* 6, 7004–7011. <https://doi.org/10.1039/c4nr01562b>.
- Zhitomirsky, D., Furukawa, M., Tang, J., Stadler, P., Hoogland, S., Voznyy, O., Liu, H., Sargent, E.H., 2012. N-type colloidal-quantum-dot solids for photovoltaics. *Adv. Mater.* 24, 6181–6185. <https://doi.org/10.1002/adma.201202825>.
- Zhou, R., Zhang, Q., Uchaker, E., Yang, L., Yin, N., Chen, Y., Yin, M., Cao, G., 2014. Photoanodes with mesoporous TiO₂ beads and nanoparticles for enhanced performance of CdS/CdSe quantum dot co-sensitized solar cells. *Electrochim. Acta* 135, 284–292. <https://doi.org/10.1016/j.electacta.2014.05.021>.